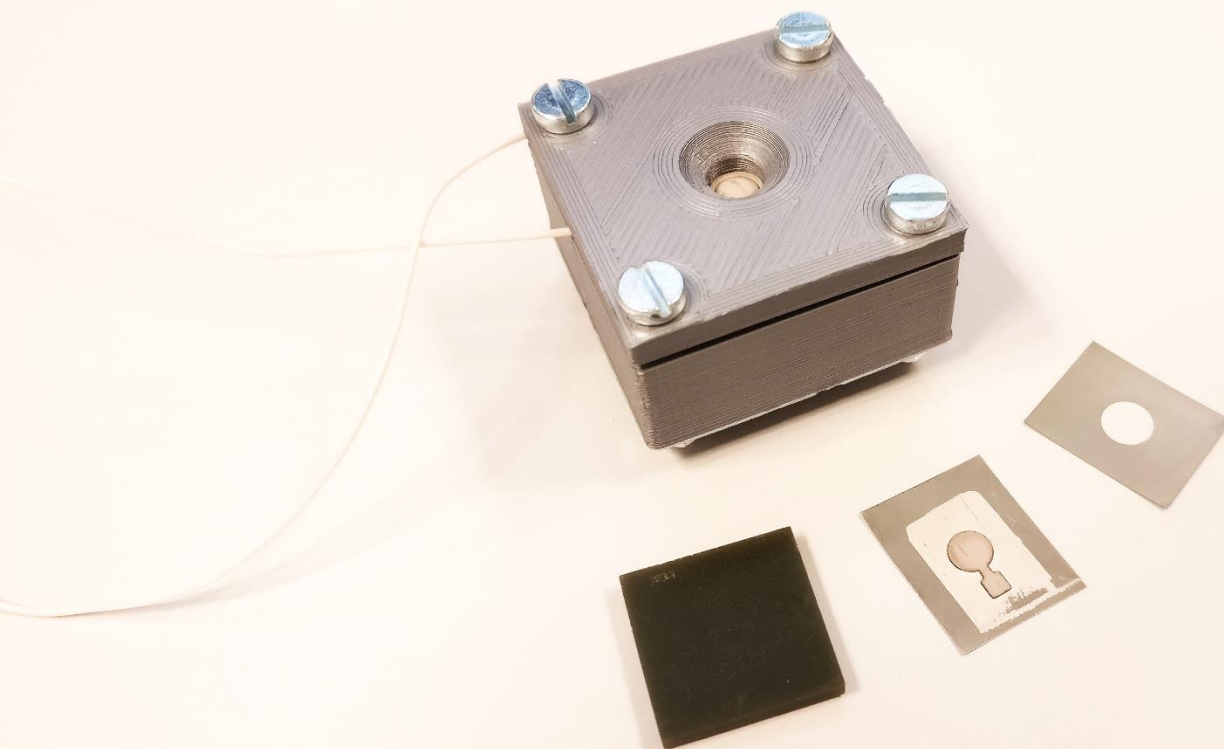# Department of Precision and Microsystems Engineering

A Proportionally Controlled Microvalve using a Piezoelectric Unimorph Microactuator

Arun Gunda

Report no	:	MNE-2019.029
Coaches	:	Ir. Gürhan Özkayar; Dr. Murali Ghatkesar
Professor	:	Dr. Ir. Marcel Tichem
Specialisation	:	Micro- and Nano- Engineering
Type of report	:	Master's Thesis
Date	:	9 August 2019

A Proportionally Controlled Microvalve using a Piezoelectric Unimorph Microactuator

by

Arun Gunda

in partial fulfilment of the requirements for the degree of

Master of Science
in Mechanical Engineering

at the Delft University of Technology

Supervisor:	Dr. Murali Ghatkesar	TU Delft
Chair:	Dr. Ir. Marcel Tichem	TU Delft
Board:	Dr. Ir. J.F.L Goosen	TU Delft
	Prof. Dr. Ir. Joost Lötters	University of Twente

Date of submission: *August 09, 2019*

Table of Contents

List of Figures

List of Tables

List of Acronyms

MEMS	Micro-Electro-Mechanical Systems
UPM	Unimorph Piezoelectric Microactuator
OOC	Organ-On-Chip
RoI	Region(s) of Interest
NO	Normally Open
NC	Normally Closed
PDMS	Polydimethylsiloxane
pMEMS	Piezo - Micro-Electro-Mechanical System
BioMEMS	Biological Micro-Electro-Mechanical System
PZT	Lead Zirconate Titanate
SOI	Silicon-on-Insulator
µ-valve	Micro-valve
µ-pump	Micro-pump
EAP	Electroactive polymer

1 Introduction

Microfluidics is the field of manipulation, control, and analysis of fluids that are restricted to channels with a hydraulic diameter in the sub-millimeter – millimeter range. Microfluidic devices consist of microchannels and active structures used for directing, modulating, mixing, and dispensing flows of different chemicals to achieve a certain purpose. The pursuit of smaller footprint devices extended to fluidics with the introduction of a novel concept called the micro-total analysis system (µTAS) by Manz et al [2] in 1990. They proposed the miniaturization of chemical analysis systems with the argument that devices with smaller microchannels and active structures would result in better chromatographic and electrophoretic separations of gases and liquids, and shorter transportation time of particulates. More importantly, they recognized that miniaturization would lead to reduced consumption of expensive reagents and mobile phases, and possible massive parallelization of chemical testing. Applications for microfluidic devices have been found in many aspects of biology and chemistry with a steady increase in the number of published papers every year. A few examples of these devices have been used for gas chromatography [3-5], drug-delivery [6-9], micro- and nano-spacecraft thermal cooling and propulsion [10-12], and lab-on-a-chip devices [13]. Lab-on-a-chip is a term loosely used to refer to any device that attempts to miniaturize biological or chemical processes. Great advances have been made in drug discovery, protein synthesis, and drug testing using these devices.

Microvalves are essential components in microfluidic devices. They, along with micropumps, are fundamental elements in various applications in fields as diverse as the life sciences and spacecraft micro-propulsion. The primary field in which microfluidic devices are currently being leveraged is in the life sciences. The present climate against the use of animals for testing and the insufficiency of in-vitro evaluation of drugs and chemicals has boosted research in tools that better recreate the human physiological system. This resulted in the introduction of the Organ-on-Chip (OOC) [14-16]. In contrast to standard static cell-culture studies where cells are grown in petri-dishes, OOCs provide an environment that can replicate the structure of the human organ in greater detail. This might be through the introduction of cyclical strains in a heart or lung OOC or the replication of nano-scale organ-wall structure in a kidney OOC. Combinations of multiple OOCs have been reported to reliably replicate the interaction of multiple organs: for instance, liver + intestine + skin + kidney OOCs for drug toxicity studies [16]. It is important to note that the mentioned study used a number of peristaltic pumps and valves to accurately control the flow of bodily fluids between the four "organs" and it is they that provide the motive and modulating force to control the flow of organic media. These fundamental components are therefore pivotal for these innovative technologies to be successful.

These components need to be reliable, occupy minimum dead volume, have a long life, and handle flows with a large dynamic range: from the pico- to micro-liter. A large body of work exists that addresses the design and fabrication of microvalves and micropumps. In this work, the device under investigation is the microvalve. Few microvalves from literature have won out in terms of use in the research lab or for commercialization. Currently, PDMS based microvalves are the most popular in biological and chemical research but they generally require bulky external peripherals like pneumatic compressors and valves. They also cannot be used for controlling gases as they are highly permeable. The alternative is to use Silicon-based microvalves, but they are hard to manufacture and require complicated infrastructure which is not readily available.

The goal of this thesis is to design and fabricate a small foot-print microvalve that can be used for both liquids and gases and without bulky external peripherals. The following chapter addresses the current state of research in microvalves and identifies a clear research gap. The third chapter is a paper that details the main work performed in this thesis to address the research gap. The thesis conclusion and the author's reflections are given in subsequent chapters.

2 Literature Survey on Microfluidic valves

This chapter consists of an exploration of existing literature regarding micro-valves and attempts to find a research gap that can be answered in a subsequent thesis.

2.1 Macro-valves

Valves are flow modulation devices used to control, direct, or regulate the flow-rate of fluids passing through a channel in a fluidic circuit. Most mechanical valves function by obstructing a flow passage. A few commonly used *macro*-valves are shown in Figure 1.
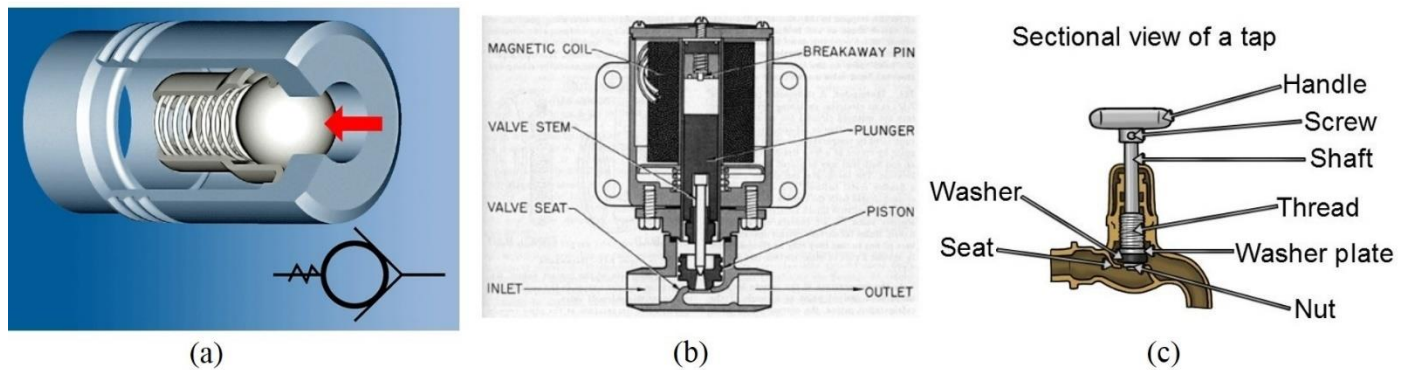
Figure 1: Common Macro-valves: (a) Check valve (b) Solenoid valve (c) Manual proportional control valve

Figure 1(a) shows a passive check valve used to allow flow in one direction. This is the simplest valve used in fluidics; it operates by inlet-pressure actuation of the ball-on-spring mechanism. Figure 1 (b) is an active valve operated using an electromagnetic solenoid actuator. Energizing the solenoid actuates a piston and opens the valve. These devices are commonly used as on-off valves. Figure 1(c) is the most recognizable of the three valves; it is a normal tap. Flow rate of water flowing through the tap can be controlled by the rotation of the handle. This is a manually-operated proportional control valve; its powered counterpart is the device that this thesis is attempting to miniaturize.

2.2 Microvalves

Microvalves (μ-valves) are fluid control devices that operate in the micro- to milli-meter length scale. They are generally fabricated using conventional microfabrication techniques (lithography, etching, etc.) and have two ports – an inlet and outlet. An active element between these ports is responsible for obstructing the passage. Some microvalves exist that operate by exploiting surface effects (as opposed to volume effects) that dominate in the small-scale. This thesis is only concerned with conventional microvalves that operate by the obstruction of a passage. Nevertheless, a brief foray is made into most types to explore the literature for regions of interest (RoI).

A large body of research in microvalves has resulted in their classification based on a number of characteristics. A few have been selected due to their relevance in this survey and are shown in Figure 2. The main classification criterion is based on their operation. A valve can be either passive or active, i.e., they might be unpowered or powered by an actuator. The actuator can, in turn, be mechanical or non-mechanical in nature. More details of active valves are given in Table 1.

Another classification can be made based on the fluid that is modulated. It is comparatively easy to test gas microvalves as evinced by a majority of relevant literature testing their valves using gases like air or nitrogen [17]. Liquid microvalves generally require more stringent conditions like the isolation of actuation electrodes from the fluid, compatibility of wetted materials with the fluid, and the requirement of an impermeable channel to transport fluid through the valve. A significant percentage of liquid microvalves utilize PDMS-based microfabrication techniques due to the availability of

easily fabricated in-channel valves (addressed in a later section) and compatibility of most liquids with common polymers.
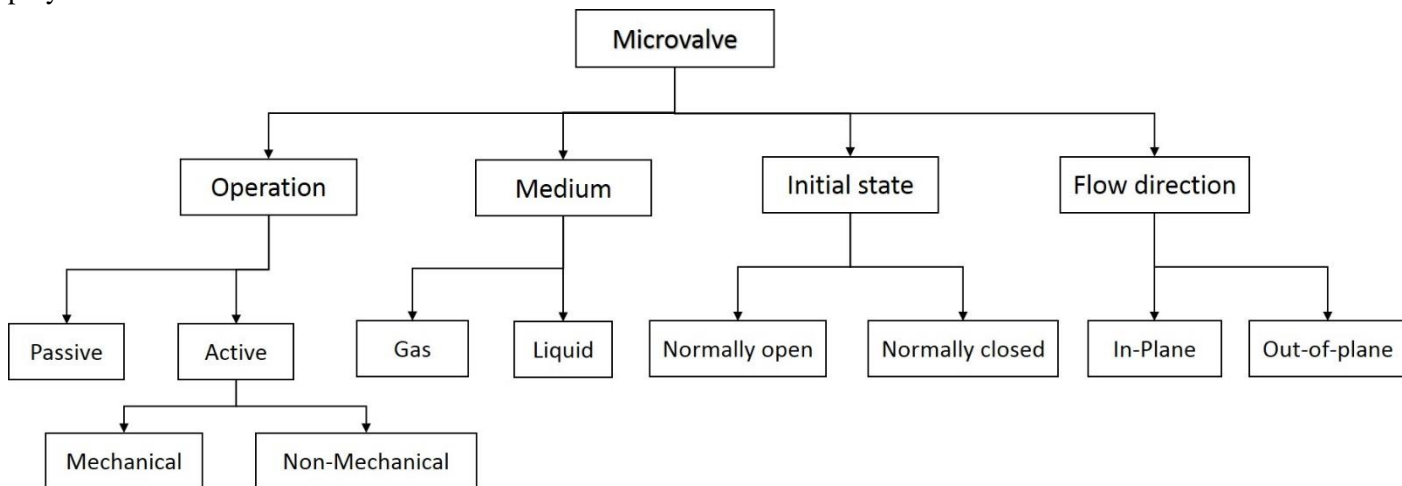
Figure 2: Classification of microvalves

The initial state of the valve is an important characteristic to consider when an application requires precise dosing, low-power, and good low-pressure performance. A normally-open (NO) configuration refers to a microvalve that, when unpowered, has free flow from inlet to outlet. The actuator has to be actuated to create any modulation or blockage. This type is not preferred in biological/chemical applications where an actuator failure can cause an uncontrolled supply of chemicals. Normally-closed (NC) valves are better suited for these applications, with the valve being closed when unpowered. A trade-off is that the flow-rate in these valves is generally lower than NO valves due to diminished stroke. NC valves are also harder to design due to the need of a spring force to move a membrane or valve plate after release of the membrane/plate. Many work-arounds have been made to achieve a normally-closed state – they will be addressed in the following sections.

The flow direction in the microvalve determines if the valve is compatible with a microfluidic circuit. Most microvalves are constructed with the inlet or outlet perpendicular to the plane of the valve. This means that off-chip tubing is required for the valve to function. This might be acceptable for a stand-alone valve, but not in a microfluidic circuit. An in-plane configuration is required when using a valve in circuits. Due to ease in design, most Si-microvalves in the literature tend to be out-of-plane. The previously mentioned PDMS-based microvalves tend to be in-plane microvalves.

Table 1: Classification of active microvalves [17]

Mechanical	Magnetic	External magnetic field
		On-board magnetic inductor
	Electric	Electrostatic
		Electro-kinetic
	Piezoelectric	Thin-film
		Thick-film
		Bulk ceramics
	Thermal	Bimetallic
		Thermo-pneumatic
		Shape memory alloy
Non-mechanical	Phase-change	Hydrogel
		Sol-gel
		Paraffin
	Rheological	Electro-rheological
		Ferro-fluids
	Electroactive	Electroactive polymers

This survey concerns itself with active microvalves and attempts to find a region of interest (RoI) to address. Table 1 lists the types of active microvalves found in the literature. As can be seen, the distinction is generally made by the actuation principle used. The following sections will offer greater detail through an explanation of working principles and examples.

2.3 Mechanical Microvalves

Microvalves that function by mechanical actuation of a valve plate/membrane to close an orifice/passage are termed as mechanical microvalves. Numerous valving schemes are possible and have been explored extensively. A succinct visual summary of valving concepts is given in Figure 3.

The concepts shown obstruct an orifice using different valving schemes. The vertical plate valve is mostly used when the valve is made of hard materials like silicon. With softer substrates like PDMS, membrane valves are preferred. Fewer examples of the other types are found due to various fabrication, sealing, or control issues encountered during their operation.
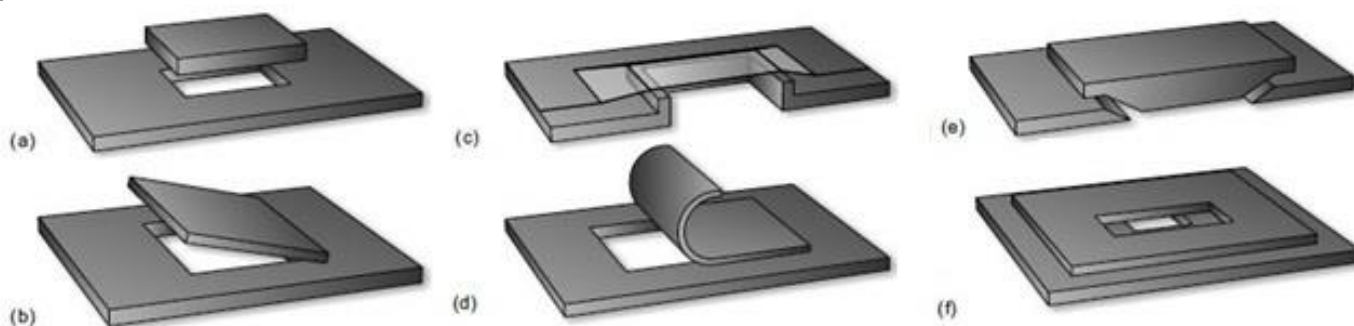
Figure 3: Valve concepts [18]: (a) Vertical plate (b) Tilting (c) Membrane (d) Bending (e) Needle (f) Sliding

The types of mechanical microvalves shown in Table 1 are explained in greater detail below.

2.3.1 Electromagnetic Microvalves

The first electromagnetic (EM) microvalve was used as an injection valve for a gas chromatography system [5]. They used a solenoid-operated actuator that depresses a silicon membrane to close an orifice. This allowed them to finely control the gas sample dispensed into the chromatography column (Figure 4(a)). These valves require a magnetic field, either generated with a coil or a permanent magnet, and a magnetic material that is influenced by this field. Power consumption can be decreased by using a permanent magnet, but it requires the introduction of a macro-scale object (the magnet). It is more common to see the use of coils as magnetic field generators. *Hirano et al* used a vacuum-deposited magnetic material (NiFe) to construct a valve plate [19]. An external coil was used to actuate the valve plate against an orifice. As shown in Figure 4(b), the construction of the valve is simple, with a valve plate moving vertically against an orifice. Contrary to most Si-based microvalves, they reported ultra-low leakages in the order of 1e-9 mbar.L/s. This was due to a tight valve seat - valve plate fit attained through a FIB etch of the valve seat. They also reported the use of a stress-controlled valve-plate anchors to attain a normally-closed initial state after release of the plate. This is an interesting concept that could be exploited in the author's thesis.

The smallest footprint is attained by a valve configuration similar to that constructed by *Bintoro et al* as shown in Figure 4(c) [20]. They use an integrated micro-coil (3) and CoNiMnP magnet (6) to create an EM actuator. The structure of the valve anchors creates an inherent bistability; this is exploited to create an on-off valve with the two stable states in the open and closed positions. Unfortunately, they also report a high operating power of 0.3W to 1.2W. This appears to be a trend in most EM valves, with a trade-off between actuation force and operating power.
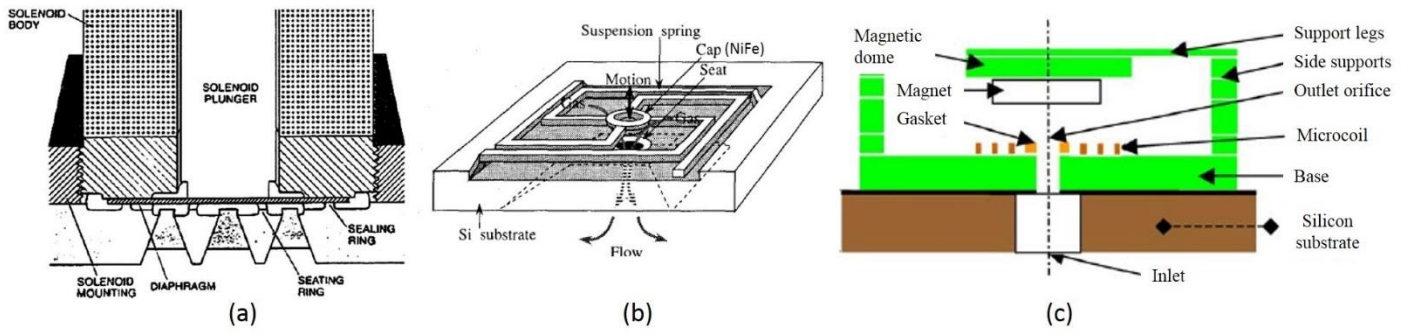
Figure 4: (a) Solenoid plunger microvalve [5] (b) Valve w/ magnetic material [19] (c) Valve w/ integrated magnetic actuator [20]

2.3.2 Electrostatic Microvalves

Although electrostatic actuators are found in a significant percentage of MEMS devices, they have some inherent drawbacks that prevent their widespread adoption in microvalves. Low force, small stroke, high voltage, and possibility of liquid electrolysis are disqualifiers for most microvalve applications. Nevertheless, there is a sizeable body of research dedicated to overcoming these issues.
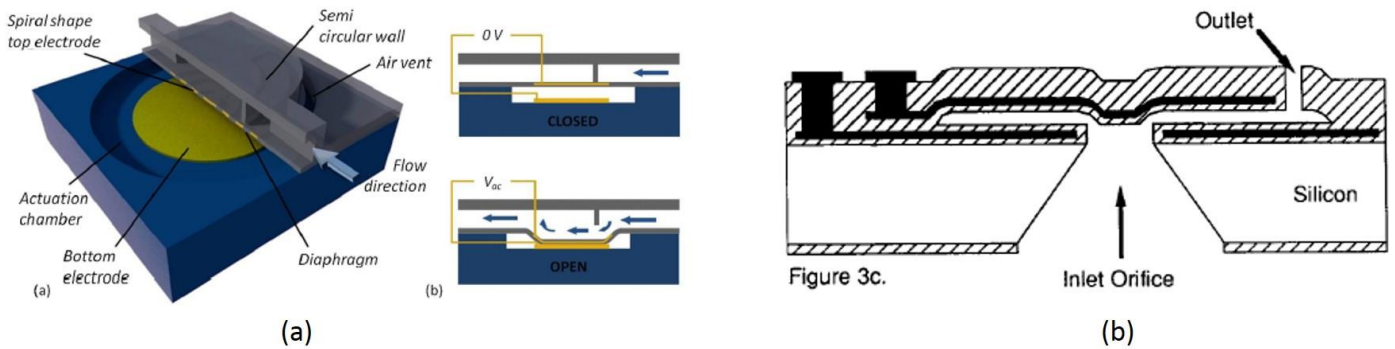
Figure 5: (a) Electrostatic membrane microvalve[21] (b) Electrostatic cantilever microvalve[22]

Recent research by *Yildirim et al* reports the fabrication of a normally-closed, electrically isolated, electrostatic microvalve constructed of parylene [21]. They obtain a normally-closed configured by depositing two parylene layers without doing a mandatory adhesion promoter step between the two depositions. This allows them to separate the two layers after resist stripping using pneumatically-applied pressure. As shown in Figure 5(a), they isolate the parallel -plate electrostatic actuator by constructing an actuator chamber underneath the valve and away from the modulated fluid. They report leakage at higher pressures due to the valve automatically opening at high inlet pressures. A more conventional Si-micromachined cantilever valve was reported in 1990 by Honeywell Inc [22]. They use a parallel plate actuator to actuate a cantilever and close an orifice as shown in Figure 5(b). Due to low actuation forces, they found significant leakage through a closed valve, even at a high actuation voltage of 30V. This valve can safely be operated with gases but might cause electrolysis when used with water or aqueous media.

Electrostatic actuators have a low stroke and a short region of influence. Parallel-plate actuators can function with an initial separation on the order of 2µm. Reliable control extends to around 1/3rd of that region, approximately 0.7µm. If the voltage is increased beyond this point, pull-in occurs, and all control is lost – the valve snaps close. Due to this, electrostatic valves are usually operated as on-off valves. Si-machined valves can also be operated in duty-cycle mode to modulate flow.

2.3.3 Piezoelectric Microvalves

Piezoelectric MEMS (pMEMS) devices have gained considerable interest in the last two decades due to the high power-density of piezoelectric materials. Advances in material sciences have resulted in ceramics with high piezoelectric coefficients. Many commercial and experimental *micropumps* utilize pMEMS actuators but their use in microvalves is still comparatively rare [9]. This is due to their low-stroke (~0.1% strain). Most reported piezo-microvalves (p-μ-valves) use a large piezo-chip/stack/disc to create a large stroke(~5-10μm). This, though functional, creates a valve in the cm length-scale. pMEMS devices integrate piezo-materials in three different ways: thin-film, thick-film, and bulk material. Currently, the material that is most used is Lead Zirconate Titanate (PZT) as it has the highest piezoelectric coefficients. Due to the importance of this topic, more detail regarding fabrication and implementation is provided.

The following list details the available methods of fabrication of each type [23].
1. Thin-Film PZT: Film thicknesses < 3μm can be deposited.
    a. Sol-gel deposition:
    b. Aerosol deposition
    c. Metal-organic Chemical Vapor Deposition
    d. Pulsed Laser Deposition
2. Thick film PZT: Film thicknesses < 50μm can be obtained.
    a. Screen printing
3. Bulk PZT ceramics: Commercially available in plate(~500μm), disc, stack, and chip form.
    a. Bonding to Si-substrate and thinning

Table 2: Comparison of PZT Integration methods [23]

	Thin Film	Thick Film	Bonded PZT ceramic
Layer Thickness	< 3μm	2 - 50μm	10 – 500μm
Processing temperature	~600°C	~900°C	~500°C
Piezoelectric coefficients	Intermediate	Least	Highest
Ability to integrate	Well-developed	Developed	Least developed
Patterning technology	Wet, dry etching	Wet and ion-milling	Wet etching, laser cutting, dicing, waterjet cutting
Applications	Sensors	Actuators	Actuators

Thin-film PZT is generally used in sensors due to their low force. This prevents their use in microvalves. Thick-film actuators have been used in micro-pumps, but their low stroke limits their use in valves. Bonded PZT actuators are a relatively new type of actuator, where commercially available 300-500μm thick plates are thinned after bonding on a substrate. The main issue with their implementation is that patterning is difficult due to the stability of the ceramic. Chemical etching tends to be too slow or highly isotropic. Physical machining like laser cutting or dicing result in rough edges and/or thermally-affected regions close to the cut that lose their piezoelectric properties. Waterjet cutting offers the best kerf and cut quality, but a backing material is required to ensure that the PZT is not shattered due to the high-pressure waterjet [24].

The requirement for amplification of stroke has resulted in ingenious, albeit sometimes impractical, designs. A more conventional valve by *Lee et al* for liquid flow control is shown in Figure 6(a) [25]. They use a wafer-bonding approach to construct a normally-closed valve for use in an integrated spacecraft micro-thruster. A custom segmented PZT actuator was used with two active PZT pillars with a central inactive zone. When powered, the two pillars increase in length to create a maximum separation of 5μm at 50V. The main issue with these types of valves are the requirement of multiple wafer bonding steps. Not only does the time and labor required increase, the chances of improper alignment are also magnified.
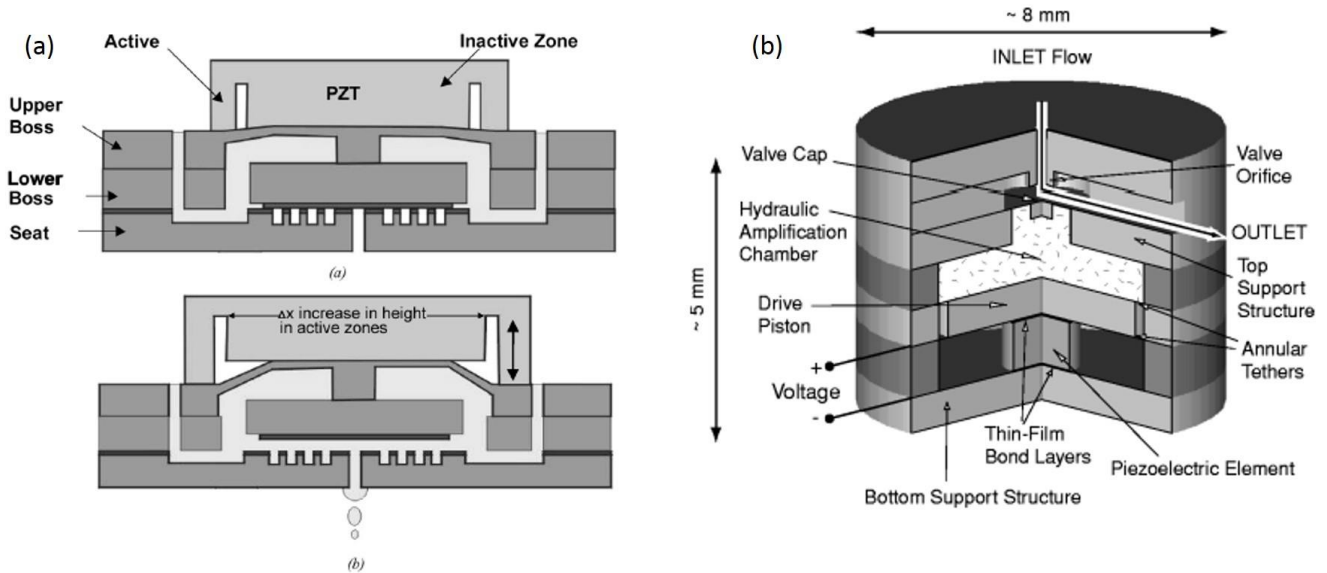
Figure 6: (a) Normally closed wafer-bonded microvalve [25] (b) Hydraulically amplified microvalve [26]

A relatively new concept (for microfluidics) was used by *Roberts et al.,* to construct a hydraulically amplified microvalve. As can be seen in Figure 6 (b), the complexity of the device is high, but the results obtained are also useful. They use four glass layers, three Silicon-on-Insulator (SOI) layers, and two Si layers to construct the microvalve. A central layer contains a chamber filled with hydraulic fluid and is sandwiched between a large membrane and a smaller membrane. The PZT element at the bottom of the valve actuates the large membrane. The structure of the hydraulic chamber causes motion amplification to occur at the small membrane. They report a maximum stroke of 30μm, which is the maximum observed in a piezoelectric microvalve, and a maximum hold-back pressure of 3 bar.
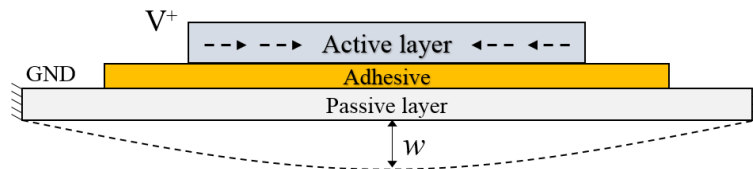
Figure 7: Unimorph Piezoelectric Actuator

Many examples of unimorph piezoelectric microactuators (UPM) for micropumps have been found in literature [27]. Unimorphs are a type of actuator that consist of an active layer that is bonded to a passive substrate. Deformation of the active layer using electrical stimulus is magnified by the bonded substrate by virtue of its physical constraints. Membrane unimorphs are constrained along the circumference. Application of stimulus causes the active layer to shrink in the lateral direction. This causes the membrane to bow down with a displacement that is amplified with respect to the active layer shrinkage as shown in Figure 7. A μ-valve using a UPM has been reported, but it has a small displacement of 1.3 µm at 250V and a large lateral dimension of 15 mm [28]. There is ample room to improve the actuation while maintaining good force characteristics.

A research gap in piezo-µ-valves is the absence of a sufficiently small piezo actuator (< 5 x 5 x 2mm) with sufficient stroke and force to overcome valve-membrane stiffness and an inlet fluid pressure of ~ 1 bar. Availability of such an actuator can fill a much-needed gap in the integrated Si-microfluidic chip field. Current piezo-actuators are usually bulky piezo-chips or stacks that increase the dimensions of the valve. Introduction of a smaller actuator can decrease the footprint and the thickness of µ-fluidic chips. As surface-micromachined Si-µ-valves usually require a small stroke of < 5 µm, a UPM might be the answer.

2.3.4 Pneumatic Microvalves

Pneumatic valves utilize pressurized air to cause membrane deformation and subsequent passage closure (or opening). They are generally used in conjunction with Polydimethylsiloxane (PDMS) to create a valve that can be easily fabricated, rapidly prototyped, and highly biocompatible. They are mostly used as liquid μ-valves as PDMS is a gas-permeable material. They require little equipment and cheap materials to fabricate due to which most chemical/biological labs that require μ-fluidics use these types of valves. The main issue is their control: they require external pneumatic control equipment to cause valving to occur due to which their use is generally limited to testing or research purposes, and are rarely commercialized [17].

PDMS-based pneumatic valves were first introduced by *Quake et al [29]*. Their paper is among the most cited in the μ-valve field and its popularity has caused these valves to be named after their inventor: Quake valves. They also introduce peristaltic pumps, switching valves, and even fabricate a seven-layer pneumatically operated logic circuit. These valves are manufactured by sandwiching multiple layers of PDMS material that are pre-fabricated with channels using soft lithography or embossing. A simple normally open microvalve is shown in Figure 8(a) [29]. Two channels are constructed on two different layers and bonded. Flow through the Flow channel can be modulated by controlling pneumatic pressure in the Control channel. For different applications, an NC valve can be constructed with a design as shown in Figure 8(b) [30]. In this configuration, negative pneumatic pressure is used to cause actuation. A vacuum pump is required instead of a conventional air compressor.
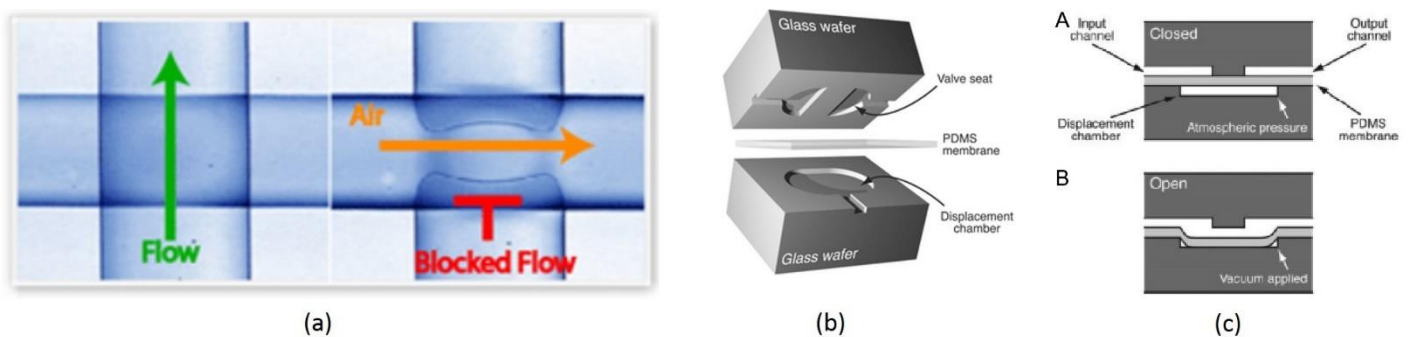
Figure 8: (a) Normally-Open (NO) PDMS μ-valve [29] (b) Exploded view: NC μ-valve [30] (c) Cross-section: NC μ-valve [30]

2.3.5 Thermo-pneumatic Microvalves

Thermo-pneumatic valves are similar to pneumatic valves in that they use pressurized fluid to cause actuation. Instead of using a compressor or external power source, they use the thermal expansion of a fluid to cause membrane deformation. Large strokes can be generated with very good force-displacement characteristics. The main disadvantage is the low speed (~1Hz) and high power requirement (>0.5W) [31, 32].
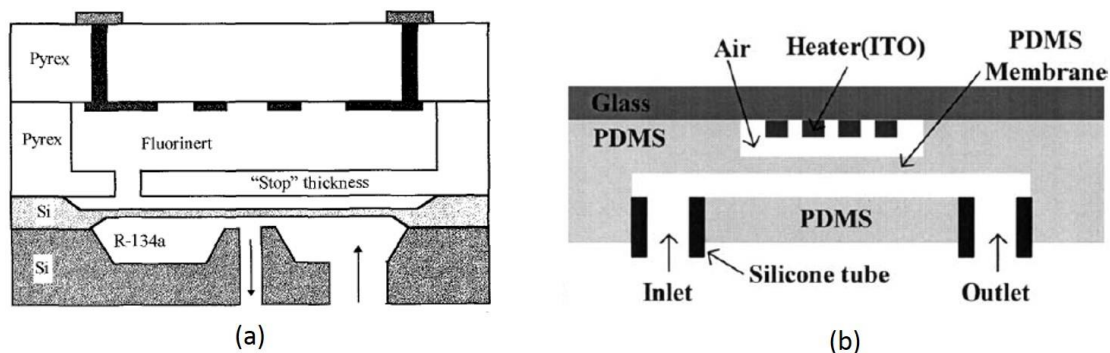
Figure 9: (a) Fluorinert Thermo-pneumatic valve [31] (b) Air Thermo-pneumatic valve [32]

Figure 9(a) is a cross-section of a thermo-pneumatic valve that is fabricated by wafer-bonding two Pyrex wafers and two Si wafers [31]. A platinum resistor is deposited on the upper Pyrex wafer and is used to heat the expansion fluid. In this case, they use Fluorinert, a low-boiling point liquid (56 °C) generally used as a refrigerant. Due to this fluid, they report a low power consumption of ~0.5W, among the lowest reported in thermo-pneumatic valves. The expansion of Fluorinert due to boiling causes the Si-membrane to deflect downwards and block the orifice. A PDMS-based equivalent is shown in Figure 9(b) [32]. The thermal expansion of air is used instead of a liquid. Due to the slow thermal conduction and expansion of air, a large time of 20-30s is required to close the valve. Due to the low stiffness of PDMS, large deflections on the order of 200μm are possible at a low power of 0.3W. This valve is meant for the control of biological media due to which they are made using cheap, disposable materials.

2.4 Unique Microvalves

Although there are many other types of microvalves, only classes with the greatest representation in the literature have been addressed in the previous sections. Of the myriad others that are available (Table 1), two interesting concepts have been chosen for their novelty and potential for RoI.

2.4.1 Electroactive Polymer Microvalve

Electroactive polymers (EAP) are a class of polymeric materials that exhibit a strain on the application of an electric field [33]. They are split into two classes: dielectric and ionic EAPs. Dielectric polymers exhibit deformations due to high electrostatic forces between two electrodes that are laid on the polymer. The Maxwell stresses caused due to the high field results in a squeezing between the two electrodes. Some materials and designs show strains in the order of 380% but require voltages on the order of 4 kV. Ionic polymers deform due to the physical motion of ions within the material on the application of an electric field. They generally require < 10 volts to function but the power consumed is higher than dielectric polymers. They also need to maintain wetness to function, i.e., they need to be within an aqueous environment. Some actuators have been packaged to ensure that they are permanently wet so that they can be used in dry conditions.
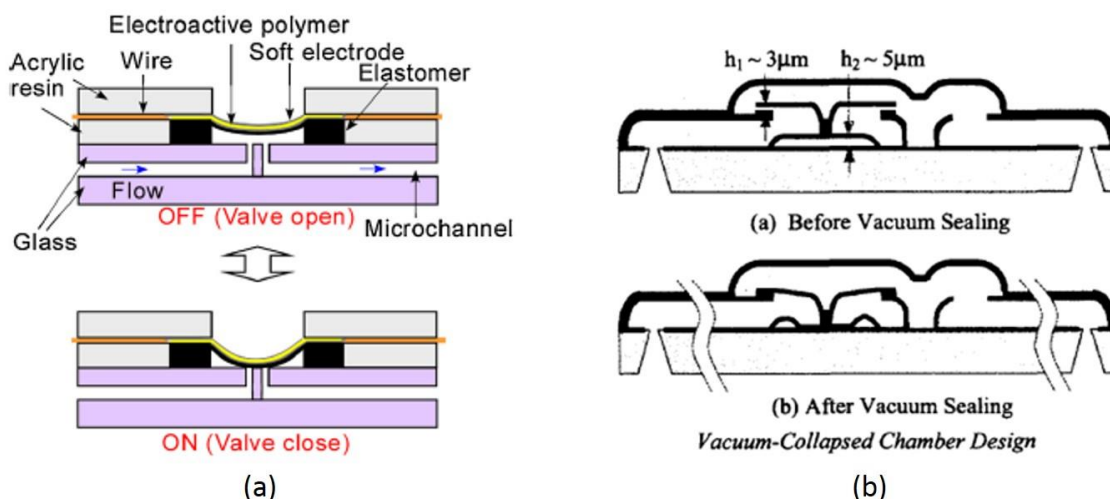
Figure 10: (a) Electroactive polymer valve [34] (b) Vacuum-collapsed passive check valve [35]

Tanaka et al reported the first dielectric EAP μ-valve [34]. As shown in Figure 10 (a), they sandwich a prestressed 18 μm-thick EAP membrane between two flexible electrodes and apply a high voltage of 900V. The resulting Maxwell stresses cause the membrane to bow downwards and block the orifice. They report a deformation of 50 μm and a response time of 0.7s to block a flow with inlet pressure of 0.04 bar. **A research gap in dielectric EAPs could be in the research of different materials and designs to improve pressure and flow characteristics.**

2.4.2 Vacuum-collapsed Microvalve

This type of valve is innovative due to it being one of the few truly normally-closed (NC) µ-valves. To understand its position in the literature, it is useful to explore the types of NC-valves that are available. A review of µ-valve literature yields seven different types of NC-µ-valves. These are:

1. Inlet-pressure closed NO valves: A normally-open valve with inlet pressure forcing the valve plate closed. The space between the valve plate and valve seat is generally on the order of 1-2 µm in Si-micromachined valves; valve plate anchors are designed to be highly compliant. Leakage is inevitable at low inlet pressures. This is a pseudo NC-valve.

2. Wafer-bonded/Assembled NC microvalves: Valve plate and valve seat are fabricated in different wafers and bonded. A normally-closed state is easily attained but at the cost of assembly and bonding [26, 36]. This is a true NC-valve.

3. Forced closure in post-fabrication: Valve is fabricated as a NO valve and forced shut by using a macro-scale actuator (piezo-stack/chip/disc) [37]. This is a pseudo NC-valve.

4. Venous valves: Inspired by valves found in the heart. Can be used as a passive check valve. Only one example has been found in literature [38]. It can only be used in polymer-based devices. This is a pseudo NC-valve.

5. Vacuum-collapsed valves: Uses an evacuated and sealed chamber with a compliant wall that buckles on the introduction of external ambient pressure to create post-release displacement of a membrane [35, 39]. This is a true NC-valve.

6. Separating layers with poor adhesion in post-processing: Some thin-film materials do not adhere well to each other. This can be used to create a valve with the two mating surfaces having poor adhesion [21]. No release step is required to separate the layers due to which it functions as a normally closed valve. This is a true NC-valve.

7. Stress-deformed Microvalve: Compressive stresses on the top-most film of the valve-plate can cause it to be pushed downwards to close an orifice [19]. This is a true NC-valve.

Among those listed above, the vacuum-collapsed microvalve appears to contain the greatest potential for research due to its rarity in literature and its potential for adaption in an active microvalve. Only two examples have been reported with both of them used only as passive check valves. Figure 10 (b) shows one of these examples by *Wang and Tai* [35]. They use parylene to fabricate the entire valve on a Si-substrate. Parylene is used as it is one of the few polymers that can be vacuum-deposited. This allows the vacuum-collapse chamber can be easily constructed. Parylene also creates highly conformal coatings and is highly biocompatible. The vacuum-chamber collapses on the introduction of ambient pressure due to its high compliance. The collapsed ceiling pulls down the connected valve plate and closes the valve. Low inlet pressures on the order of 0.02 bar can push the valve open. Reverse pressures on the order of 2-3 bar is required to cause the valve to fail. Flows in the range of 100nl/min can be controlled with no detectable leakage.

A research area could be in the conversion of the vacuum-collapse check valve to a proportionally controlled valve. There is ample design space available that can be exploited with the collapsed chamber concept.

In this section, a brief overview of relevant microvalve concepts has been provided with a commentary about potential research gaps. The following section elaborates these areas with further detail and attempts to determine the feasibility of pursuing these regions of interest in a subsequent thesis.

2.5 Exploration of Research Gaps

In the previous sections, three tentative areas of research have been identified. This section goes into greater detail to determine the region with the highest feasibility in the given timeframe and available resources. These are listed in order below:

1. Research of different EAP materials and designs to improve pressure and flow characteristics

2. Conversion of a vacuum-collapse check valve to a proportionally controlled active valve
3. Small piezo actuator (< 5 x 5 x 2 mm) using a PZT unimorph for the actuation of Si-µ-valves

The above research questions will be explored in greater detail to decide if they contain intellectual value. Table 4 contains a final comparison of the above regions of interest (RoI). Sections 2.5.1 - 2.5.3, contain detailed explanations of each RoI.

2.5.1 Dielectric EAP Microvalve

The microvalve shown in Figure 10 (a) requires a high voltage of 4 kV to achieve a central membrane displacement of ~50 µm [34]. The material used is a nitrile rubber with significant processing required to obtain a membrane. This is then laminated with electrode layers to create an actuator. It is evident from this procedure that the fabrication of the membrane is highly unwieldy with many steps involved.

Table 3: Response of some elastomers [40]

Polymer (Specific Type)	Elastic Energy Density (J/cm³)	Pressure (MPa)	Strain (%)	Young's Modulus* (MPa)	Electric Field (V/mm)	Dielectric Constant (at 1 kHz)	Coupling Efficiency, k^2 (%)
Silicone Nusil CF19-2186	0.15	0.72	32	1.0	235	2.8	54
Silicone Dow Corning HS3 (centrifuged to remove particulates)	0.038	0.13	41	0.125	72	2.8	65
Polyurethane Deerfield PT6100S	0.20	3.8	11	17	160	7.0	21
Silicone Dow Corning Sylgard 186	0.10	0.50	32	0.7	144	2.8	54
Fluorosilicone Dow Corning 730	0.051	0.29	28	0.5	80	6.9	48

Table 3 shows some commercially available elastomers that have been characterized. The highest strains have been observed in some silicones based on PDMS (120%), and an acrylate elastomer by 3M named VHB-4910 (380%). The above table and strain values are representative of the fact that there are many more alternatives available that could be explored as a microvalve actuator. It must also be noted that pre-stretching is a necessary step to obtain good deformation. No dielectric EAP microvalve has been implemented with a pre-stretched elastomer state. This can significantly decrease the potential strain output and could be an area of contribution for future work.

Unfortunately, no solution currently exists for the reduction of operating voltage to a level that is more feasible for portable applications. The voltage applied in most research papers is close to the breakdown voltage of the dielectric used (~200V/µm). This might be a large disqualifier for this µ-valve as even high piezo- and electrostatic voltages (~200V) are frowned upon in the MEMS industry. Breakdown of air is also possible if the electrodes are not designed well or if there are fabrication errors.

2.5.2 Active Vacuum-collapsed Microvalve

The vacuum-collapse concept is an innovative technique to obtain a post-release spring force. The operation of the vacuum collapse chamber is explained in detail in Sec. 2.4.2. The primary reason for its lack of use in conventional valves is the requirement of a compliant material (generally a polymer) and the need for a vacuum within the vacuum-collapse chamber. The author who pioneered this technique is a proponent for the large-scale use of parylene for microfluidics due to its biocompatibility, gas and liquid-impermeability, and high compliance [35]. The main reason for why PDMS is preferred as a polymer for microfluidics is because parylene can only be vacuum deposited. The deposition rate is generally slow and can be as low as 2 µm/hr for certain parylene variants. Another issue that is more relevant to the check valve shown in Figure 10 (b) is the need for multiple patterning steps; six photolithography steps were required.

A variant of the valve required eight photolithography steps [39]. Nevertheless, the concept itself is sound and the possibility of a novel μ-valve cannot be ignored without a more detailed exploration.

To investigate the concept further, two designs for a vacuum-collapsed pneumatic microvalve were made. A pneumatic power source was considered due to its ease of testing and troubleshooting. An integrated actuator like an electrostatic membrane valve will require more photolithography steps and this might cause budgeting and fabrication issues that might not be solved within the given time constraints of a thesis.
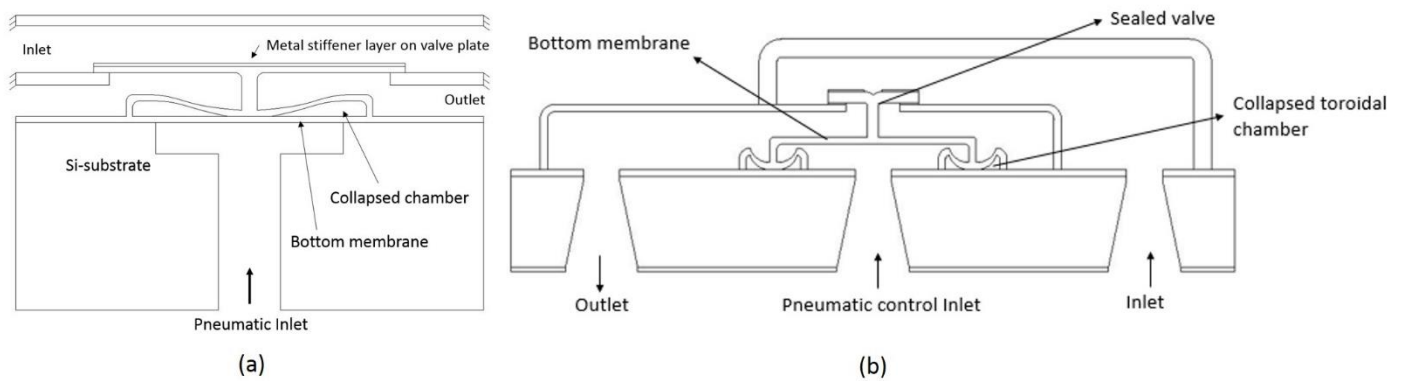
Figure 11: (a) Simple active μ-valve (b) Bidirectional Normally-closed μ-valve

The simple μ-valve in Figure 11 (a) shows its state after the vacuum collapse chamber has been collapsed. The valve plate has contacted the valve seat and the device is normally closed. Regardless of the inlet pressure, the valve remains closed as the valve plate is pushed downwards. Application of control pressure through the Pneumatic inlet causes the bottom membrane to bow upwards and push the valve plate open. Control of pneumatic pressure proportionally affects valve separation and therefore the flow-rate. A major disadvantage with this design is the low-impedance during backflow. If the outlet pressure is greater than the inlet pressure, fluid can readily flow backwards from outlet to inlet.

A slightly more involved design is required to eliminate the risk of back-flow. This is shown in Figure 11 (b). It is an extension of the designs by *Tai's* group [35, 39]. Its operation when the inlet pressure is greater than outlet pressure is the same as the previous example. Conversely, when outlet-pressure is greater than the inlet pressure, the bottom membrane deflects downwards and pulls the valve-plate closed. The valve can only be opened by application of a positive control pressure to push the valve-plate up. This design is therefore an intrinsically bi-directional, normally-closed, pneumatically-operated, single-wafer valve. There are few, if any, valves in the literature that can boast the same characteristics. Most bidirectional, normally-closed valves require an external force to hold them closed (Figure 6(a)).

It is apparent from Figure 11 (b) that it requires a large number of parylene layers and therefore, many photolithography steps. A quick process sequence showed that at least 10 lithography steps are needed to realize the valve (including channel fabrication). In MEMS fabrication, it is generally preferred to limit the number of steps to below four, both to decrease mask cost and fabrication risk. As the number of steps increases, it is more probable for the design to fail, either due to stress, misalignment, or plain human error. Moreover, the cost of a single mask is upwards of EUR500; we require at least ten of these. It is possible to have multiple designs on the same mask to decrease the total number of masks, but this is only when fabricating the μ-valve alone. This design, although highly novel, requires the sacrifice of both time (long fabrication process), and cost (mask fabrication, time on machine).

2.5.3 Piezoelectric Unimorph Microvalve

Microvalves using piezoelectric actuation schemes typically use an actuator in the cm-scale to actuate a microvalve in the mm-scale. This has resulted in devices that are much larger than they need to be, with the actuator dominating the volume of the valve [36, 37, 41]. Figure 6 (a) shows an example of a μ-valve where it is clear that the actuator is greater than 90% of the device volume. The only reason for their use is the availability of commercial piezo-actuators and the

possibility of easy integration to the valving structure. The development of an actuator in the mm-length scale that has sufficient force to actuate a valve at 1-3 bar inlet pressure and sufficient stroke to close the separation between valve plate and valve seat can be of great significance to the μ-valve field.

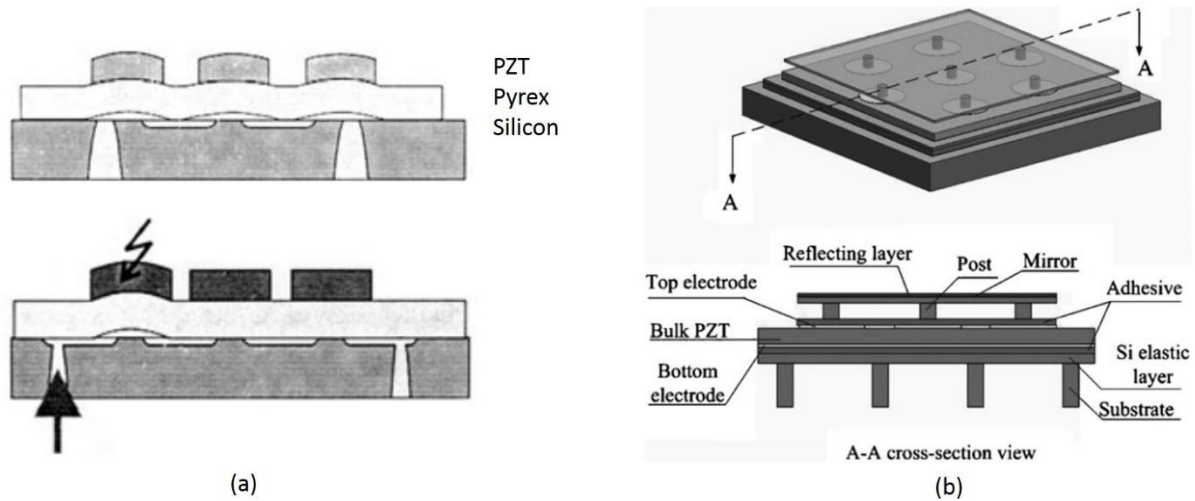**Figure 12: (a) Peristaltic Micropump [42] (b) Deformable Micromirror [43]**

In μ-fluidics, unimorph membrane actuators (UPM) have been used in micro-pumps. They generally follow the same principle as that shown by *Veenstra et al.,* in Figure 12 (a). Peristaltic micropumps use sequential actuation of membranes to pull and push liquid from the inlet to outlet. In *Veenstra et al*, three PZT discs are epoxy-bonded to a Pyrex substrate [42]. This actuator is then anodically bonded to a Silicon substrate with pre-built channels and access ports. The actuator uses its d_{31} mode; the small lateral deformation ($< 0.5\,\mu m$) of the PZT is converted to a large out-of-plane deformation due to the attached membrane. This is similarly used in Figure 12 (b) to obtain a deformable micromirror. Selective operation of the array of UPMs can deform the mirror as required.

Bulk-PZT ceramics are commercially available and possess the highest piezoelectric coefficients in comparison to their thin- and thick-film counterparts. Their use in μ-devices is generally restricted to high-frequency applications like ultrasonic and acoustic transducers due to their nm-scale deflection. In the last decade, a new methodology was explored where wafer-bonding of PZT and Si with an intermediate Au layer was performed [1]. Other

Figure 13: Bulk-PZT-Si μ-device Process Sequence [1]

intermediate layers like polymers (Cytop, Parylene), AuSn, AuIn, and InSn have also been tested successfully [44]. The procedure of bonding and subsequent machining using Au is shown in Figure 13. From a budgetary point-of-view, the costliest operations (time, equipment required) in these steps are bonding (Step 5), thinning (Step 7), and patterning (Step 6).

It has been shown that laser cutting may result in thermally-affected regions near the cut where piezoelectric properties are lost. An alternative is the use of Abrasive Water-jet cutting (as opposed to laser-cutting and dicing), where the best kerf quality was observed [24]. No thermally-affected regions are present and complex shapes can be cut (unlike dicing, where only straight cuts are possible). Of course, this is only possible before the PZT is bonded to the Silicon wafer. This method, then, is applicable when the PZT size is large enough to handle manually ($> 2\,mm$).

SOI-based µ-valves are the simplest Si-micromachined µ-valves that can be fabricated. They consist of a valve-membrane (device layer), valve-seat (handle-layer), and an initial separation that is defined by the buried-oxide (BOX) layer. Assuming that the valving is achieved using an SOI µ-valve, the µ-actuator must be able to force the valve-plate against the valve-seat after displacing the valve-plate across the initial separation. Assuming a BOX-thickness of 2µm, we would need a µ-actuator that has a stroke greater than 2µm to ensure proper sealing. COMSOL studies have been conducted that prove the feasibility of a Bulk-PZT µ-actuator as a viable research project. Note that the unimorph can be fabricated using different substrate materials like steel. This means that Si-micromachining is not the only option to construct the microvalve. In fact, high resolution 3D-printing is a viable option to manufacture a µ-channels that are then integrated with a steel unimorph. This would greatly decrease the cost and time required in comparison to Si-micromachining.

2.6 Selection of a Microvalve

To aid in easy selection of a RoI, the following table has been constructed. The distinguishing characteristics attempt to encompass the entire process of the project – from design to testing. The cost of the project is measured coarsely using $-symbols.

Table 4: Comparison of identified Regions of Interest

Characteristics	Dielectric EAP µ-valve	Vacuum-collapsed µ-valve	Piezo unimorph µ-valve
Design Freedom	• Material choices – Many • Pre-stretching methods – Few • Design of actuator – Mostly a membrane actuator • Simulation – Hard to simulate and verify designs	• Vacuum-collapse chamber - Circular, toroidal • Valve configuration – High design freedom	• Low design freedom – Membrane actuator is the only option available
Fabrication	• Will require wafer-bonding and alignment • Membrane pre-stretching is complicated • Material procurement will be expensive and comprehensive testing is required	• Mainly involves parylene vacuum-deposition, some metal sputtering, some Si wet-etching • Many masks required, 10 photolithography steps, might require 1-2 months to fabricate one batch	• Large freedom in deciding cutting, bonding, and thinning methods • Dimensions are in the mm-scale, so manual handling is possible
Actuation	Electrostatic: Extremely high voltages required (1-4kV) Deformation: 50µm at 4kV [34]	Pneumatic: Cheaply available and controllable Electrostatic and Piezoelectric membranes possible, not pursued in current time-frame Deformation: < 6 µm required	Novel bulk-PZT piezoelectric actuation method is used. Deformation: < 5 µm required
Estimated Fluid working conditions	Pressure: < 0.5 bar [34] Flow rate: - Response time: ~700ms	Pressure: < 2 bar [35] Flow rate: 2.5ml/min air at 0.07 bar Response time: ~40ms	Pressure: < 2 bar (according to COMSOL) Flow rate: 25 g/h N_2 at 1 bar [18]
Simple Cost Comparison [$-$$$]	**$$** (Requires procurement of materials, extensive testing time, fabrication time, high-voltage power supply)	**$$$** (Many masks required so high mask cost, long machine time during fabrication, pneumatic components)	**$** (piezoelectric plate is available, AWJ/laser cutting is free, comparatively little fabrication time, bonding adhesives are the primary expense)
Potential for future use	Low potential as high-voltages are not preferred and not portable	Medium potential as parylene is currently not widely used in µ-fluidics	High potential due to wide-spread requirement of mm-scale piezo µ-actuators

Table 4 clearly shows the advantages and disadvantages of each RoI. The EAP microvalve requires high voltages to operate and this is its greatest disqualifier. The Vacuum-collapse μ-valve, though novel, requires great effort to realize. It might also not be feasible to explore electrostatic or piezoelectric actuation principles within the given time-frame. The expense involved, and fabrication time required are its greatest disqualifiers. The Bulk-PZT μ-valve is straightforward to fabricate, requires cheap or available components, and does not require many complex fabrication steps to achieve.

It appears that the most important practical characteristics are the cost and fabrication. It is evident that the third RoI, the Piezo unimorph μ-valve is the best choice to explore in this thesis. Not only is it economical to work on this RoI, it also has the highest potential for future use.

2.7 Target Specifications

To formalize this study, the following target specifications (TS) are stated. The specifications are used as a general guideline to aid in quantifying the results from this thesis and are not rigid requirements that need to be satisfied to prove the concept.

Table 5: Microvalve Target specifications

Specification	Target value [45]
Flow range	0 - 100 µL/min (liquids), 0 - 100sccm (gases)
Flow control resolution	0.1 µL/min (liq), 0.1 sccm (gas)
Leakage	$< 10^{-6}$ mbar L/s He
Max. differential pressure	≥ 1 bar
Static power consumption	< 10 mW
Typical response time	< 5 ms
Dimensions	$< 5 \times 5 \times 2$ mm^3

Goal: Design and fabricate a proportionally-controlled microvalve actuated by a unimorph piezoelectric actuator with a maximum inlet pressure requirement of 1 bar.

The following chapter consists of a paper that contains the primary work performed in this thesis to address the target specification.

3 Paper – A Hybrid 3D-Printed Piezoelectric Unimorph Microvalve

A Hybrid 3D-printed Piezoelectric Unimorph Microvalve

Arun Gunda

Department of Precision and Microsystems Engineering
TU Delft, Delft, The Netherlands
a.gunda@student.tudelft.nl

Abstract—**Microvalves are important flow-control devices in many standalone and integrated microfluidic applications. PDMS-based (Polydimethylsiloxane) pneumatic microvalves are the most commonly used type for research purposes, but they require large peripheral connections and cannot be used for controlling gases due to the high gas permeability of PDMS. There are many alternatives found in the literature that use Si-based microvalves, but variants that can throttle even moderate pressures ($1\,\mathrm{bar}$) tend to be bulky (cm-range) or consume high power. This paper details the development of a low-power, normally-open piezoelectric microvalve to control flows with a maximum driving pressure of $1\,\mathrm{bar}$, but also retain a small effective form-factor of $5\,\mathrm{mm} \times 5\,\mathrm{mm} \times 1.8\,\mathrm{mm}$. A novel combination of rapid prototyping methods like stereolithography and laser-cutting have been used to realize this device. The maximum displacement of the fabricated microactuator was measured to be $8.5\,\mu\mathrm{m}$ at $150\,\mathrm{V}$. The fabricated microvalve has a flow range of 0 - $90\,\mu\mathrm{L}\,\mathrm{min}^{-1}$ at $1\,\mathrm{bar}$ inlet pressure. When fully closed, a leakage of $0.8\,\%$ open-flow was observed with a power-consumption of $37.5\,\mu\mathrm{W}$. A flow resolution of $0.2\,\mu\mathrm{L}\,\mathrm{min}^{-1}$ - water was measured at $0.5\,\mathrm{bar}$ pressure.**

I. INTRODUCTION

The need for techniques that more efficiently utilize chemical and biological reagents in chemical analysis systems led to the introduction of micro-total analysis systems (μTAS) [1]. The versatility of miniaturizing fluidics was realized and subsequently utilized in applications like drug-delivery [2], micro- and nano-spacecraft thermal cooling and propulsion systems [3], and lab-on-a-chip devices [4].

An essential component in integrated microfluidic devices is the microvalve. In conjunction with a pressure source, it is used to control, direct, or regulate the pressure or flow rate of media within these microfluidic circuits. Valves that operate in the μm- to cm- length scales are generally classified as microvalves and they are usually fabricated using microfabrication techniques like (soft-)lithography, etching. Conventional microvalves contain a flow-channel that is obstructed by an active/passive element.

Active microvalves, as opposed to their passive counterparts, have a controllable element within the device. These valves are usually classified by the working principle of the active element. One of the first reported microvalves used an electromagnetic solenoid actuator to control the separation between a valve-membrane and inlet-orifice [5]. A valve membrane or valve plate has since been one of the most used valving mechanisms to control fluid flow, with large variations in the actuation scheme. Principles like electrostatic actuation [6], piezoelectric actuation [7], pneumatic actuation [8], and thermopneumatic actuation [9] have been used with varying degrees of success.

Each actuation principle has one or more unique disadvantages that prevent a single scheme to become widely adopted. For instance, scaling laws prevent the wide-spread adoption of electromagnetic micro-actuators as has been seen in macro-scale applications. The low-force and low region-of-influence characteristics of electrostatics prevent their use in high-pressure, high-stroke microvalving applications. Pneumatic actuation is the most used method in polymer-based microvalves (eg., Polydimethylsiloxane), but it requires a bulky pressure source and pressure control elements. Thermo-pneumatic microvalves consume a lot of power and are prone to wear and subsequent failure due to extensive thermal cycling.

Piezoelectric Micro-Electromechanical Systems (pMEMS) are a growing field of research due to the high power-density and low power requirement of piezoelectric materials like Lead Zirconate Titanate (PZT), and the possibility to manufacture high-sensitivity thin-film PZT MEMS sensors [10]. However, high-quality thin-film PZT is hard to obtain due to strict stoichiometry and high thermal processing conditions. They also require many fabrication steps and expensive, specialized equipment to manufacture.

In this work, an active proportional microvalve was designed, fabricated and characterized based on a piezoelectric actuation method that uses a commercially available PZT-5H plate as the active element. As the active element works without any processing, all the advantages of piezoelectric actuation were retained while the manufacturing disadvantages were eliminated. The valve deflection was controlled by applying a desired voltage across the piezoelectric material. Thus, the fluid flow-rate in the microvalve was proportionally controlled. The following sections detail the design, optimization, fabrication, and characterization of the microactuator and the microvalve.
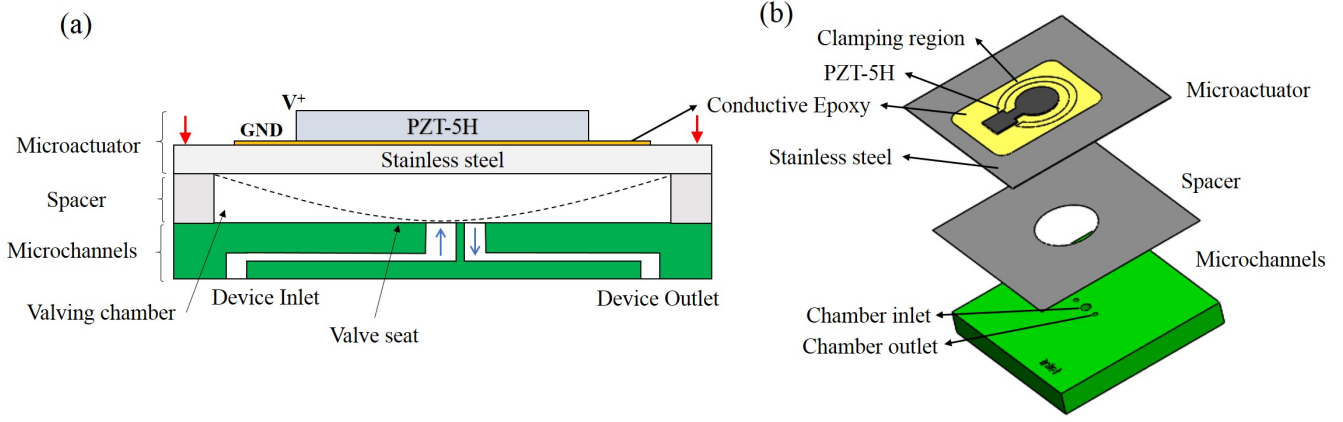
Fig. 1: (a) Schematic of the microvalve: It consists of a piezoelectric unimorph microactuator, a spacer, and 3D-printed microchannels. The microactuator is placed on top of the microchannels with an intermediate spacer and the entire assembly is clamped. Red arrows indicate the direction of the clamping force. Black dashed lines indicate the membrane deformation when actuated. (b) Exploded 3D view of the microvalve.

II. MATERIALS AND METHODS

A piezoelectric microvalve with a small footprint of $5\,\text{mm} \times 5\,\text{mm} \times 1.8\,\text{mm}$ that can withstand a pressure of $1\,\text{bar}$ and compatible with both liquids and gases was developed in this work. As shown in Fig. 1, the piezoelectric actuator modulates the flow-rate in the microvalve by closing the inlet orifice upon actuation. The fabrication approach that was used is a hybrid-integration method, using a combination of 3D-printing, laser-machining and epoxy-bonding to achieve the desired device. No microvalve was found in the literature that uses this combination of rapid prototyping methods and piezoelectric actuation mechanism.

As shown in Fig. 1, a thin PZT plate was laser-cut to the desired shape and was glued with conductive epoxy to a stainless steel (SS) foil to form a unimorph piezoelectric microactuator (UPM). A detailed study of the microactuator is given in Sec. II-A. The microchannels are printed using stereolithography, a 3D-printing technique that uses UV-light to selectively polymerize a UV-sensitive resin layer-by-layer. The spacer in the middle defines the initial separation between the actuator membrane and valve seat. A detailed explanation of the microchannels and spacer is given in Sec. II-B. In this work, the entire assembly needs to be clamped for the microvalve to function as designed. This means that a clamping holder is required. Many bonding techniques exist to permanently bond the constituents parts, but they were not explored due to time constraints [11].

A. Microactuator

A unimorph piezoelectric microactuator (UPM) has been designed and fabricated. A unimorph refers to an actuator that has an active layer that is bonded to a passive substrate. Deformation of the active layer due to electrical stimulus
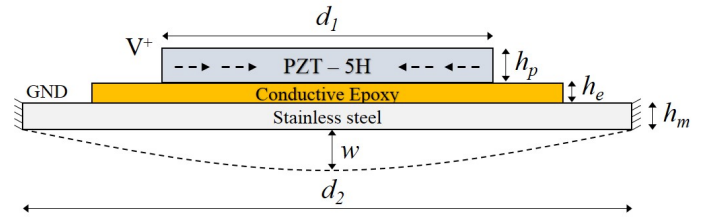

Fig. 2: Schematic of the piezoelectric unimorph microactuator: Design parameters are the PZT diameter (d_1), PZT thickness (h_p), epoxy thickness (h_e), steel membrane diameter (d_2), and thickness (h_m). Positive (V^+) and ground terminals are indicated.

causes a bending stress in the passive substrate. In this work, the active piezoelectric layer was Lead Zirconate Titanate (PZT-5H, Piezo Systems T105-H4E-602) and the passive layer was a stainless steel plate (Jeveka H+S 0.05mm flat sheet). The PZT-5H plate was provided with vacuum-deposited nickel electrodes on both sides. An Optec Micro laser-etching machine was used to laser-cut the PZT. The laser parameters used are provided in the supplementary paper.

The active and passive layers were bonded using conductive epoxy (CircuitWorks CW2400). A thin layer of epoxy was applied onto the steel membrane using a $20\,\mu\text{m}$ Jeveka shim-steel stencil. The PZT part was then gently pressed to ensure good contact. The assembled UPM was then cured at $75\,°\text{C}$ in a furnace for twenty minutes. The fabrication process is shown in the supplementary paper. The epoxy should be conductive to transfer the PZT bottom terminal to the stainless steel. The steel membrane was then clamped along its circumference and the piezoelectric layer was subjected to an electric field along its poling direction.

Due to the inverse piezoelectric effect, the active layer exhibits inward lateral deformation (dashed arrows in Fig. 2). This causes a bending moment that forces the stainless steel membrane downwards. In this case, the transverse displacement of the steel membrane was amplified by a factor of ≈ 10 with respect to the free lateral motion of the PZT.

The main design parameters of the UPM are shown in Fig. 2 and the optimized values for these parameters are given in Table II. The objective function that was maximized is the central displacement of the UPM. The analytical and numerical formulation of the UPM behaviour are provided in the following sections.

1) Analytical formulation: The deflection of a UPM where the two layers have unequal diameters ($d_1 < d_2$ from Fig. 2) was derived by *Mo et al* [12]. Eq. 1 shows the relationship between the downward displacement of the membrane (w), and the parameters of the unimorph (Fig. 2) [12]. These parameters are given in Table. I. Note that a lateral dimensional constraint of $5\,\text{mm} \times 5\,\text{mm}$ was assumed to provide a starting point. The primary control variables are the PZT layer dimensions.

TABLE I: Microactuator parameters

Material	Parameter	Symbol	Value
PZT	Young's Modulus	E_{11}	$62\,\text{GPa}$
	Compliance constant	S_{11}^E	$1/E_{11}$
	Piezoelectric constant	d_{31}	$-350 \times 10^{-12}\ \text{m V}^{-1}$
	Poisson's ratio	ν	0.31
	Thickness	h_p	**To be optimized**
	Radius	r_1	**To be optimized**
	Polarization field	E_p	$1.5 \times 10^6\ \text{V m}^{-1}$
	Voltage	V	$0 \leq V \leq E_p \times h_p$
Steel	Young's Modulus	E_m	$193\,\text{GPa}$
	Compliance constant	S_m	$1/E_m$
	Thickness	h_m	$\geq 50\,\mu\text{m}$
	Radius	r_2	$\leq 2.5\,\text{mm}$
Adhesive	Young's Modulus	E_e	$760\,\text{MPa}$
	Poisson's ratio	ν_e	0.3
	Density	ρ_e	$2440\,\text{kg/cm}^3$
	Thickness	h_e	**To be optimized**

The maximum voltage that can be applied to the UPM is given in the table above. This is the potential that was applied during poling of the material by the manufacturer. Increasing the voltage beyond this can degrade PZT behaviour.

$$w(r) = \begin{cases} \dfrac{C_1\left\{2r_1^2\ln\left(\frac{r_1}{r_2}\right) + \left[1 - \left(\frac{r_1}{r_2}\right)^2\right]r^2\right\}V}{C_2 - C_3\left(\frac{r_1}{r_2}\right)^2 + \frac{1}{2}h_p^4 S_m^2(1+v)\left(\frac{r_1}{r_2}\right)^4} \\ \qquad\qquad r \leqslant r_1 \\[2ex] \dfrac{C_1\left\{2r_1^2\ln(r) - r_1^2[2\ln(r_2)-1] - \left(\frac{r_1}{r_2}\right)^2 r^2\right\}V}{C_2 - C_3\left(\frac{r_1}{r_2}\right)^2 + \frac{1}{2}h_p^4 S_m^2(1+v)\left(\frac{r_1}{r_2}\right)^4} \\ \qquad\qquad r_1 < r \leqslant r_2 \end{cases} \quad (1)$$

where
$C_1 = 3d_{31}h_m S_{11}^E S_m (h_m + h_p)$
$C_2 = 4S_{11}^E h_p h_m^3 S_m + 6S_{11}^E h_m^2 h_p^2 S_m + 4S_{11}^E h_m h_p^3 S_m$
$\qquad + \frac{1}{2}h_p^4 S_m^2(1+v) + \frac{2h_m^4 S_{11}^{E^2}}{1+v}$
$C_3 = 4S_{11}^E h_p h_m^3 S_m + 6S_{11}^E h_m^2 h_p^2 S_m + 4S_{11}^E h_m h_p^3 S_m$
$\qquad + h_p^4 S_m^2(1+v)$
$\qquad\qquad\qquad\qquad\qquad\qquad\qquad (2)$

where $w(r)$ is the transverse displacement of the membrane along the radius r.

It was desirable in this work to maximize the central displacement of the actuator. A parametric study was performed using Eq. 1 to determine the optimal combination of parameters to obtain highest displacement. Note that the adhesive layer is ignored in the above formulation. To determine whether it plays a large role in the obtained displacement, a numerical study was performed.

2) Numerical formulation: COMSOL Multiphysics ®(v5.3) was used to simulate the UPM. A 2D-axisymmetric model with the Piezoelectric Devices module was used to conduct Stationary and Eigenfrequency studies. The material properties and initial dimensions used are given in Table. I. The full COMSOL model is shown in greater detail in the supplementary paper. The adhesive thickness and material properties are additional parameters in the numerical optimization.

The maximum force that a piezoelectric actuator can apply is called the blocking force. The actuator exhibits zero displacement in this state. It is calculated as:

$$F_b = k_{mem} \times x_{act} \qquad (3)$$

where k_{mem} is the membrane stiffness, x_{act} is the central displacement of the actuator when fully actuated (maximum operating voltage) without any load, and F_b is the blocking force.

B. Microchannels and spacer

The microchannel part plays two primary roles: it allows interfacing with the macro-world and provides the base for the valving chamber with inlets and outlets. The former means that there are orifices in the microvalve structure that are far enough apart to interface with external microfluidic connections, and the latter means that a flat valve-seat with small ($\leq 500\,\mu\text{m}$) and accurate chamber orifices is realizable. A 3D-model and a schematic of the microchannels are shown in Fig. 3.

To obtain such a finely machined part, a desktop stereolithography (SLA) printer (Envision-TEC GmbH. Micro Plus Hi-Res) was used. An XYZ resolution of $30\,\mu\text{m} \times 30\,\mu\text{m} \times 25\,\mu\text{m}$ can be obtained with Envision-TEC's proprietary methacrylate/acrylate-based resin (HTM140V2M). The fabrication process involves preliminary UV-curing of the desired device in the SLA printer, ultrasonication of the part in
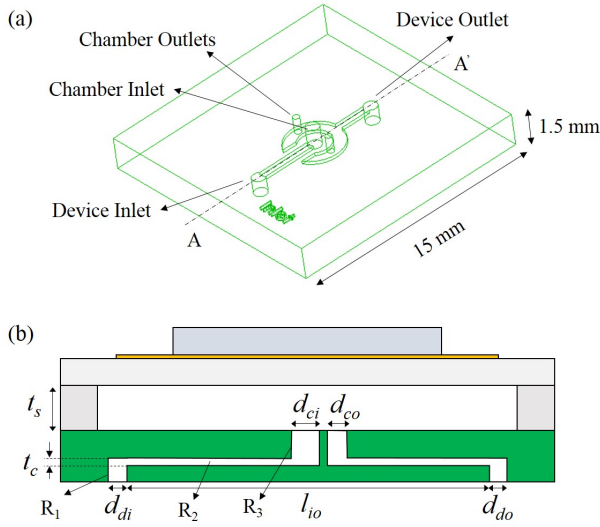
Fig. 3: (a) Transparent view of the microchannels: Internal channels are visible. The microchannel part is large (15 mm) to enable easy manual handling. (b) Cross-section of microchannels along A-A' with spacer and microactuator: Design parameters are spacer thickness (t_s), device inlet diameter (d_{di}), device outlet diameter (d_{do}), distance between device orifices (l_{io}), chamber inlet diameter (d_{ci}), chamber outlet diameter (d_{co}), internal channel thickness (t_c). Static resistances are represented as R_i.

Isopropyl Alcohol (IPA) to remove uncured resin, and a final curing step in a UV oven to fully polymerize the part.

The spacer was laser-cut to shape using the same laser cutter as used above. As the spacer thickness decides the valving-chamber height, a very thin machinable material is required. If the thickness is too large ($\geq 10\,\mu\text{m}$), the microactuator might not be able to close the inlet. For this purpose, $3\,\mu\text{m}$, $5\,\mu\text{m}$, or $8\,\mu\text{m}$ thick Jeveka shim-steel can be used. They can be machined using the laser-cutter with minimal warping. Laser parameters are given in the supplementary paper.

The microchannel design parameters given in Fig. 3 were optimized for one objective: minimization of dimensions while maintaining manufacturability. This was so that static resistance of the hydraulic circuit was maximized. Increasing static resistance provides greater control over the flow [13]. An important concern with making internal structures in an SLA printer is the removal of uncured resin from the channels during ultrasonication. Too small a channel can prevent removal of resin, which can then block the channel permanently during the final curing step. An experimental study using different internal channel and chamber orifice dimensions was performed to determine the smallest dimensions realizable using the available SLA printer (Table. IV).

The flow through the microvalve can be analytically and numerically estimated. This was used to determine parameter values that result in flow-rates that could be measured with the available equipment. Too high a flow-rate will result in saturation of the flow-sensor and too low a flow-rate cannot be detected (see Sec. II-D for flow-sensor details). It was expected that the valving chamber would be the greatest source of hydraulic resistance due to its low height ($t_s << t_c$ in Fig. 3). As the spacer thickness determined the height of the chamber, it could be optimized with the formulations shown in the following sections.

1) Analytical formulation: An electrical analogy is best suited for calculating flow-rates in microfluidic circuits. In such an analogy, the pressure differential is similar to potential difference, fluid flow is similar to current, and the drag or pressure drop due to the wetted path is similar to electrical resistance. Also, high pressures can deform channels and cause flow-rate to increase. This is modelled as a capacitance. In this case, capacitance is neglected due to its low influence.

All the channels were modelled as static resistances and the valving chamber was modelled as a variable resistance [13]. Rectangular and circular channel resistances are shown in Eq. 4 and 5 respectively.

$$R_{sr} = \frac{12l\mu}{wh^3(1 - 0.63\frac{h}{w})} \tag{4}$$

$$R_{sc} = \frac{8\mu l}{\pi r^4} \tag{5}$$

where μ is the dynamic viscosity, l is channel length, w is rectangular channel width, h is channel height, and r is circular channel radius.

The variable chamber resistance is:

$$R_{var} = \frac{6\mu \ln \frac{a_2}{a_1}}{\pi s^3} \tag{6}$$

where a_1 is chamber inlet radius, a_2 is valve seat radius ($\approx 5a_1$), and s is the chamber height (= spacer thickness, t_s).

Based on the channel configuration, channel resistances can be added up to obtain the total static resistance R_s. The flow-rate Q is then calculated as:

$$Q = \frac{\Delta P}{R_s + R_{var}} \tag{7}$$

where ΔP is the pressure differential.

A more accurate numerical flow-model including all the geometric features of the microchannels was made. This is briefly explained in the following section.

2) Numerical formulation: A 3D-study using the Laminar Flow physics in COMSOL Multiphysics ®(v5.3) was used to simulate the flow. Due to the high computational power
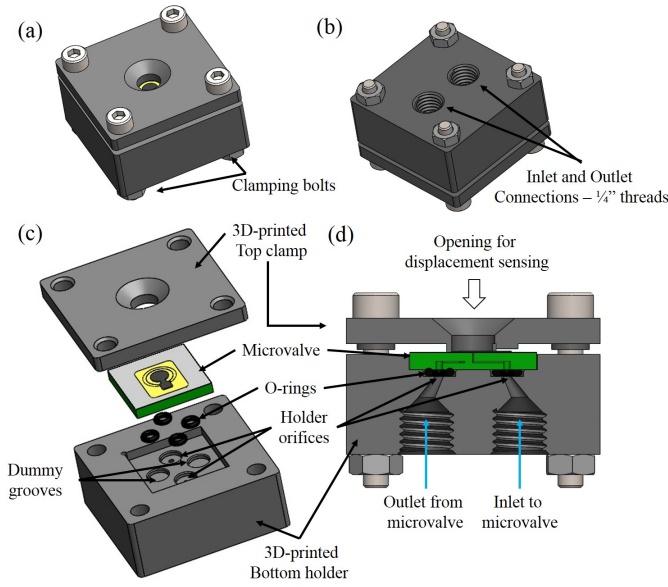
Fig. 4: (a) Top isometric view of the microvalve in its 3D-printed holder. An opening is provided on top to allow displacement sensing (b) Bottom isometric view of the microvalve holder with 3D-printed threads for enabling microfluidic connections to the macro-world (c) Exploded view of the microvalve holder (d) Cross-section of the assembled microvalve holder.

required to run this model, the results obtained were mainly used to validate the analytical model.

Water at standard temperature was used as the medium. Pressure constraints were used as inlet and outlet conditions. To ensure convergence, a boundary layer mesh with high density was used at the valving chamber. The COMSOL model is explained in greater detail in the supplementary paper.

C. Device holders

The UPM and the microvalve had to be clamped and interfaced to testing rigs for characterization. Two special holders were built to enable quick and temporary connections. The UPM holder is shown in the supplementary paper and the microvalve holder is detailed below.

The microvalve holder is required for the main flow measurements conducted in this work. The holder was 3D-printed using a Prusa Mk2 Multi Material 3D printer with grey Polylactic Acid (PLA) filament. A 30% hexagonal infill was found to be acceptable in both printing speed and product rigidity. A 50 μm vertical resolution can be obtained with this printer but the 100 μm setting was used to decrease printing time.

It had two primary purposes: to provide clamping force to the UPM membrane and to enable interfacing between the microvalve and microfluidic circuit. The clamping force was achieved with a knife-edge clamping surface. Microvalve interfacing requires a leakage-proof connection. For this, O-rings (Ebele Viton $1.5\,\text{mm} \times 1\,\text{mm}$ O-rings) were used with recesses designed in the holder. The microfluidic circuit interfacing was done by incorporating 1/4" threaded ports into the design. Elveflow 1/4"-28 TPI microfluidic connectors were used to connect the holder to the rest of the microfluidic circuit as detailed in Sec. II-D.

D. Experimental setup

The main experiments that were conducted are related to the central displacement of the microactuator and the flow rate controlled by the microvalve. The three experimental setups used to do so are detailed below.

1) **Microactuator - Static measurement:** The static displacement of the microactuator can be measured using the test-setup shown in Fig. 5, with the microvalve replaced with the UPM (in its holder). The fluidic connections are not required. The UPM was controlled by a high-voltage, current-limited, programmable DC power-supply (Delta Elektronika ES0300-0.45). A voltage resolution of 0.5V can be obtained using the programmable interface and a maximum voltage of $300\,\text{V}$ can be applied. The current was limited to $1\,\text{mA}$ for safety. The central displacement of the UPM was measured using a high-resolution laser displacement sensor (Keyence LC-2420 sensor-head with a Keyence LC-2400W laser displacement meter). The sensor head has a resolution of $0.01\,\mu\text{m}$ and a working range of $\pm 200\,\mu\text{m}$. The sensor-head was mounted on a stiff Z-stage for easy adjustment. Command signals to the voltage-source and measurement signals from the displacement sensor were routed through a data-acquisition device (National Instruments NI-DAQ USB-6211) to a computer. The control program was made using Python (2.7) and is given in the supplementary material.

2) **Microactuator - Dynamic measurement:** Frequency response curves (FRC) have been obtained using a Polytec PSV-400 scanning laser doppler vibrometer. In this experiment, a low voltage pseudo-random signal (1 V) was used to excite the actuator. The eigen-frequency of the actuator can be obtained from the FRC and compared to numerical results. Stiffness of the membrane can be calculated using its eigen-frequency with the following equation:

$$k_{mem} = \omega_{mem}^2 \times m_{mem} \tag{8}$$

where m_{mem} is the mass of the membrane, and ω_{mem} is the measured eigen-frequency in rad s^{-1}.

3) **Microvalve - Fluidic measurement:** The main characterization of the microvalve is done using this experimental setup. The layout of the setup is shown in Fig. 5. The microvalve is connected to a microfluidic circuit consisting of a pressure source (Elveflow OB1 Mk3+) which can apply pressure from $-1\,\text{bar}$ to $6\,\text{bar}$, and a thermal flow-sensor (Elveflow MFS3)
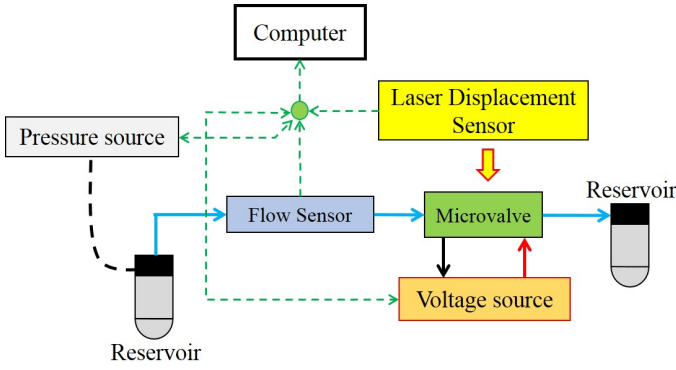
Fig. 5: Layout of the test set-up for measuring flow-rate and displacement of the microvalve: Green dashed arrows are signal wires, red and black arrows are terminal wires of the microvalve, blue arrows are microfluidic tubing, and the black dashed line is tubing from the pressure source.

which can measure a maximum flow-rate of $90\,\mu\mathrm{L\,min^{-1}}$ (accuracy: 5% measured value). The microvalve structure must be optimized such that the flow-rate at maximum pressure is within the range of the flow-sensor.

A similar setup to that shown in Sec. II-D1 is replicated to apply voltage to the actuator and measure its displacement. Control signals to the pressure source and measurement signals from the flow-sensor are routed directly to a computer via USB using Elveflow's software development kit (SDK). A Python (v2.7) program is used for the overall control of this setup.

III. RESULTS

The results are detailed in the following order: design optimization, fabrication results, actuation behaviour, and valving behaviour.

A. *Design Parameter Optimization*

The microactuator was optimized for maximum central displacement and the microvalve was optimized such that the static resistance is maximum and the flow rate was in range of the flow-sensor. They are discussed separately in the following sections.

1) Microactuator optimization: In this work, $50\,\mu\mathrm{m}$ thick steel was ùsed as it has sufficient stiffness for manual handling but much lower stiffness than similar substrates used in literature [14, 15]. The lateral dimensions were constrained to $5\,\mathrm{mm} \times 5\,\mathrm{mm}$, thereby limiting the steel membrane diameter (d_2 in Fig. 2) to $5\,\mathrm{mm}$. The remaining parameters to optimize were the PZT thickness, PZT radius, and adhesive thickness.

The analytical formula given in Sec. II-A1 was used to obtain a heat-map of the central displacement and is shown in Fig. 6 (a). The optimal set of values was obtained using Matlab's *fmincon* optimizer. Similar numerical results are shown in Fig.
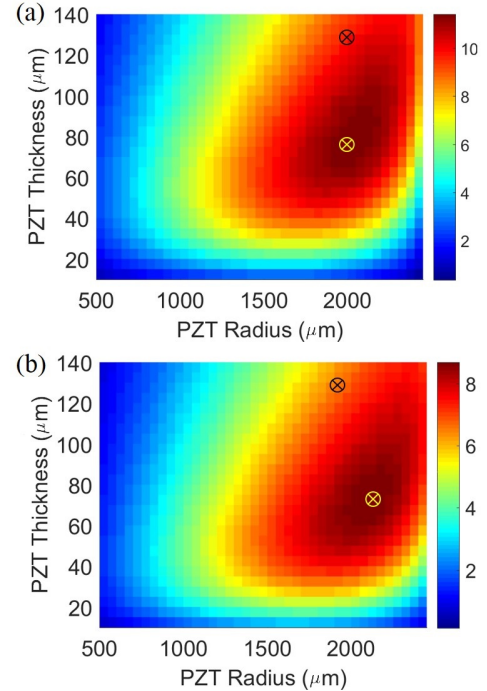

Fig. 6: (a) Central displacement plotted for different PZT parameters using the analytical formulation (b) Central displacement plotted for different PZT parameters using the numerical simulation (adhesive was not considered). Yellow crosses are optimal parameters, black crosses are fabricated parameters.
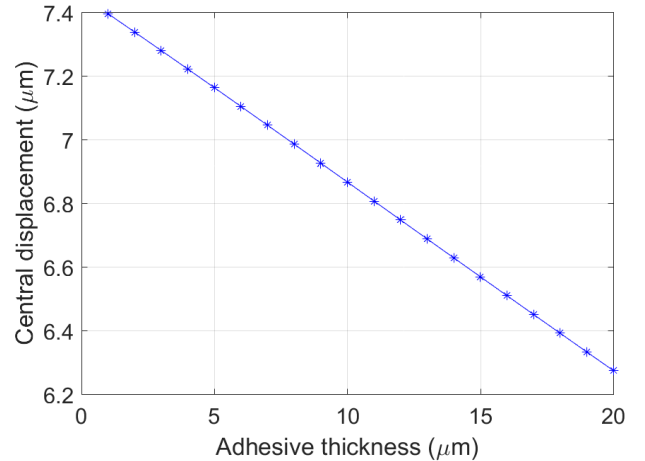

Fig. 7: Dependence of Microactuator displacement on Adhesive Thickness: PZT Radius = $2\,\mathrm{mm}$, PZT Thickness = $127\,\mu\mathrm{m}$, Voltage = $190\,\mathrm{V}$.

6 (b). An in-built COMSOL Optimization study was used to obtain the optimal dimensions. The results are tabulated in Table. II. The adhesive layer was not considered in this case.

The optimal dimensions for the PZT were obtained and the adhesive layer was introduced. The central displacement with

TABLE II: Microactuator Design Parameters

Parameter	Analytical	Numerical	Fabricated
PZT diameter (d_1)	$4\,\text{mm}$	$4.2\,\text{mm}$	$4\,\text{mm}$
PZT thickness (h_p)	$76\,\mu\text{m}$	$68\,\mu\text{m}$	$127\,\mu\text{m}$
Epoxy thickness (h_e)	-	$< 5\,\mu\text{m}$	$< 15\,\mu\text{m}$
Membrane diameter (d_2)	$5\,\text{mm}$	$5\,\text{mm}$	$5\,\text{mm}$
Membrane thickness (h_m)	$25\,\mu\text{m}$	$25\,\mu\text{m}$	$50\,\mu\text{m}$

varying adhesive thickness is plotted in Fig. 7.

2) Microvalve optimization: An experimental study was performed to determine the smallest microchannel dimensions that resulted in a reproducible device. The main issues encountered were clogging of the channels and bowing of the flat valve-seat surface. Clogging was solved by increasing the internal channel dimensions and bowing was mitigated by introducing supports in the channels. Failed microchannels are shown in the supplementary paper. The set of smallest manufacturable dimensions are given in Table. IV.

The static resistances of the micro-channels are tabulated in Table. III. The resistance indices are shown in Fig. 3 (b). $R_{chamber}$ refers to the static resistance of the chamber with a $5\,\mu\text{m}$ height. The chamber height is determined by the spacer thickness.

TABLE III: Microfluidic resistances

Resistance	Value [Pas/m^3]
R_1	1.7×10^8
R_2	4.81×10^4
R_3	4.5×10^{10}
$R_{chamber}$	2.2×10^{13}

It is evident from Table. III that the valve chamber resistance is much higher than any other part of the circuit. Fig. 8 shows the dependence of the flow rate on the spacer thickness.
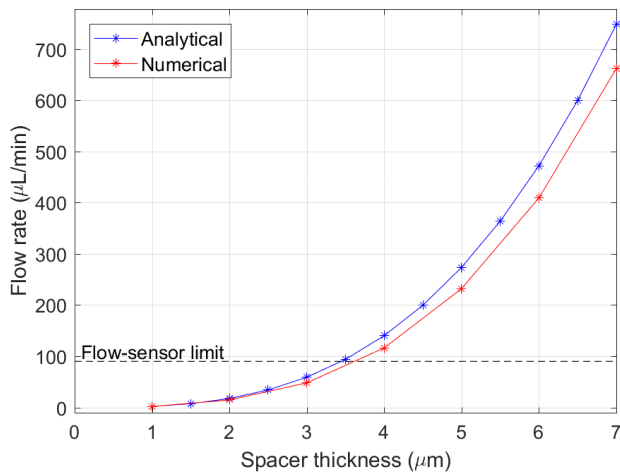

Fig. 8: Flow rate dependence on spacer thickness with a $1000\,\text{mbar}$ pressure differential

The flow sensor can measure a maximum flow rate of $90\,\mu\text{L}\,\text{min}^{-1}$. It can be inferred from Fig. 8 that the spacer

TABLE IV: Microchannel and Spacer Design Parameters

Parameter	Value
Chamber inlet dia (d_{ci})	$0.2\,\text{mm}$
Chamber outlet dia (d_{co})	$0.2\,\text{mm}$
Internal Channel thickness (t_c)	$0.2\,\text{mm}$
Internal Channel width	$0.2\,\text{mm}$
Distance b/w device orifices (l_{io})	$8\,\text{mm}$
Device orifice dia (d_{di}, d_{do})	$0.8\,\text{mm}$
Spacer thickness t_s	$5\,\mu\text{m}$

must be $\approx 3.5\,\mu\text{m}$ thick to be able to measure the flow rate at $1\,\text{bar}$ using this flow sensor. The thinnest shim-steel that was available was $5\,\mu\text{m}$ thick, which means that there will be a maximum flow rate of $\approx 260\,\mu\text{L}\,\text{min}^{-1}$ at $1000\,\text{mbar}$. Tightening the bolts in the valve-holder caused a small decrease in the chamber height by pushing the spacer into the microchannel part.

B. Fabrication Results

The fabricated devices shown below correspond to those discussed in Sec. II and are introduced in the same order.

1) Microactuator: A top-view of the microactuator is shown in Fig. 9. The PZT part consists of a circular actuation section that is connected to a square pad. The top terminal wire was placed on the pad and then forced down to ensure connectivity by the UPM holder.
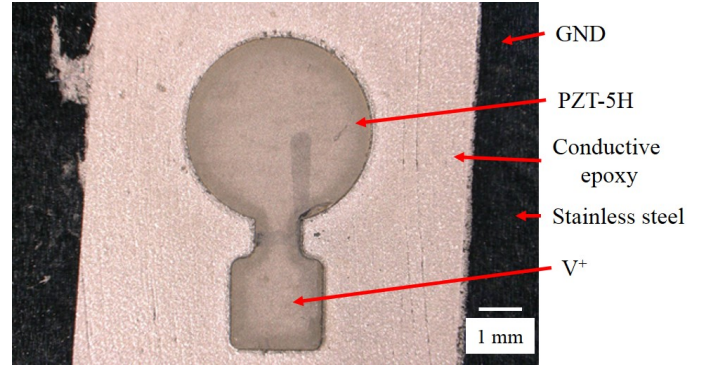

Fig. 9: Fabricated microactuator with a laser-cut PZT part bonded to a stainless steel membrane using conductive epoxy. Positive (V^+) and Ground (GND) terminals are indicated. Wires were attached using conductive tape (bottom terminal) and a press-fit (top terminal).

The surface profile of the microactuator was measured using a Bruker Contour Elite-K White Light Interferometer to determine the adhesive thickness. It was found that the thickness varied from $3\,\mu\text{m}$ to $15\,\mu\text{m}$ as the epoxy application was done manually.

2) Microchannels: The optimal design parameters given in Table. IV were used to fabricate the microchannels shown in Fig. 10. As the material is translucent, light can be shined
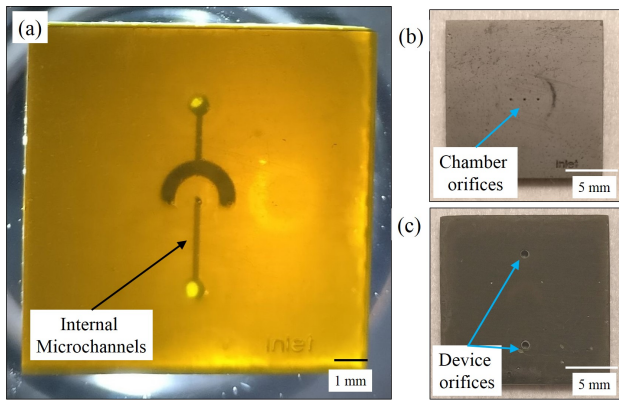
Fig. 10: (a) Microchannels with a light source underneath to illuminate the internal channels (b) Top view: Central orifice is the valve chamber inlet, neighbouring orifices are chamber outlets (c) Bottom View: Top orifice is the device inlet, bottom orifice is the device outlet, surface is sanded with 1000-grit sandpaper.
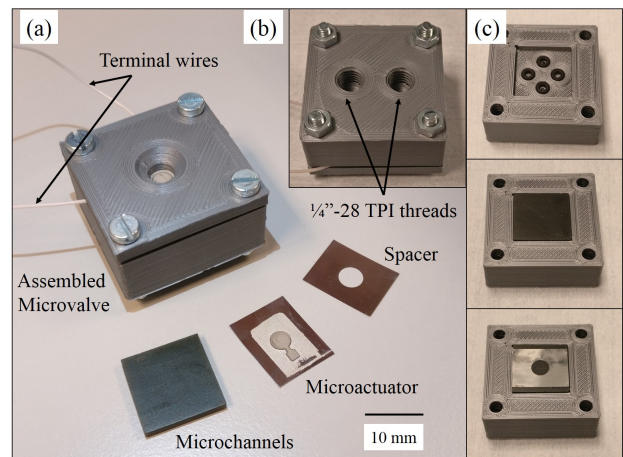

Fig. 11: (a) Assembled microvalve holder with constituent parts. Terminal wires are copper with $0.5\,\mathrm{mm}$ diameter. (b) Bottom viw of the holder (c) First step: O-rings placed in grooves, Second step: Microchannels placed in groove, Third step: Spacer placed over microchannels, Fourth step (not shown): Actuator is placed and then assembly is clamped.
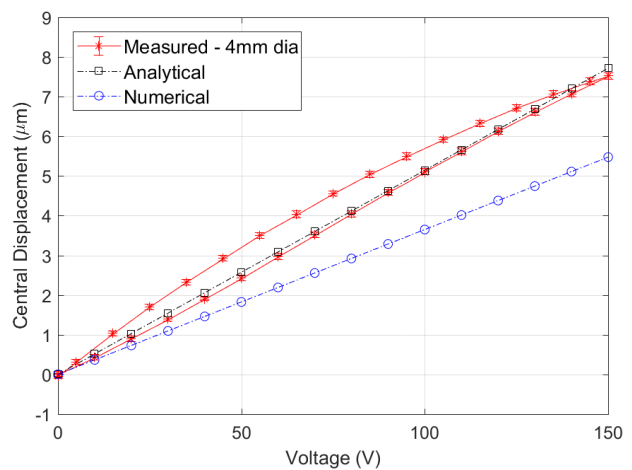
through to observe the internal channels. The faint circular scuffing around the orifices in Fig. 10 (b) shows the clamping region where the UPM was clamped.

The microchannels were initially printed with supports underneath where the device orifices were present. These supports were removed with a scalpel, and the rough surface was sanded using 1000-grit waterproof sandpaper with water as a lubricant. The sanded surface had low roughness ($R_a \approx 10\mu m$) which enabled a leakage-proof connection with the O-rings. The process is shown in the supplementary paper.

3) Device holder: The assembled microvalve holder is shown in Fig. 11 (a) along with its constituent parts. The microfluidic coupling ports are shown in Fig. 11 (b). The assembly steps are shown in Fig. 11 (c). After assembly, the microvalve was flushed with IPA and DI-water at $1\,\mathrm{bar}$ for ten minutes to remove any residue from the manufacturing processes. White residue from the sanding operation of the microchannels was the only visible impurity observed.

4) Test setup: The microvalve test-setup is shown in Fig. 22. The Z-stage was used to position the microvalve in range of the displacement sensor, and the XY-stage was used to position the center of the PZT membrane to the laser-spot from the sensor.

C. Actuation behaviour

The dimensions given in Table. II were used to manufacture the microactuator shown in Fig. 9. The UPM was clamped in a UPM holder and a voltage was applied. For a $127\,\mu m$ thick PZT plate, a maximum voltage of $190\,\mathrm{V}$ can be applied by the criteria given in Table. I. In this work, the voltage was limited to $150\,\mathrm{V}$. The measured displacement is plotted alongside the predicted displacements in Fig. 12.

Fig. 12: Comparison of measured and predicted displacement for a $4\,\mathrm{mm}$ actuator in the UPM holder: The bottom part of the red curve is measured during voltage up-sweep and the top part of the red-curve is during voltage down-sweep. Error-bars indicate one standard deviation of three measurements.

Microactuators with different PZT diameters were tested to investigate how the diameter affects displacement. The measured central displacement at $150\,\mathrm{V}$ has been plotted in Fig. 13 with the predicted values.

The frequency-response curve of a microactuator (PZT dia = $4\,\mathrm{mm}$) is shown in Fig. 14. The first natural frequency is located at $25.3\,\mathrm{kHz}$. The numerical formulation predicts a natural frequency of $26.5\,\mathrm{kHz}$. The stiffness of the membrane is found using Eq. 8. The mass of the microactuator was measured using a Scaltec SBC33 digital weighing scale with a resolution of $0.1\,\mathrm{mg}$. Once the stiffness is known, blocking
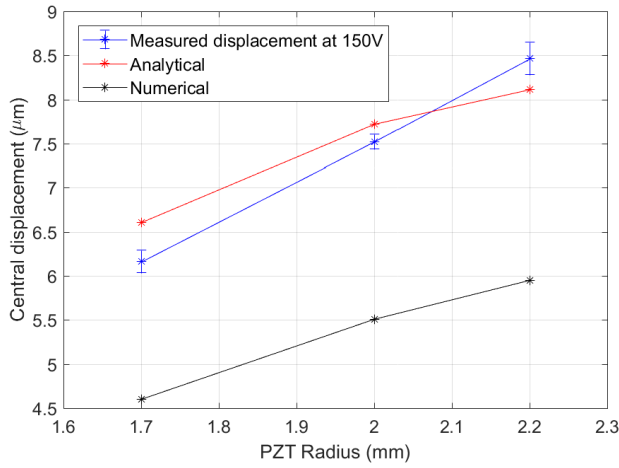
Fig. 13: Displacement of different actuators at $150\,\mathrm{V}$. The predicted displacements are plotted for comparison. Error bars indicate one standard deviation of three measurements in each sample.
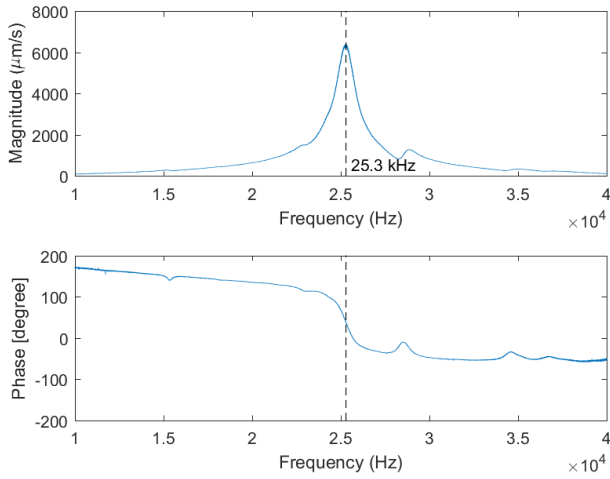

Fig. 14: Frequency response curve of a UPM (PZT dia = $4\,\mathrm{mm}$) centered around the first eigen-frequency.

force of the actuator can be calculated using Eq. 3. The results are shown in Table. V.

TABLE V: Stiffness and Blocking force calculations

Parameter	Value
Frequency ω_{mem} [kHz]	25.3
Mass m_{mem} [mg]	25
Stiffness k_{mem} [N $\mu\mathrm{m}^{-1}$]	0.63
Deflection x_{act} [$\mu\mathrm{m}$]	7.5
Blocking force F_b [N]	4.74

D. *Valving behaviour*

The validity of the analytical and numerical flow models shown in Sec. II-B1 and II-B2 need to be tested. To do so, fluid was forced through the microvalve at different pressures
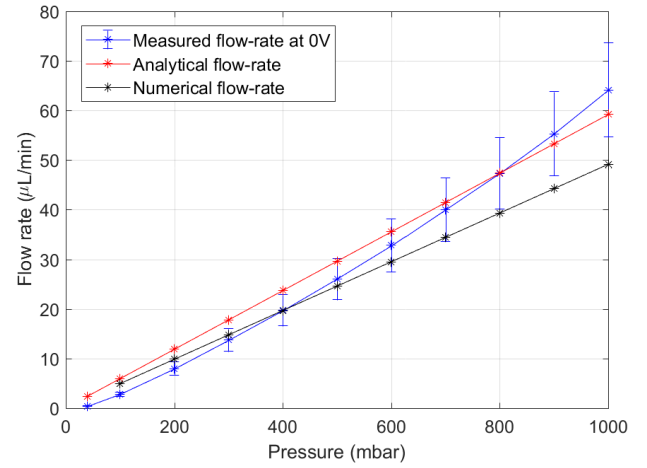

Fig. 15: Comparison of predicted and measured flow rate in the microvalve assuming a valving chamber height of $3\,\mu\mathrm{m}$.
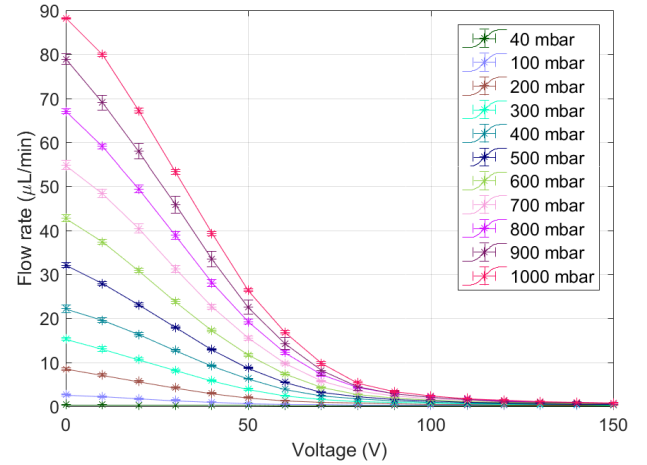

Fig. 16: Proportional control of flow rate at different pressures. Error-bars indicate one standard-deviation of three measurements.

and the measured flow rate is plotted alongside the predicted flow rate (Fig. 15). The UPM was inactive in this study. The analytical and numerical values assume a $3\,\mu\mathrm{m}$ spacer thickness (or chamber height).

The main objective of this work was to prove proportional control of fluid flow. This is shown in Fig. 16. For a set pressure, the voltage was increased from $0\,\mathrm{V}$ to $150\,\mathrm{V}$ and the flow rate was measured.

The flow rate at fully-open and fully-closed positions at different pressures are shown in Fig. 17. The overlaid leak-rate graph is the ratio of the flow rate at closed and open conditions.

Fine control of the flow rate has been shown in Fig. 18. A linear region was observed from 0 - $50\,\mathrm{V}$. Here, a flow rate change of $0.2\,\mu\mathrm{L\,min}^{-1}$ was measured for a voltage increment of $0.5\,\mathrm{V}$.
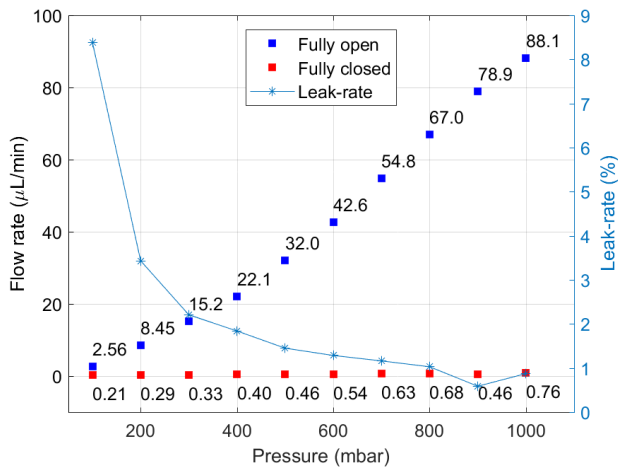
Fig. 17: On-off behaviour and leak-rate of the microvalve at different pressures: The numbers are the flow rates at those data points. Leak-rate is the ratio of closed and open flow rates.
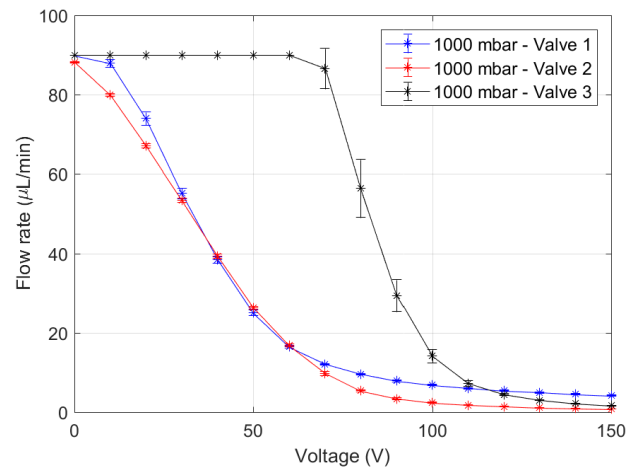

Fig. 19: Reproducibility of flow rate behaviour at $1000\,\mathrm{mbar}$ with three microvalves. The flow sensor has a limit of $90\,\mu\mathrm{L\,min^{-1}}$.
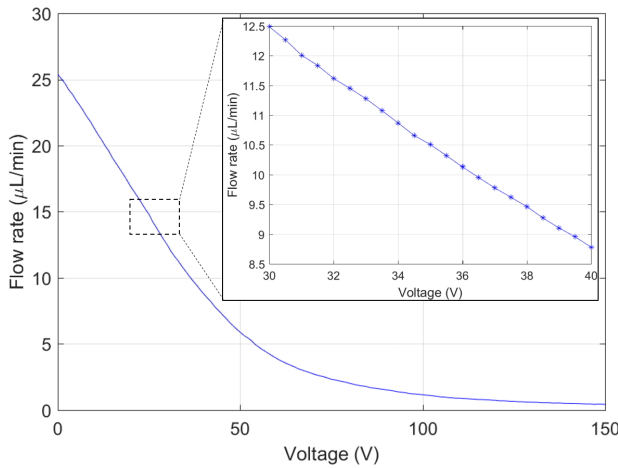

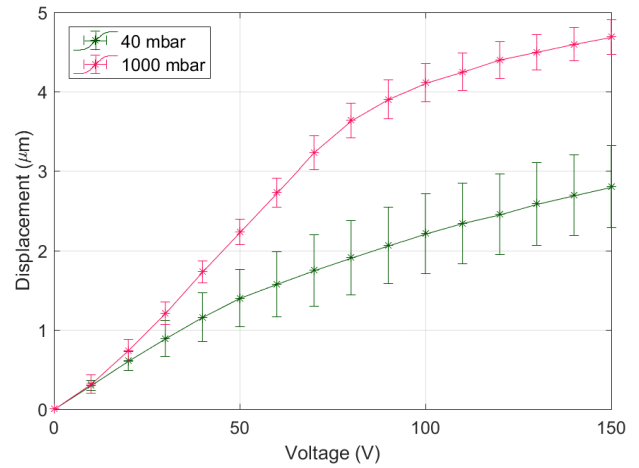Fig. 18: Fine microvalve control at $500\,\mathrm{mbar}$ pressure.

Fig. 20: Displacement behaviour of the UPM when assembled in the microvalve and the voltage is swept up.

The reproducibility of the microvalve is shown in Fig. 19. Two microvalves with different UPMs and microchannels were assembled in two different microvalve holders and their flow rate behaviour is observed. Here, a single flow rate curve at $1000\,\mathrm{mbar}$ is shown for each valve.

The displacement behaviour of the UPM when assembled in the microvalve is shown in Fig. 20. The displacement behaviour at the lowest measured pressure ($40\,\mathrm{mbar}$) and highest measured pressure ($1000\,\mathrm{mbar}$) is shown.

The UPM behaves like a capacitor. When fully charged, there should ideally be no current flowing through the circuit. This means that there is zero power consumption. In practice, there is always a small leakage current in the order of micro-Amperes due to the high internal resistance of the material. A Keithley 2400 Sourcemeter was used to measure the current flowing through the circuit at maximum load ($1\,\mathrm{bar}$) and

maximum voltage ($150\,\mathrm{V}$). A leakage current of $0.25\,\mu\mathrm{A}$ was observed. This means that a power of $37.5\,\mu\mathrm{W}$ (Power = Voltage x Current) was drawn.

The response time of the microvalve was measured by using a square wave that varied from 0-150 V. An Agilent 33220A function generator was used with an amplifier to generate the input signal. An example of the valve closing time measurement is given in Fig. 21. The closing time is defined as the time required to reach 90% of the final flow rate. As the acquisition frequency of the DAQ is not high enough, a smooth measured curve is not observed. Due to this, a sigmoidal fit has been used. Some accuracy has been sacrificed, but a repeatable estimate is obtained. A valve-closing time of $38\pm2\,\mathrm{ms}$ and valve-opening time of $41\pm2\,\mathrm{ms}$ was measured at $500\,\mathrm{mbar}$.
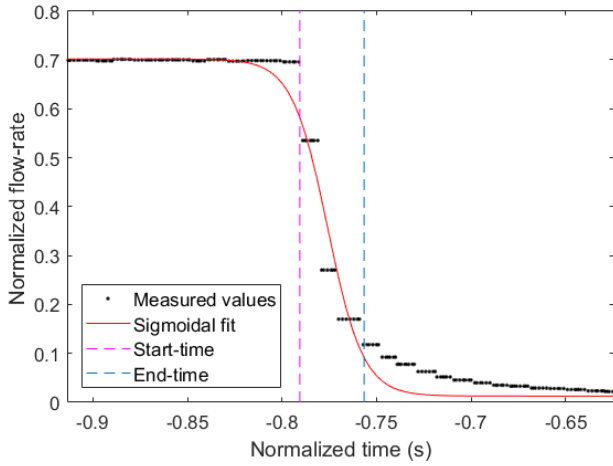
Fig. 21: Valve closing behaviour at $500\,\mathrm{mbar}$: The difference between the start and end-time is the closing time. The closing time is defined as the time required to reach 90% of the final flow rate.

IV. DISCUSSION

The results given in the previous section are discussed here in greater detail. The microactuator and microvalve are explored in different subsections.

A. *Microactuator*

1) Optimization: The microactuator was optimized to maximize its central displacement. This objective function was chosen as it was assumed that this would enable the microvalve to be operated at a lower voltage. As the size of the PZT-5H plate available was limited, it was essential that the best parameters were chosen to prevent wastage of material. To ensure this, both analytical and numerical optimization was performed.

From the displacement heat-maps given in Fig. 6, it is evident that the *shape* of the displacement distribution is the same, even though the values are different. The optima found using both methods are also very close to each other (Table. II). This shows that the underlying physics behind the derivation of the analytical formulation appears to match the numerical formulation. It was initially assumed that the measured displacement would be closer to the numerical simulation results due to its general reliability. The fabricated parameters are different due to unavailability of the required facilities to decrease PZT thickness. Two reported techniques for PZT thinning are lapping and chemical-mechanical polishing [16].

The adhesive layer does not appear to play a significant role in the deformation of the actuator as shown in Fig. 7. Nevertheless, it is preferred to keep the thickness $<15\,\mu\mathrm{m}$ thick to prevent other issues like electrical shorting, which is discussed in the following section.

2) Fabrication: The assembly process of the microactuator is highly manual, meaning that there is room to improve in reproducibility. The main step where uncertainty is introduced is during the application of epoxy to the steel membrane. Too thick an epoxy layer can not only decrease actuation (as shown in Fig. 7), it can also cause an electrical short circuit at low actuation voltages.

It was found that too thick a conductive epoxy layer ($>20\,\mu\mathrm{m}$) can cause epoxy to creep up the side-walls of the PZT when it is pressed before curing. This effectively decreases the minimum distance between the two terminals of the PZT. Assuming that there is no epoxy creeping, there is a minimum distance of $127\,\mu\mathrm{m}$ (PZT thickness) between the two electrodes. Using the dielectric breakdown strength of air ($3\,\mathrm{V}\,\mu\mathrm{m}^{-1}$), it is estimated that a maximum voltage of $380\,\mathrm{V}$ can be applied before the device electrically shorts. However, some actuators were found to short even at $80\,\mathrm{V}$. Shorting did not necessarily mean that the device failed. Some actuators continued functioning even after shorting, which is usually evidenced by sharp, loud pops. Upon later disassembly, small blackened spots were found at the shorted regions. The continued working of these actuators might be because the conductive epoxy that had crept up was vaporized due to the arc that was created. No more current could pass through that path, so no more shorting occurred.

The best way to minimize this issue was to change how the epoxy was applied. Initial experiments used a $25\,\mu\mathrm{m}$ Kapton film as a stencil. This was then replaced with a much more robust $20\,\mu\mathrm{m}$ steel stencil that was accurately cut using a laser-cutter. A clean glass-slide was used to squeegee the epoxy over the stencil to leave behind a thin layer in the negative space of the stencil. Using the steel stencil improved the success rate of actuators that could handle $150\,\mathrm{V}$ from 30% to 60%. This was further improved to 80% when a new batch of conductive epoxy was used. The previous batch had expired.

The PZT part was laser-cut to shape; this means that there is a Heat-Affected-Zone (HAZ) in the cut region. As the temperature goes beyond $250\,^\circ\mathrm{C}$ (Curie Temperature) during the laser ablation process, the material depolarizes in this region. The optimal parameters to minimize the HAZ were used, but a small zone of depolarized PZT is always present. Studies have shown Abrasive Waterjet (AWJ) cutting to be superior to laser-cutting in terms of cut quality and the absence of a HAZ [17]. AWJ was initially experimented with in this work but as the facility was not easily accessible, laser-cutting was preferred. The only test that was performed with AWJ cutting required the PZT to be clamped between two $1\,\mathrm{mm}$ steel plates to prevent shattering. The cut was successful and the cut region appeared smooth, but the cutting parameters had to be optimized to decrease material loss.

A $50\,\mu\mathrm{m}$ stainless steel plate was chosen as the substrate after preliminary tests were conducted with 25, 50, and $100\,\mu\mathrm{m}$ plates. Although it was possible to fabricate an actuator with a $25\,\mu\mathrm{m}$ plate, it was found to be very easy to break the bonded
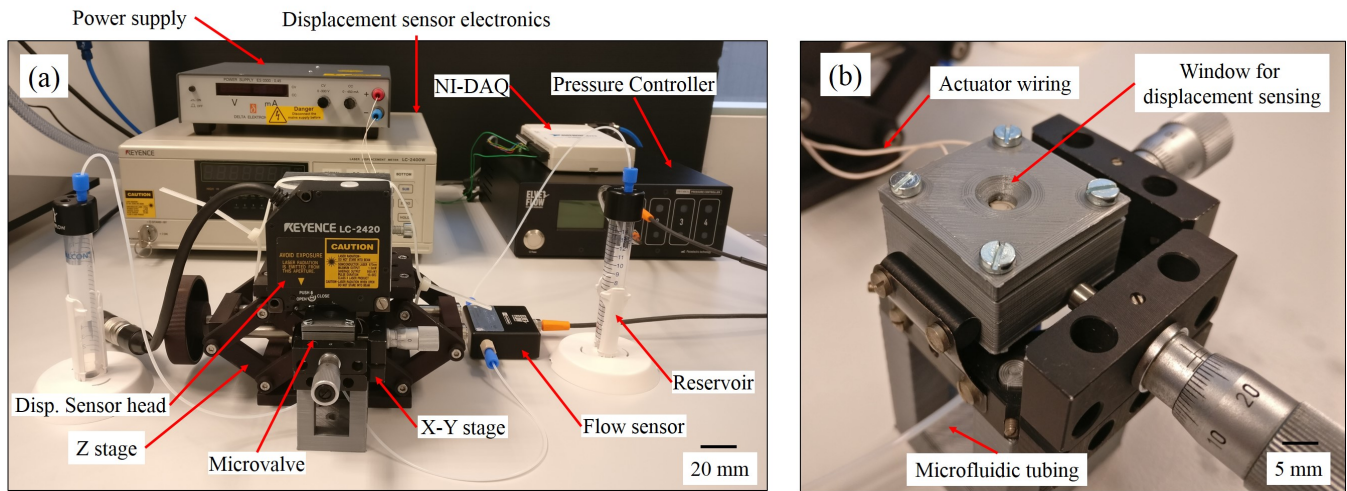
Fig. 22: (a) Microvalve test-setup (b) Microvalve holder mounted on an XY-stage for fine control

PZT if the substrate was bent even slightly. The other two thickness' proved to be more robust, but the $100\,\mu m$ plate was too stiff to provide the required actuation. The $50\,\mu m$ thickness was found to be optimal for this purpose.

3) Behaviour: A surprising result from the central displacement measurement was that the analytical formulation matched very closely to the measured result (2.6% error at 150V, Fig. 12). It was initially assumed that the numerical simulation would be more accurate (27.2% error at 150V, Fig. 12). A more accurate numerical solution might be reached if a Membrane model is used instead of a high mesh density Solid Mechanics model.

In Fig. 12, piezoelectric hysteresis is clearly evidenced by how the up-sweep path is different from the down-sweep path. Hysteresis in piezoelectric actuators is one of the major causes for positioning inaccuracies [18]. Hysteresis models exist that could be used to relate the voltage to displacement, but it is beyond the scope of this work.

There are two other solutions towards controlling the displacement of the actuator. One is simply to introduce a feedback loop in the system, but this means that a displacement sensor is necessary. Another method is to use charge-steering instead of traditional voltage-steering. Hysteresis has been shown to decrease significantly using this technique [19]. A detailed explanation about charge-steering can be found in [19]. A brief explanation is given below.
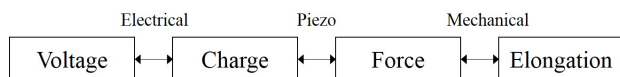

Fig. 23: Physics of a piezo-actuator [20]

In general, the inverse piezoelectric effect follows the order shown in Fig. 23. As piezoelectric materials are insulators, an applied voltage results in the development of charge across the terminals. As they are dielectric materials, the external charge causes a reorientation of internal electric dipoles. This results in a force that causes an elongation of the material. This is then exploited in actuators. The non-linearity occurs in the voltage - charge relation. This causes the undesired hysteresis effect. If the charge can be controlled directly, then the hysteresis will be avoided. The method to do so is called the charge drive. It would be interesting to find if a charge drive changes the microvalve behaviour shown in Fig. 16.

The displacement behaviour for UPMs with different PZT diameters was tested and has been shown in Fig. 13. Note that only one sample of each was tested formally. The error bars indicate the standard deviation of three cycles of actuation (One cycle = 0V → 150V → 0V) of each UPM. It is clear that the analytical values are much closer to experimental results than the numerical results. The measured results show a slightly different trend than that predicted. It appears that deflection is increasing at a constant rate in the measurements, but the analytical and numerical values show a clear decrease in slope as the radius increases. Actuators with higher radii PZT need to be tested to find where the slope changes.

A central displacement of $8.5\,\mu m$ at $150\,V$ has been measured using the $4.4\,mm$ dia UPM. A similar microvalve in literature used a UPM that reported a displacement of $1.3\,\mu m$ at $250\,V$ [15]. Assuming their UPM is linear, it is expected that they measured $\approx 0.8\,\mu m$ at $150\,V$. This means that the UPM developed in this work is ≈ 11 times better in terms of displacement. Some thick-film diaphragm actuators have been reported to produce similar deflection but their blocking force is negligible in comparison to that measured in this work [21].

The frequency-response behaviour shown in Fig. 14 clearly shows a peak at $25.3\,kHz$, denoting the first eigen-frequency of the actuator. A numerical simulation shows the first eigen-frequency at $26.5\,kHz$. The 4.7% error between the two is reasonable considering that the manufactured UPM could be

slightly different in both dimensions and clamping conditions. The eigen-frequency and mass of the membrane are then used to calculate the blocking force of the UPM in Table. V. This is the total force that needs to be applied to the membrane to prevent any motion when maximum voltage is applied. Converting this to blocking pressure (Pressure = Force/Area), we find that $2.4 \, \text{bar}$ is required to prevent any motion. This means that no flow modulation will be observed at and beyond this pressure using this microvalve.

It was observed that the recommended curing time for the conductive epoxy (65 - 120 °C for 5 - 10 minutes) was not sufficient to obtain good stability of the actuator [22]. This means that in its fully actuated state, the actuator drifted backwards at a rate of $\approx 0.5 \, \mu\text{m} \, \text{min}^{-1}$. This was because the epoxy was still quite compliant in its partially cured state. After increasing the oven-curing time to 20 minutes and allowing the actuator to rest for three hours at room temperature, no drift was observed.

To test reproducibility of the adjusted fabrication procedure, three UPMs (PZT dia - $4 \, \text{mm}$) were fabricated in the same batch and subjected to $150 \, \text{V}$. The central displacement measured was $7.41 \pm 0.36 \, \mu\text{m}$. The primary difference between the actuators was the adhesive thickness, which was measured to be $12.6 \pm 3.7 \, \mu\text{m}$. Automating the process of applying epoxy might be a good solution to improving repeatability.

B. Microvalve

1) *Optimization*: Experimental testing was done to find the smallest set of dimensions that could be fabricated with the available SLA printer. The results are shown in Table. IV. The static resistance was maximized in this study, but it was found that the valving-chamber resistance was much higher due to which the dimensions of these channels do not play a significant role in deciding the flow rate. A useful by-product of the study was that the minimum chamber inlet diameter was found. This played a large role in minimizing the leakage of the valve by decreasing the area required to be closed by the UPM.

The spacer thickness is the primary factor that decides the flow rate in an un-actuated microvalve. Fig. 8 shows that the spacer must have a thickness less than $3.5 \, \mu\text{m}$ for the flow rate to be measurable over the full-range of the study (0 - $1 \, \text{bar}$) with the available flow-sensor. This is obviously a limitation of the available equipment. As the UPM shows a maximum displacement of $7.5 \, \mu\text{m}$, it is expected that the microvalve should be able to close the inlet even if the spacer-thickness is $\approx 7 \, \mu\text{m}$. This means that the microvalve can theoretically control a maximum flow rate of $750 \, \mu\text{L} \, \text{min}^{-1}$ as per Fig. 8. The best way to test the limits of this microvalve is to use an $8 \, \mu\text{m}$ thick Jeveka shim-steel spacer with a $4.4 \, \text{mm}$ PZT diameter UPM and check if the flow rate goes to zero at $1 \, \text{bar}$ pressure.

2) *Fabrication*: The main issue with the fabrication of the microchannels was a downward bowing of the valve seat. This is an effect that had been previously encountered with the SLA printer, but no solution had been found. In this case, the bowing was minimized by increasing the number of supports in the internal channels. This decreased the bowing from $5 \, \mu\text{m}$ at the middle of the valve seat to $3 \, \mu\text{m}$. The bowing was measured from the edge of the valving chamber to the center. Images are shown in the supplementary paper.

The laser-cutting of the spacers proved to be a challenge due to warping of the ultra-thin shim steel. The $5 \, \mu\text{m}$ Jeveka shim steel was the thinnest material cut using the available laser-cutter. Due to this, the laser parameters had to be optimized with multiple trials until the warping was minimized.

3) *Behaviour*: Fig. 15 clearly shows that the microvalve behaviour can be predicted with good accuracy using both the analytical and numerical models. This, of course, is dependent on our assumption that the spacing of the microvalve has decreased to $3 \, \mu\text{m}$ due to tightening of the holder bolts. This was verified with reasonable confidence by observing the displacement of the UPM at $40 \, \text{mbar}$ relative pressure. This is shown in Fig. 20, where the maximum displacement is $\approx 3 \, \mu\text{m}$.

It is seen from Fig. 15 that the measured flow rate matches accurately with the numerical model at lower pressures, but diverges at $500 \, \text{mbar}$. This is because the valve-chamber expands slightly at these pressures, allowing a higher flow rate to pass. The numerical model did not account for this expansion as the computing time was too high. The analytical formulation predicts a higher flow rate so it is a good conservative metric to use when designing future microvalves. Including fluidic capacitance in the analytical expression will allow the trends of the two curves to match.

From Fig. 20, it can be seen that the displacement behaviour of the UPM varies significantly when assembled in the microvalve holder in comparison to the UPM holder. It was initially thought that the microvalve would close the inlet orifice at a much lower voltage as the UPM showed $3 \, \mu\text{m}$ displacement at $70 \, \text{V}$ (Fig. 12). This might be because the clamping conditions are quite different in the UPM and the microvalve holders. There is free space underneath the UPM in the UPM holder, while only a small valve-chamber in the valve holder. The microvalve rests on compliant O-rings, which might cause a further divergence in behaviour.

Proportional control of flow rate in the microvalve is clearly observed in Fig. 16. A uniform upward shift in the flow rate curve is seen in relation to the pressure differential. The small standard deviation (error bars) shows that there is good repeatability of the valving behaviour.

It can also be seen that, at all pressures, a bulk of the valving is done from 0 - $100 \, \text{V}$. The slope changes rapidly from $90 \, \text{V}$ and the flow rate appears to asymptotically decrease to zero. In the $1000 \, \text{mbar}$ curve, flow rate decreases at an average rate of $0.95 \, \mu\text{L} \, \text{min}^{-1} \, \text{V}^{-1}$ till $100 \, \text{V}$, but this changes

to $0.04\,\mu\text{L}\,\text{min}^{-1}\,\text{V}^{-1}$ in the latter half of the curve. It is hypothesized that the UPM membrane contacts the valve-seat at $100\,\text{V}$, but due to surface defects, a large leakage flow is still observed. Increasing the voltage further causes the membrane to flatten itself against the valve seat and close the chamber orifice more efficiently. This hypothesis is backed by the $1000\,\text{mbar}$ curve shown in Fig. 20. The displacement of the UPM increases at a constant rate till $100\,\text{V}$ where the slope decreases suddenly. The shift in the final displacement of the red curve shown in Fig. 20 is because the membrane is forced away from the valve seat initially due to the high pressure. This shift is added to the final displacement of the actuator.

The leakage behaviour of the microvalve is shown in Fig. 17. Here, leakage rate is defined as the ratio of closed and open flow rates. Generally, leakage is measured using Helium gas but this facility was not available. A high leakage-rate is observed at low pressures; this is because flow rate at open condition is low, but a constant leakage is always present due to valve seat defects. As pressure increases, open flow rate increases while closed flow rate remains relatively constant, effectively decreasing the leakage-rate. Some methods to decrease leakage include decreasing the valve-seat area by using a knife-edge contact and introducing a soft material like PDMS or a parylene layer to the actuator or valve-seat.

To investigate fine control of the flow, voltage increments of $0.5\,\text{V}$ were applied to the microvalve at $500\,\text{mbar}$ pressure. This was the voltage resolution of the power supply. The resulting curve is shown in Fig. 18. In the linear regime, a flow rate change of $0.2\,\mu\text{L}\,\text{min}^{-1}$ was measured. This is dependent on the pressure differential across the microvalve. Higher flow rate changes are expected at higher pressures and vice versa.

An important characteristic of any device is its reproducibility. The flow rate behaviour of three different microvalves are shown in Fig. 19. The dimensions of the microvalves were similar, but there is a clear difference in their behaviour. Although valves 1 and 2 show similar behaviour, valve 3 acts very differently. This is because lower torque was applied while tightening the microvalve holder bolts. Decreasing the torque results in a lower clamping force on the microvalve. This directly affects the valve chamber height. Larger the valve chamber height - higher the fluid flow rate. Valve 1 and 2 on the other hand, have bolts that were tightened with higher torque, resulting in a lower valve chamber height and a lower flow rate. This was done so that the flow rate could be measured using the available flow sensor over the entire pressure range of the experiment. The decrease in valve-chamber height is due to the spacer being pushed into the microchannel material, thereby permanently deforming it. Lower clamping force is therefore preferred. The reproducibility appears to be linked closely to the clamping force applied to the microvalve. This can be corrected by bonding the UPM to the microchannels instead of clamping them.

As this is a normally-open microvalve, for applications that require long periods of closed state, it is essential that the power

consumption be minimal. Due to the quasi-static nature of this microvalve, only a small leakage current will flow through the piezoelectric material during operation. A minuscule power consumption of $37.5\,\mu\text{W}$ was measured. Similar piezoelectric microvalves have shown a static power consumption of $2500\,\mu\text{W}$ [23], and $3000\,\mu\text{W}$ [24]. No microvalve has been found by the author in the literature that reports a lower static power consumption in this pressure range.

A switching time of $\approx 40\,\text{ms}$ was measured at $500\,\text{mbar}$. The fastest microvalve that was found in literature reported a settling time of $30\,\mu\text{s}$, but they used a custom-made PZT-chip that is both expensive and bulky [24]. The main reason for the higher switching time in this UPM is that membrane actuators have lower stiffness and higher damping. This decreases the reaction time of the actuator. If faster reaction times are desired using a UPM, then a simple modification must be made. The PZT radius must be larger than the membrane radius. A valving time of $1\,\text{ms}$ has been reported with this configuration [15]. However, this greatly decreases the displacement of the actuator due to added stiffness.

V. Conclusion

A proportionally-controlled piezoelectric microvalve was designed, fabricated and characterized. De-ionized water at room temperature was used for characterization. Most piezoelectric devices use MEMS fabrication techniques which are not very accessible. Here, a novel combination of accessible rapid-prototyping methods were used to fabricate an active piezo-electric microfluidic device. The specifications of the final microvalve are given in Table. VI.

A thorough characterization of the unimorph microactuator was performed and a good match was found between the analytical and measured results. A high central displacement of $7.5\,\mu\text{m}$ was observed with an estimated blocking pressure of $2.4\,\text{bar}$ for an actuator dimension of $5\,\text{mm} \times 5\,\text{mm} \times 0.2\,\text{mm}$ (PZT dia = $4\,\text{mm}$).

TABLE VI: Obtained Microvalve specifications

Specification	Measured value
Flow range	0 - 90 $\mu\text{L}\,\text{min}^{-1}$
Flow control resolution	0.2 $\mu\text{L}\,\text{min}^{-1}$ at 500 mbar
Leakage	0.8% open-flow at 1000 mbar
Max. differential pressure	1 bar
Static power consumption	37.5 μW
Operating voltage	0 - 150 V
Typical response time	40 ms
Dimensions (effective)	5 mm $\times$ 5 mm $\times$ 1.8 mm

Due to limitations in the available flow sensor, the full potential of the microvalve could not be explored. The projected flow-range for this microvalve is 0 - $750\,\mu\text{L}\,\text{min}^{-1}$ (water). Recommendations have been given to improve the leakage behaviour of the microvalve. A low power consumption of $37.5\,\mu\text{W}$ has been measured, which, to the best of the author's

knowledge, is the lowest reported in literature for this pressure range.

REFERENCES

[1] A. Manz, N. Graber, and H. á. Widmer, "Miniaturized total chemical analysis systems: a novel concept for chemical sensing," *Sensors and actuators B: Chemical*, vol. 1, no. 1-6, pp. 244–248, 1990.

[2] S. Böhm, B. Timmer, W. Olthuis, and P. Bergveld, "A closed-loop controlled electrochemically actuated micro-dosing system," *Journal of Micromechanics and Microengineering*, vol. 10, no. 4, p. 498, 2000.

[3] G. C. Birur, T. W. Sur, A. D. Paris, P. Shakkottai, A. A. Green, and S. I. Haapanen, "Micro/nano spacecraft thermal control using a mems-based pumped liquid cooling system," in *Microfluidics and BioMEMS*, vol. 4560, pp. 196–207, International Society for Optics and Photonics, 2001.

[4] P. S. Dittrich and A. Manz, "Lab-on-a-chip: microfluidics in drug discovery," *Nature reviews Drug discovery*, vol. 5, no. 3, p. 210, 2006.

[5] S. C. Terry, J. H. Jerman, and J. B. Angell, "A gas chromatographic air analyzer fabricated on a silicon wafer," *IEEE transactions on electron devices*, vol. 26, no. 12, pp. 1880–1886, 1979.

[6] T. Ohnstein, T. Fukiura, J. Ridley, and U. Bonne, "Micromachined silicon microvalve," in *IEEE Proceedings on Micro Electro Mechanical Systems, An Investigation of Micro Structures, Sensors, Actuators, Machines and Robots.*, pp. 95–98, IEEE, 1990.

[7] D. C. Roberts, H. Li, J. L. Steyn, O. Yaglioglu, S. M. Spearing, M. A. Schmidt, and N. W. Hagood, "A piezoelectric microvalve for compact high-frequency, high-differential pressure hydraulic micropumping systems," *Journal of Microelectromechanical Systems*, vol. 12, no. 1, pp. 81–92, 2003.

[8] M. A. Unger, H.-P. Chou, T. Thorsen, A. Scherer, and S. R. Quake, "Monolithic microfabricated valves and pumps by multilayer soft lithography," *Science*, vol. 288, no. 5463, pp. 113–116, 2000.

[9] J.-H. Kim, K.-H. Na, C. Kang, and Y.-S. Kim, "A disposable thermopneumatic-actuated micropump stacked with pdms layers and ito-coated glass," *Sensors and Actuators A: Physical*, vol. 120, no. 2, pp. 365–369, 2005.

[10] S. Trolier-McKinstry and P. Muralt, "Thin film piezoelectrics for mems," *Journal of Electroceramics*, vol. 12, no. 1-2, pp. 7–17, 2004.

[11] S. J. Bleiker, V. Dubois, S. Schröder, G. Stemme, and F. Niklaus, "Adhesive wafer bonding with ultra-thin intermediate polymer layers," *Sensors and Actuators A: Physical*, vol. 260, pp. 16–23, 2017.

[12] C. Mo, R. Wright, W. S. Slaughter, and W. W. Clark, "Behaviour of a unimorph circular piezoelectric actuator," *Smart Materials and Structures*, vol. 15, no. 4, p. 1094, 2006.

[13] I. Fazal and M. C. Elwenspoek, "Design and analysis of a high pressure piezoelectric actuated microvalve," *Journal of micromechanics and microengineering*, vol. 17, no. 11, p. 2366, 2007.

[14] D. Accoto, M. Carrozza, and P. Dario, "Modelling of micropumps using unimorph piezoelectric actuator and ball valves," *Journal of Micromechanics and Microengineering*, vol. 10, no. 2, p. 277, 2000.

[15] M. Sobocinski, J. Juuti, H. Jantunen, and L. Golonka, "Piezoelectric unimorph valve assembled on an ltcc substrate," *Sensors and Actuators A: Physical*, vol. 149, no. 2, pp. 315–319, 2009.

[16] Z. Wang, J. Miao, C. W. Tan, and T. Xu, "Fabrication of piezoelectric mems devices-from thin film to bulk pzt wafer," *Journal of electroceramics*, vol. 24, no. 1, pp. 25–32, 2010.

[17] M. Annoni, F. Arleo, A. Trolli, A. Suarez, A. Alberdi, and R. Tecnalia, "Fine abrasive water jet machining of piezoelectric ceramics: cutting parameters optimization," in *Proceedings of the 21st International Conference on Water Jetting, Ottawa, Canada*, pp. 67–80, 2012.

[18] D. Damjanovic, "Hysteresis in piezoelectric and ferroelectric materials," *The science of hysteresis*, vol. 3, pp. 337–465, 2006.

[19] R. H. Comstock, "Charge control of piezoelectric actuators to reduce hysteresis effects," Apr. 21 1981. US Patent 4,263,527.

[20] H. Adriaens, W. L. De Koning, and R. Banning, "Modeling piezoelectric actuators," *IEEE/ASME transactions on mechatronics*, vol. 5, no. 4, pp. 331–341, 2000.

[21] E. Hong, S. Trolier-McKinstry, R. L. Smith, S. V. Krishnaswamy, and C. B. Freidhoff, "Design of mems pzt circular diaphragm actuators to generate large deflections," *Journal of Microelectromechanical systems*, vol. 15, no. 4, pp. 832–839, 2006.

[22] "Circuitworks cw 2400 conductive epoxy datasheet." https://www.mouser.com/datasheet/2/69/Cw2400tds-1224167.pdf. Accessed: 2019-07-22.

[23] C. Lee, E.-H. Yang, S. M. Saeidi, and J. M. Khodadadi, "Fabrication, characterization, and computational modeling of a piezoelectrically actuated microvalve for liquid flow control," *Journal of Microelectromechanical Systems*, vol. 15, no. 3, pp. 686–696, 2006.

[24] E.-H. Yang, C. Lee, J. Mueller, and T. George, "Leak-tight piezoelectric microvalve for high-pressure gas micropropulsion," *Journal of Microelectromechanical Systems*, vol. 13, no. 5, pp. 799–807, 2004.

4 Conclusion and Recommendations

4.1 Conclusion

A comprehensive literature review was conducted to identify a research gap in the field of microvalves. A gap was found in the absence of a small foot-print microvalve for flow modulation of both liquids and gases. A hybrid-integrated microvalve controlled by a unimorph piezoelectric actuator was developed using a combination of 3D printing and laser-cutting. These fabrication methods are much more accessible than Silicon-microfabrication techniques. The target and final specifications of the microvalve are shown in Table 6.

Table 6: Target and obtained specifications

Specification	Target value	Obtained value
Flow range	0 - 100 µL/min (liquids), 0 - 100sccm (gases)	0 - 90 µLmin^{-1} V^{-1} (water, measured) 0 - 750 µLmin^{-1} V^{-1} (water, projected)
Flow control resolution	0.1 µL/min (liq), 0.1 sccm (gas)	0.2 µLmin^{-1} (water, 500 mbar)
Leakage	$< 10^{-6}$ mbar L/s He	0.8% open-flow at 1 bar (water)
Max. differential pressure	≥ 1 bar	1 bar
Static power consumption	< 10 mW	37.5 µW
Typical response time	< 5 ms	40 ms
Dimensions	$< 5 \times 5 \times 2$ mm^3	$5 \times 5 \times 1.8$ mm^3

4.2 Recommendations and Future Work

It was found that a unimorph microvalve is both simple to fabricate and easy to integrate. The main issue that can be solved in the immediate future is the leakage of the microvalve. This can be done by using soft materials at the interface. One method is to print a ~2 µm thick valve boss underneath the actuator using two-photon polymerization (NanoScribe). Another method is to spin-coat and pattern a very thin layer of PDMS (~2 µm) on the valve-seat or actuator. Leakage can be reduced significantly using these methods. A unimorph microvalve could also be fabricated using Si-MEMS technology as has been discussed in Appendix B. The surface of the valve-seat is expected to be smooth and this can mean a decrease in the leak-rate. Also, the microvalve still requires a holder that provides clamping force. This increases the dimensions of the microvalve. Adhesive or metal-metal bonding can be used to permanently bond the microactuator to the microchannels, thereby decreasing the overall size. In metal-metal bonding, gold can be sputtered on the actuator and the microchannels in the required regions. High pressure and temperature are then required to bond them together. The thickness of the gold layer determines the height of the valving chamber. This is similar in adhesive bonding.

A broader recommendation for further research is to implement the hybrid-fabrication approach to fabricate other microfluidic devices like a micropump. This can even be done using the device that has been fabricated in this work, with the only addition being two check valves on either side of the device. It would be interesting to integrate this micropump with a microvalve and test their behavior to check if an integrated microfluidic system can be built.

5 Reflection

The following chapter contains the details of the author's personal scientific pursuit while executing this thesis work. The design and selection process, the time-line, and the problems faced are detailed below in chronological order.

The initial research question that was posed was simply to design a microvalve that could handle a certain pressure. Little information was given about dimensional and flow constraints. The main intention of having such an open-ended question was to allow an unfettered view of the available literature. This resulted in the *novelty* becoming the primary criterion of comparison between designs as that was thought to bring about the highest scientific value. The fabrication complexity was not considered with the importance that it deserved by the author. The first design that was proposed was an EAP (Electroactive polymer) microvalve. A closer look at the working principle and fabrication complexity resulted in its quick rejection (operating voltage > 1000 V). The next proposal was of a parylene based microvalve that was certainly novel, but highly complex to fabricate with more than eight photolithography steps. Almost three weeks were expended on designing this microvalve even though the complexity was known from the outset by the author. This was again turned down after a meeting with Bronkhorst B.V. (a stakeholder in the project) where they expressed interest in a microvalve that used hard materials (unlike parylene or EAPs), was easy to fabricate, and required minimal peripherals to operate.

The above wishes/constraints provided a filter that quickly eliminated many actuation concepts. Piezoelectricity was chosen as the final actuation principle with a focus on the unimorph configuration. Unimorph piezoelectric microactuators (UPM) were frequently encountered in micropumps but only one example was later found in microvalves. They are simple in structure and their main advantages are the small size, good force, and fast reaction time (compared to other actuation principles). The main problem was that most of the micropump examples used actuators which exhibited low displacements (~1 µm). This is insufficient for microvalves. Preliminary simulations using COMSOL provided evidence that it is possible to obtain > 5 µm actuation if the right materials and right dimensions were used. This was certainly sufficient to obtain good flow-rate (>200 µL/min) at moderate pressures of 1 bar. This was then proposed and enthusiastically agreed upon as it matched the expectations of both Bronkhorst and TU Delft.

The initial design required two parts that were both Si-microfabricated (Appendix B). One part would be used for the UPM and the other would contain the valving mechanism. They would be clamped together to obtain a working microvalve. The designs were given to the Else Kooi Lab (EKL) for fabrication. It was expected that they would take two months to deliver so a proof-of-principle UPM was constructed using a steel substrate during the time.

Abrasive-waterjet cutting (AWJ) was initially considered to be a good option to cut PZT. DEMO (Dienst Elektronische en Mechanische Ontwikkeling), a facility with an AWJ cutting machine was approached and a preliminary square cut was made to find if the 127 µm PZT sample was machinable. A good quality cut was observed but with large material losses as the process was not optimized for this material. Further attempts to optimize could not be made as the AWJ machine was constantly being used. This forced us to use the laser-cutter as it was readily available. The laser parameters for PZT had been optimized by a previous student so the cut quality was good and the heat-affected-zone of the PZT was minimal. This cutter was used for the remainder of the project to cut PZT and stainless steel.

After a month (in April '19), it became evident that the delivery from EKL would be postponed by at least two more months. This meant that a Plan B would be required in case the chips arrived too late (August '19 was the thesis deadline). A brainstorming session was arranged with the supervisor to decide on a plan of action. It was assumed that the EKL chips would not arrive during my thesis period. By this time, the proof-of-principle actuator was working well so the UPM-portion of the thesis was well underway. It was considered whether the thesis could be pivoted to concentrate on characterizing the UPM but the plan was discarded as time was still available to work on an alternative fabrication

sequence to make a microvalve. The Envision-TEC SLA printer was recommended as it was used exclusively to create high-resolution parts. The NanoScribe (two-photon polymerization tool, TPP) was also considered as an option. Two options were then available to explore.

A new design was made that would use the SLA printer to create microchannels. The resolution of the printer was still too coarse to be able to create the final structure required. Due to this, a combined approach of using both the SLA printer and the NanoScribe was considered. In this, a portion of the microchannels would be built using the SLA printer and the rest would be completed using the NanoScribe. Unfortunately, it was found during the first test that it was not easy to construct TPP structures on an SLA part due to bubbling of the SLA material. This plan was quickly discarded as time was insufficient to optimize these parameters.

The main issue was that the valve chamber height of the microchannel has to be within 10 µm for the UPM to be able to close the orifice. It was thought that this spacing could be obtained through printing (SLA+TPP). On speaking to lab technicians, it was realized that ultra-thin shim-steel was available (5 µm). Another re-design was made to incorporate the shim-steel into the microvalve structure.

All the constituent parts of the microvalve were coming together, but there was still no way to test it. Fortunately, a pressure controller had just been purchased along with a liquid flow-sensor that had a usable range. A microvalve holder was then developed using a conventional 3D-printer. It was tricky to introduce threaded ports in the holder that could directly interface with Elveflow microfluidic connectors. A few trials were required to finalize the thread design and the 3D printer parameters. O-rings had been purchased previously anticipating that they would be required for interfacing. Once everything was available, the testing phase of the thesis began.

The failure rate of the UPMs immediately increased as their clamping conditions had been modified. Adjustments were made to the holder design to prevent breakage. The microchannel design had to be modified with smaller chamber inlets to decrease leakage. A new batch of conductive epoxy arrived and the quality of the UPMs increased. The voltage applied could be increased from 80V to 150V as the chances of shorting the UPM decreased. The leakage was initially very high (30% open-flow), but these incremental improvements to the design decreased the leakage to 0.8% open-flow. Reproducibility is still an issue, but proposals have been made to improve it.

The research that has been conducted in this work fits into the iMicrofluidics project at the MNE specialization. The main focus of this project is a microfluidic platform that stresses on miniaturization of peripherals. This work requires only electrical peripherals and can be used in a general platform for both liquids and gases.

In conclusion, these past nine months have been filled with steep drops and sudden jumps. A combination of bad luck and some fortunate events have resulted in a functioning microvalve that can be manufactured relatively easily (compared to Si-MEMS), has good reaction time, ultra-low power consumption, and a good dynamic range of flow control for both liquids and, potentially, gases. I cannot profess to have done exactly what I set out to do in the beginning, but I am confident that this work will be useful for future students and is publishable.

Bibliography

[1] K. Tanaka, T. Konishi, M. Ide, Z. Meng, and S. Sugiyama, "Fabrication of microdevices using bulk ceramics of lead zirconate titanate," *Japanese journal of applied physics,* vol. 44, no. 9S, p. 7068, 2005.

[2] A. Manz, N. Graber, and H. á. Widmer, "Miniaturized total chemical analysis systems: a novel concept for chemical sensing," *Sensors and actuators B: Chemical,* vol. 1, no. 1-6, pp. 244-248, 1990.

[3] E. S. Kolesar and R. R. Reston, "Review and summary of a silicon micromachined gas chromatography system," *IEEE Transactions on Components, Packaging, and Manufacturing Technology: Part B,* vol. 21, no. 4, pp. 324-328, 1998.

[4] A. Manz, Y. Miyahara, J. Miura, Y. Watanabe, H. Miyagi, and K. Sato, "Design of an open-tubular column liquid chromatograph using silicon chip technology," *Sensors and actuators B: Chemical,* vol. 1, no. 1-6, pp. 249-255, 1990.

[5] S. C. Terry, J. H. Jerman, and J. B. Angell, "A gas chromatographic air analyzer fabricated on a silicon wafer," *IEEE transactions on electron devices,* vol. 26, no. 12, pp. 1880-1886, 1979.

[6] S. Böhm, B. Timmer, W. Olthuis, and P. Bergveld, "A closed-loop controlled electrochemically actuated micro-dosing system," *Journal of micromechanics and microengineering,* vol. 10, no. 4, p. 498, 2000.

[7] D. Maillefer, H. van Lintel, G. Rey-Mermet, and R. Hirschi, "A high-performance silicon micropump for an implantable drug delivery system," in *Micro Electro Mechanical Systems, 1999. MEMS'99. Twelfth IEEE International Conference on*, 1999, pp. 541-546: IEEE.

[8] D. Reynaerts, J. Peirs, and H. Van Brussel, "An implantable drug-delivery system based on shape memory alloy micro-actuation," *Sensors and Actuators A: Physical,* vol. 61, no. 1-3, pp. 455-462, 1997.

[9] F. E. Tay, W. Choong, H. Liu, and G. Xu, "An intelligent micro-fluidic system for drug delivery," in *Industrial Technology 2000. Proceedings of IEEE International Conference on*, 2000, vol. 2, pp. 70-75: IEEE.

[10] G. C. Birur, T. W. Sur, A. D. Paris, P. Shakkottai, A. A. Green, and S. I. Haapanen, "Micro/nano spacecraft thermal control using a MEMS-based pumped liquid cooling system," in *Microfluidics and BioMEMS*, 2001, vol. 4560, pp. 196-207: International Society for Optics and Photonics.

[11] C. M. Marrese-Reading, J. Mueller, and W. C. West, "Microfluidic electrospray thruster," ed: Google Patents, 2014.

[12] A. D. Paris, G. C. Birur, and A. A. Green, "Development of MEMS microchannel heat sinks for micro/nano spacecraft thermal control," in *ASME 2002 International Mechanical Engineering Congress and Exposition*, 2002, pp. 25-31: American Society of Mechanical Engineers.

[13] P. S. Dittrich and A. Manz, "Lab-on-a-chip: microfluidics in drug discovery," *Nature reviews Drug discovery,* vol. 5, no. 3, p. 210, 2006.

[14] D. Huh *et al.*, "A human disease model of drug toxicity–induced pulmonary edema in a lung-on-a-chip microdevice," *Science translational medicine,* vol. 4, no. 159, pp. 159ra147-159ra147, 2012.

[15] D. Huh, B. D. Matthews, A. Mammoto, M. Montoya-Zavala, H. Y. Hsin, and D. E. Ingber, "Reconstituting organ-level lung functions on a chip," *Science,* vol. 328, no. 5986, pp. 1662-1668, 2010.

[16] I. Maschmeyer *et al.*, "A four-organ-chip for interconnected long-term co-culture of human intestine, liver, skin and kidney equivalents," *Lab on a Chip,* vol. 15, no. 12, pp. 2688-2699, 2015.

[17] K. W. Oh and C. H. Ahn, "A review of microvalves," *Journal of micromechanics and microengineering,* vol. 16, no. 5, p. R13, 2006.

[18] M. Groen, "Microvalves for precise dosing: proportional flow control on a chip," 2015.

[19] M. Hirano, K. Yanagisawa, H. Kuwano, and S. Nakano, "Microvalve with ultra-low leakage," in *Micro Electro Mechanical Systems, 1997. MEMS'97, Proceedings, IEEE., Tenth Annual International Workshop on*, 1997, pp. 323-326: IEEE.

[20] J. S. Bintoro, P. J. Hesketh, and Y. H. Berthelot, "CMOS compatible bistable electromagnetic microvalve on a single wafer," *Microelectronics Journal,* vol. 36, no. 7, pp. 667-672, 2005.

[21] E. Yıldırım, M. S. Arıkan, and H. Külah, "A normally closed electrostatic parylene microvalve for micro total analysis systems," *Sensors and Actuators A: Physical,* vol. 181, pp. 81-86, 2012.

[22] T. Ohnstein, T. Fukiura, J. Ridley, and U. Bonne, "Micromachined silicon microvalve," in *Micro Electro Mechanical Systems, 1990. Proceedings, An Investigation of Micro Structures, Sensors, Actuators, Machines and Robots. IEEE*, 1990, pp. 95-98: IEEE.

[23] Z. Wang, J. Miao, C. W. Tan, and T. Xu, "Fabrication of piezoelectric MEMS devices-from thin film to bulk PZT wafer," *Journal of electroceramics,* vol. 24, no. 1, pp. 25-32, 2010.

[24] M. Annoni, F. Arleo, A. Trolli, A. Suarez, A. Alberdi, and R. Tecnalia, "Fine abrasive water jet machining of piezoelectric ceramics: cutting parameters optimization," in *Proceedings of the 21st International Conference on Water Jetting, Ottawa, Canada*, 2012, pp. 67-80.

[25] C. Lee, E.-H. Yang, S. M. Saeidi, and J. M. Khodadadi, "Fabrication, characterization, and computational modeling of a piezoelectrically actuated microvalve for liquid flow control," *Journal of microelectromechanical systems,* vol. 15, no. 3, pp. 686-696, 2006.

[26] D. C. Roberts *et al.*, "A piezoelectric microvalve for compact high frequency high differential pressure micropumping systems," *Journal of Microelectromechanical Systems,* vol. 12, no. 1, pp. 81-92, 2003.

[27] H. Van Lintel, F. Van de Pol, and S. Bouwstra, "A piezoelectric micropump based on micromachining of silicon," *Sensors and actuators,* vol. 15, no. 2, pp. 153-167, 1988.

[28] M. Sobocinski, J. Juuti, H. Jantunen, and L. Golonka, "Piezoelectric unimorph valve assembled on an LTCC substrate," *Sensors and Actuators A: Physical,* vol. 149, no. 2, pp. 315-319, 2009.

[29] M. A. Unger, H.-P. Chou, T. Thorsen, A. Scherer, and S. R. Quake, "Monolithic microfabricated valves and pumps by multilayer soft lithography," *Science,* vol. 288, no. 5463, pp. 113-116, 2000.

[30] W. H. Grover, R. H. Ivester, E. C. Jensen, and R. A. Mathies, "Development and multiplexed control of latching pneumatic valves using microfluidic logical structures," *Lab on a Chip,* vol. 6, no. 5, pp. 623-631, 2006.

[31] A. Henning *et al.*, "A thermopneumatically actuated microvalve for liquid expansion and proportional control," in *Solid State Sensors and Actuators, 1997. TRANSDUCERS'97 Chicago., 1997 International Conference on*, 1997, vol. 2, pp. 825-828: IEEE.

[32] J.-H. Kim, K.-H. Na, C. Kang, and Y.-S. Kim, "A disposable thermopneumatic-actuated micropump stacked with PDMS layers and ITO-coated glass," *Sensors and Actuators A: Physical,* vol. 120, no. 2, pp. 365-369, 2005.

[33] Y. Bar-Cohen, *Electroactive polymer (EAP) actuators as artificial muscles: reality, potential, and challenges*. SPIE press Bellingham, WA, 2004.

[34] Y. Tanaka, T. Fujikawa, Y. Kazoe, and T. Kitamori, "An active valve incorporated into a microchip using a high strain electroactive polymer," *Sensors and Actuators B: Chemical,* vol. 184, pp. 163-169, 2013.

[35] X.-Q. Wang and Y.-C. Tai, "A normally closed in-channel micro check valve," in *Micro Electro Mechanical Systems, 2000. MEMS 2000. The Thirteenth Annual International Conference on*, 2000, pp. 68-73: IEEE.

[36] J. M. Park *et al.*, "A piezoelectric microvalve for cryogenic applications," *Journal of Micromechanics and Microengineering,* vol. 18, no. 1, p. 015023, 2007.

[37] E.-H. Yang, C. Lee, J. Mueller, and T. George, "Leak-tight piezoelectric microvalve for high-pressure gas micropropulsion," *Journal of Microelectromechanical systems,* vol. 13, no. 5, pp. 799-807, 2004.

[38] I. Klammer, A. Buchenauer, G. Dura, W. Mokwa, and U. Schnakenberg, "A novel valve for microfluidic PDMS-based systems," in *2008 IEEE 21st International Conference on Micro Electro Mechanical Systems*, 2008, pp. 626-629: IEEE.

[39] P.-J. Chen, D. C. Rodger, E. M. Meng, M. S. Humayun, and Y.-C. Tai, "Surface-micromachined parylene dual valves for on-chip unpowered microflow regulation," *Journal of Microelectromechanical Systems,* vol. 16, no. 2, pp. 223-231, 2007.

[40] F. Carpi, D. De Rossi, R. Kornbluh, R. E. Pelrine, and P. Sommer-Larsen, *Dielectric elastomers as electromechanical transducers: Fundamentals, materials, devices, models and applications of an emerging electroactive polymer technology*. Elsevier, 2011.

[41] I. Fazal and M. C. Elwenspoek, "Design and analysis of a high pressure piezoelectric actuated microvalve," *Journal of micromechanics and microengineering,* vol. 17, no. 11, p. 2366, 2007.

[42] T. Veenstra, J. W. Berenschot, R. G. Sanders, J. G. Gardeniers, M. C. Elwenspoek, and A. Van Den Berg, "A simple selfpriming bubble-tolerant peristaltic micropump," in *Sensor Technology 2001*: Springer, 2001, pp. 125-129.

[43] X.-H. Xu, B.-Q. Li, Y. Feng, and J.-R. Chu, "Design, fabrication and characterization of a bulk-PZT-actuated MEMS deformable mirror," *Journal of Micromechanics and Microengineering,* vol. 17, no. 12, p. 2439, 2007.

[44] E. Aktakka, H. Kim, and K. Najafi, "Wafer level fabrication of high performance MEMS using bonded and thinned bulk piezoelectric substrates," in *Solid-State Sensors, Actuators and Microsystems Conference, 2009. TRANSDUCERS 2009. International*, 2009, pp. 849-852: IEEE.

[45] M. S. Groen, D. M. Brouwer, R. J. Wiegerink, and J. C. Lötters, "Design considerations for a micromachined proportional control valve," *Micromachines,* vol. 3, no. 2, pp. 396-412, 2012.

Appendix A – Supplementary Material

The supplementary material discusses the following topics.

1. Laser parameters used for cutting PZT and stainless steel
2. Fabrication process
   a. PZT Microactuator
   b. Microchannels
3. COMSOL model
   a. Microactuator displacement
   b. Microvalve flow-rate
4. Failure modes:
   a. PZT microactuator
   b. Microchannels
5. Additional microvalve results
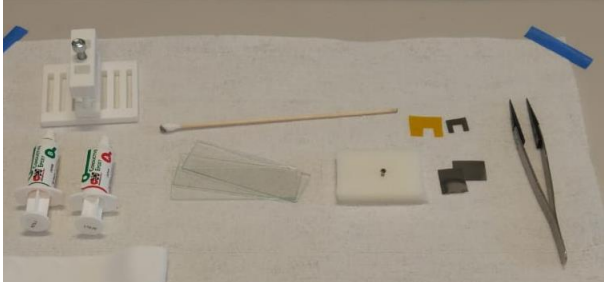6. Program – Microvalve Data Acquisition

A.1   Laser Parameters

The parameters given in Table 7 are applicable to an Optec laser micro-etching machine.
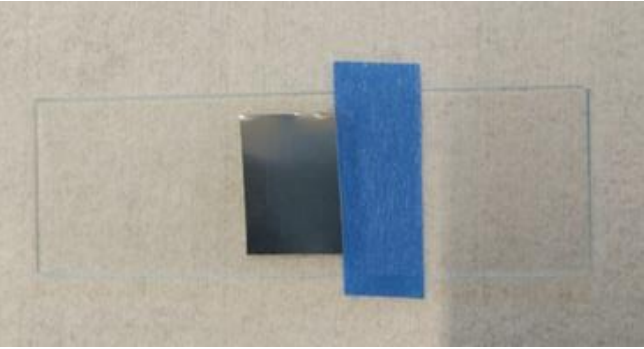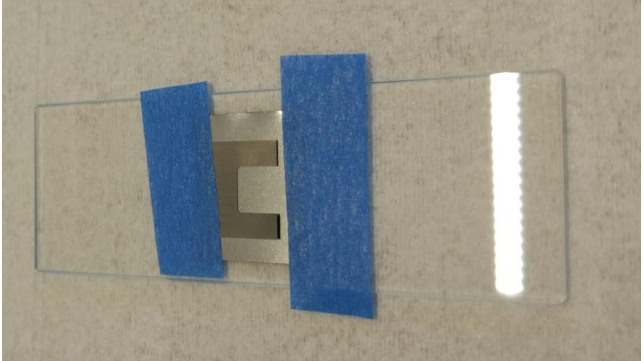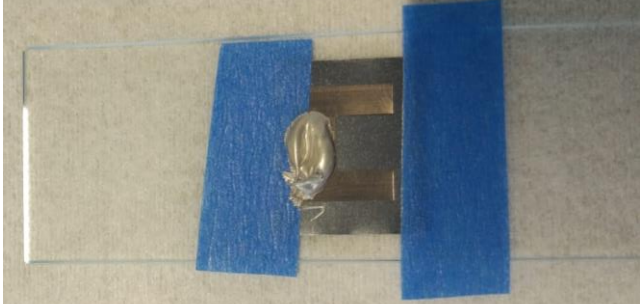
Table 7: Laser parameters for the materials used
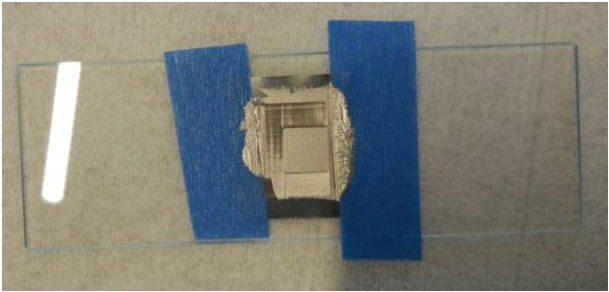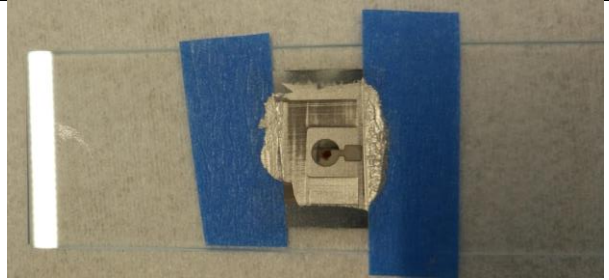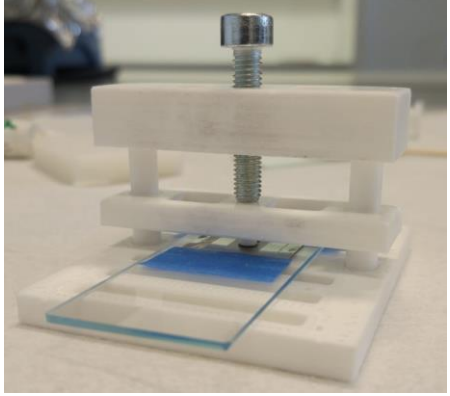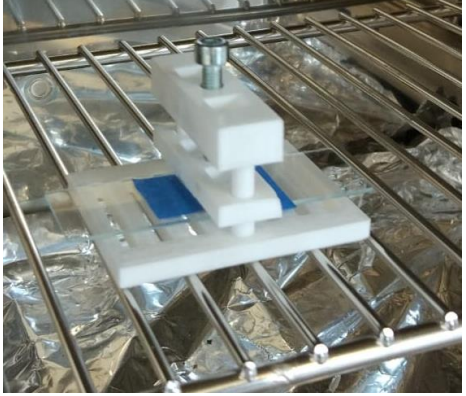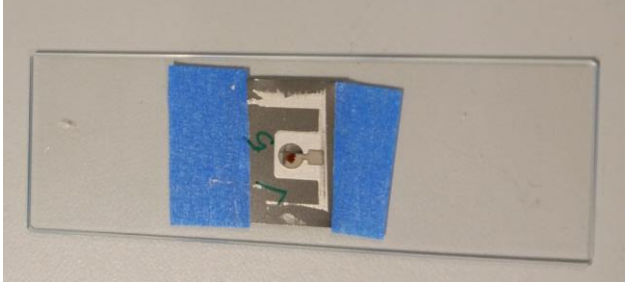
Parameter	PZT- 5H	Stainless steel	
Thickness (µm)	127	5	20
Current (A)	6	3	3
Laser frequency (kHz)	15	50	50
Laser cutting speed (mm/s)	60	20	20
Number of repetitions	30	4	8
Number of levels	4	1	1
Distance between levels (µm)	25	-	-
Number of offset lines	5	0	0
Distance between offset lines (µm)	20	-	-

A.2   Fabrication Process

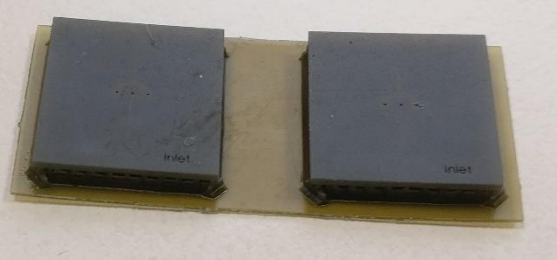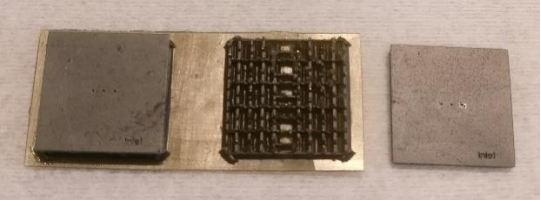### A.2.1 PZT Microactuator
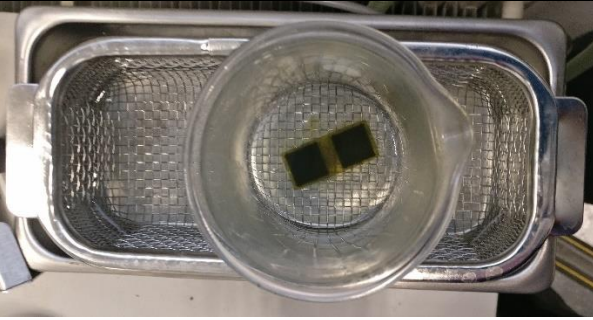
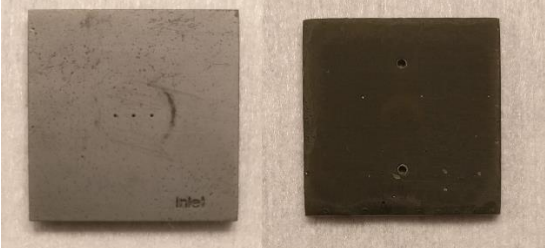| S.No	Image	Description	Notes
1		Arrange everything that is necessary before you begin	1. Conductive epoxy 2. Clamp 3. Glass slides 4. Cut PZT part 5. Stencil 6. Steel substrate 7. Vacuum/manual tweezers

2		Affix steel substrate to glass slide using tape	
3		Affix steel stencil centrally	
4		Dispense two small globs of both components of epoxy and mix them for two minutes	
5		Put a glob of mixed epoxy on the stencil.	Make sure that the negative space of the stencil is free of epoxy in this step

6		Squeegee the epoxy with the short edge of a clean glass slide	This is the trickiest step. Best results were noticed when the glass-slide is angled at 45°. The example shown in the image is a non-optimal result.
7		Place PZT centrally on the epoxy using tweezers	Using vacuum tweezers is recommended. The coloring on the top face of the PZT is to indicate the positive terminal.
8	-	Remove the stencil carefully and clean the surface using IPA to remove any epoxy. The stencil can now be re-used.	
8		Clamp the PZT gently, do not use excessive force.	
9		Cure in a furnace at 75°C for 20 minutes	
10		Enjoy your new piezoelectric unimorph microactuator!	

A.1   Microchannels

The microchannels are printed using an EnvisionTec Micro-plus Hi-Res SLA printer, but it should be possible with any SLA printer that has a ≤ 25 μm vertical resolution. The steps taken to set up the print are not covered here.

S. No	Image	Description	Notes
1		Two microchannel parts after printing	
2		Ultrasonicate the part for 5 minutes, remove, use compressed air to remove remaining uncured polymer, repeat ultrasonication step.	
3		Do a post-cure step for three minutes.	
4		Final product with supports	
5		Remove the part using a scalpel and sand the bottom with 1000 grit sandpaper	

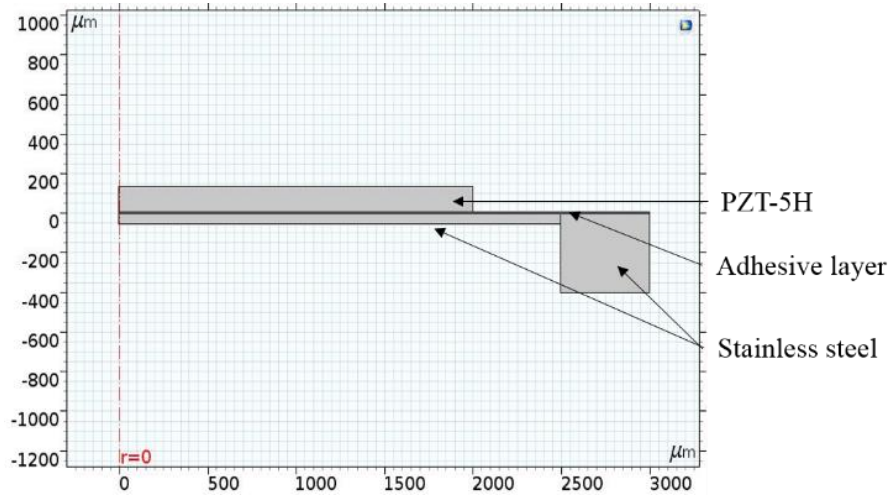| 6 | | Enjoy your new microchannels! | |

A.3 COMSOL Models

A.3.1 Microactuator displacement

The COMSOL model is explained in the following sections:
1. Geometry and Materials
2. Setting up the physics
3. Results

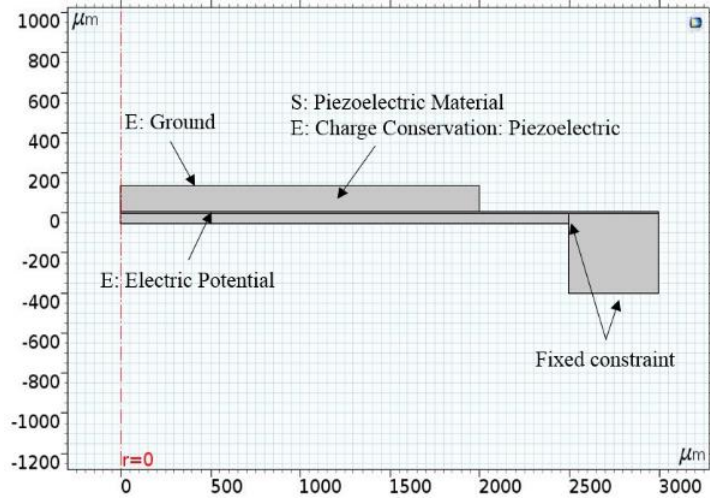### A.3.1.1 Geometry and Materials
Geometry type: 2D – axisymmetric

A.3.1.2 Setting up the Physics
Physics: Solid Mechanics (S) and Electrostatics (E)
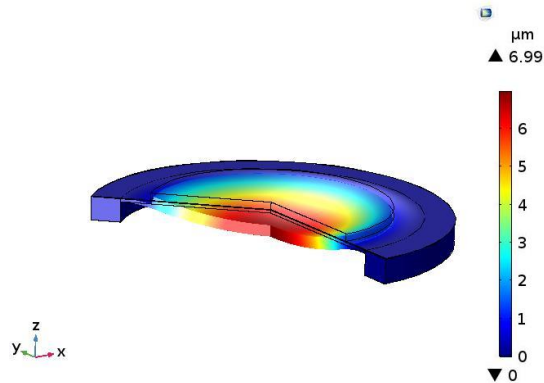**Multiphysics:** Piezoelectric Devices
Mesh: Boundary layer mesh with maximum element size of 1 µm

A.3.1.3 Results
Displacement results

PZT Radius	= 2 mm
PZT Thickness	= 127 µm
Membrane thickness	= 50 µm
Membrane radius	= 2.5 mm
Adhesive thickness	= 10 µm
Voltage	= 190V

A.3.2 Microvalve Flow rate

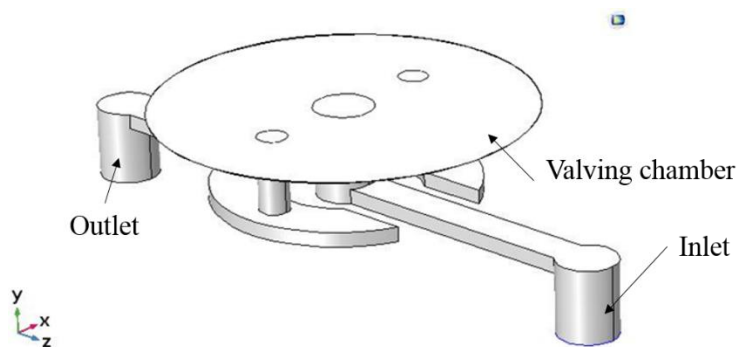The COMSOL model is explained in the following sections:
1. Geometry and Materials
2. Setting up the physics
3. Results

A.3.2.1 Geometry and Materials
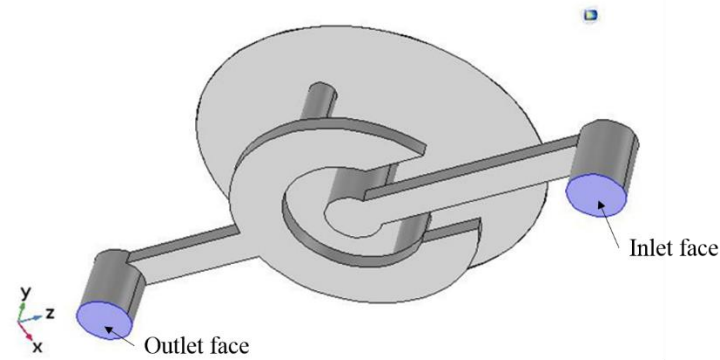The geometry given below shows the wetted path of the valve.
Material: Water

A.3.2.2 Setting up the physics
Physics: Laminar Flow
Mesh: Boundary layer mesh with maximum element size of 0.25 µm
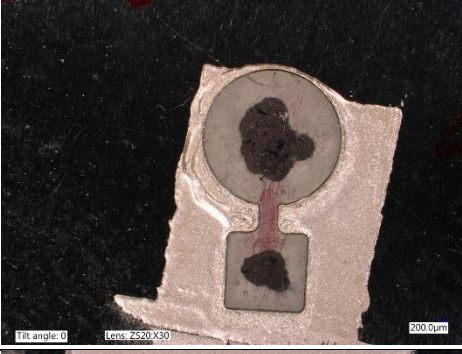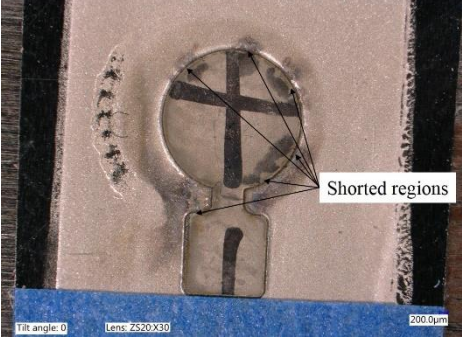
Inlet face

Outlet face

A.3.2.3 Results

The main result that is extracted is the volume flow-rate. It is calculated using the Surface Integration tool (Derived value). The velocity of the fluid (spf.U) is integrated over the inlet face. This results in the volume flow-rate.
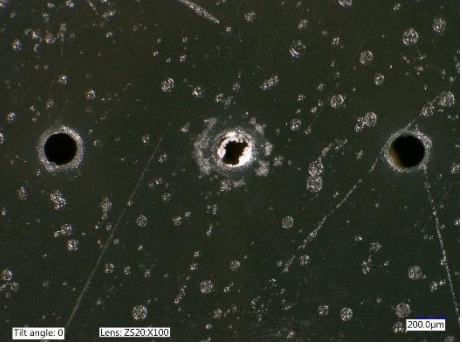
A.4 Failure Modes
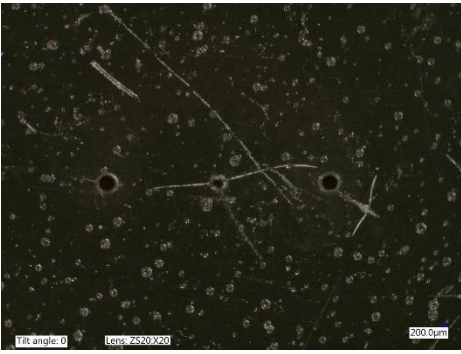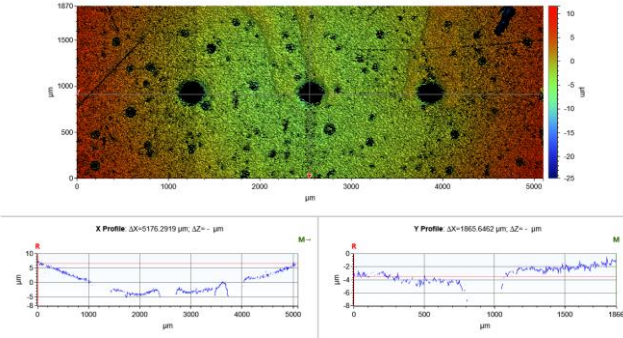
A.4.1 PZT Microactuator

S.No	Image	Failure Mode	Description	Measures
1		Near-invisible micro-cracks on the top metal layer of the PZT	These cracks can break electrical continuity between the square pad and the main disc and are generally due to mishandling or excess downward force on the pad.	**Preventive:** Careful handling. Low electrode wire diameter (< 0.5 mm).
				Corrective: No measures found. Device has to be discarded.
2		Complete breakage at the neck-region between the disc and pad	Generally due to excessive flexing of the metal substrate	**Preventive:** Careful handling. No flexing of steel membrane.
				Corrective: No measures found. Device has to be discarded.
3		Misalignment of PZT during assembly of the actuator.	Misalignment is due to the use of manual tweezers. Shorting is	**Preventive:** Use vacuum tweezers for handling PZT. Take your time when placing it on epoxy.

S.No	Image	Failure Mode	Description	Measures
		Shorting of PZT can be seen as black patches near the square pad.	due to thick epoxy layer.	**Corrective:** If before oven-curing, use vacuum tweezers to carefully pick up misaligned PZT and re-align.
4		Extremely thick layer of epoxy with the two terminals physically shorted.	Similar reason as above.	**Preventive:** Use clean, 20 µm stencil with a glass slide.
				Corrective: No measures found. Device has to be discarded.
5		An actuator with many shorted regions due to thick epoxy.	The actuator shorted at different places from 80V to 150V.	**Preventive:** Same as above.
				Corrective: No measures found. Device has to be discarded.

A.4.2 Microchannels

S.No	Image	Failure Mode	Description	Measures
1		Clogging of central inlet due to residue from sanding	The bottom face of the microchannels need to be sanded, but some particulates tend to enter the channels during this operation.	**Preventive:** Flush microchannels with IPA and DI water frequently while sanding.
				Corrective: If channel is completely blocked, try with syringe pump to unclog. Else, discard.

|				
2		Absence of microchannels after printing	It was found during some prints that some microchannels were completely absent.	**Preventive:** Increase thickness of microchannels
				Corrective: No measured found. Device has to be discarded.
3		Clogging of microchannels due to size of orifices	This is a limitation of the fabrication process and cannot be changed.	**Preventive:** Ensure that the dimensions are larger than the minimum possible dimension.
				Corrective: No measures found. Device must be discarded.
4		Bowing of the membrane	The bottom left image shows the surface profile in the X-direction. A clear bowing is visible.	**Preventive:** Add more supports within the microchannels in the design. Add more supports underneath the *part* in the 3D printing software.
				Corrective: Try the microvalve without spacers.

A.5 Microvalve Details

A.5.1 UPM Holder
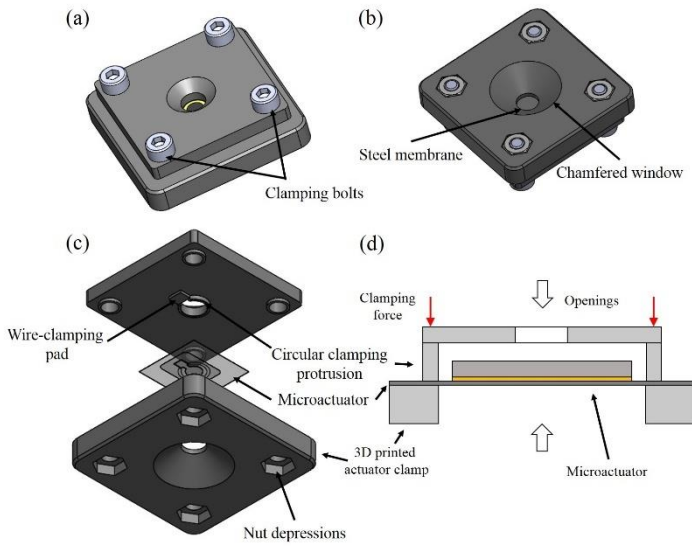
Figure 15: UPM holder schematic

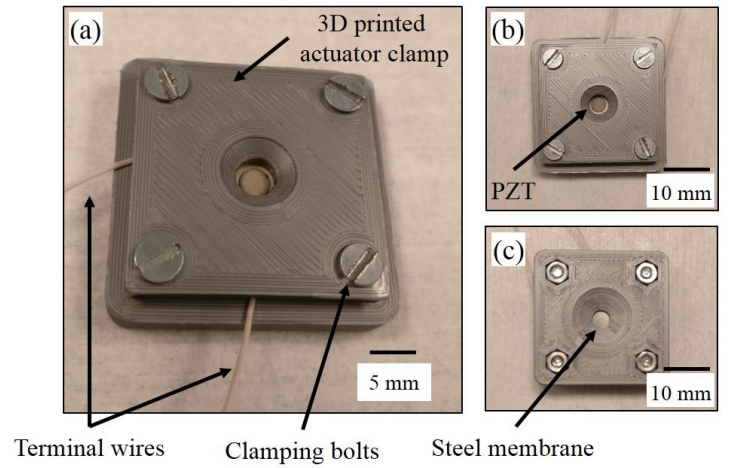**Figure 14: Fabricated UPM holder**

A.5.2 Microvalve results with a 5 µm spacer

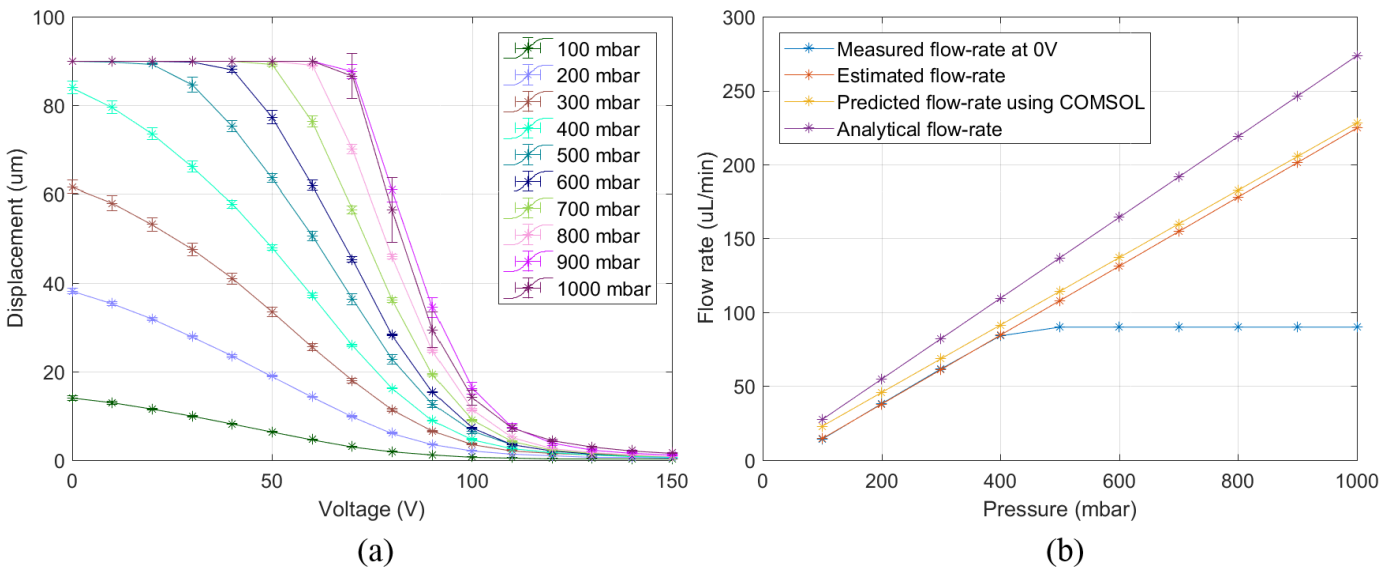**Figure 16: Voltage vs. Flow-rate for a microvalve with a 5 µm spacer**

A.6   Program – Microvalve Data-Acquisition
A.6.1 Main Program

```python
import numpy as np
import time, csv
from OB1 import OB1
from interfaceNI import niDAQ
from analogGeneration import changeVoltage

NI = niDAQ()
mfControl = OB1()

pressures = [40] + range(100, 1100, 100)
pressures = [500]
voltages = np.arange(0, 150.5, 0.5)
repetitions = 3

log_file_path = <file_path>

start_time = time.time()

with open(log_file_path, 'wb') as f:
    writer = csv.writer(f)
    writer.writerow(['Pressure (mbar)', 'Rep', 'Voltage (V)', 'Flow-rate (uL/min)', 'Displacement (um)', 'Time-stamp'])
f.close()
try:
    print('Setting voltage to zero')
    changeVoltage(0)
    print('Flushing..')
    mfControl.setPressure(500)
    time.sleep(20)
    print('Flushing completed')
    mfControl.setPressure(40)
    time.sleep(5)
    for pressure in pressures:
        mfControl.setPressure(pressure)
        time.sleep(10)
        for rep in range(0, repetitions):
            for voltage in voltages:
                # try:
                changeVoltage(voltage+0.2)
                flowRate = mfControl.getFlowRate(num = 500)
                disp = NI.readDisp(port = 3, channel = 9, num_samples = 2000)
                with open(log_file_path, 'ab') as f:
                    writer = csv.writer(f)
                    writer.writerow([pressure, rep+1, voltage, flowRate, disp, time.time()])
                f.close()
                print('%d, %d, %f, %.2f, %.2f' %(pressure, rep+1, voltage, flowRate, disp))
            voltages.reverse()
            for voltage in voltages:
                # try:
                changeVoltage(voltage+0.2)
                flowRate = mfControl.getFlowRate(num = 500)
                disp = NI.readDisp(port = 3, channel = 9, num_samples = 2000)
                with open(log_file_path, 'ab') as f:
                    writer = csv.writer(f)
                    writer.writerow([pressure, rep+1, voltage, flowRate, disp, time.time()])
                f.close()
                print('%d, %d, %f, %.2f, %.2f' %(pressure, rep+1, voltage, flowRate, disp))
            voltages.reverse()
    mfControl.destroy_OB1()
    changeVoltage(0)
    print('All done!')

except KeyboardInterrupt:
    mfControl.abort_OB1()
    changeVoltage(0)
    print('Encountered keyboard interrupt')
except:
    mfControl.abort_OB1()
    changeVoltage(0)

end_time = time.time()

print('Total time taken: %f seconds' %(end_time - start_time))
```

A.6.2 NI DAQ Interfacing

```python
import ctypes
import numpy
class niDAQ:
    def __init__(self):
        self.nidaq = ctypes.windll.nicaiu
        self.int32 = ctypes.c_long
        self.uInt32 = ctypes.c_ulong
        self.uInt64 = ctypes.c_ulonglong
        self.float64 = ctypes.c_double
        self.TaskHandle = self.uInt32
        # the constants
        self.DAQmx_Val_Cfg_Default = self.int32(-1)
        self.DAQmx_Val_Volts = 10348
        self.DAQmx_Val_Rising = 10280
        self.DAQmx_Val_FiniteSamps = 10178
        self.DAQmx_Val_GroupByChannel = 0

    def CHK(self, err):
        if err < 0:
            buf_size = 100
            buf = ctypes.create_string_buffer('\000' * buf_size)
            self.nidaq.DAQmxGetErrorString(err,ctypes.byref(buf),buf_size)
            raise RuntimeError('nidaq call failed with error %d: %s'%(err,repr(buf.value)))

    def analogRead(self, port = 3, channel = 9, num_samples = 5000):
        pin = 'Dev' + str(port) + '/ai' + str(channel)
        # print(pin)
        taskHandle = self.TaskHandle(0)
        max_num_samples = num_samples
        data = numpy.zeros((max_num_samples,),dtype=numpy.float64)
        self.CHK(self.nidaq.DAQmxCreateTask("",ctypes.byref(taskHandle)))
        self.CHK(self.nidaq.DAQmxCreateAIVoltageChan(taskHandle, pin, "",
                                        self.DAQmx_Val_Cfg_Default,
                                        self.float64(-10.0), self.float64(10.0),
                                        self.DAQmx_Val_Volts,None))
        self.CHK(self.nidaq.DAQmxCfgSampClkTiming(taskHandle,"",self.float64(10000.0),
                                        self.DAQmx_Val_Rising,self.DAQmx_Val_FiniteSamps,
                                        self.uInt64(max_num_samples)))
        self.CHK(self.nidaq.DAQmxStartTask(taskHandle))
        read = self.int32()
        self.CHK(self.nidaq.DAQmxReadAnalogF64(taskHandle,max_num_samples,self.float64(10.0),
                                        self.DAQmx_Val_GroupByChannel,data.ctypes.data,
                                        max_num_samples,ctypes.byref(read),None))
        averagedData = numpy.mean(data)

        if taskHandle.value != 0:
            self.nidaq.DAQmxStopTask(taskHandle)
            self.nidaq.DAQmxClearTask(taskHandle)

        return averagedData
    def readDisp(self, port = 3, channel = 9, num_samples = 5000):
        voltage = self.analogRead(port, channel)
        return voltage*25
```

A.6.3 Elveflow Interfacing

Note that the Elveflow SDK needs to be available in the path. Here, the Python32 SDK is used.

```python
import sys
sys.path.append('E:\Delft\Thesis\ELVEFLOW\ESI
SOFTWARE_&_SDK\ESI_V3_02_05\SDK_V3_02_05\SDK_V3_02_05\Python_32\DLL32'.encode('ascii')) #add the path of the library here
sys.path.append('E:\Delft\Thesis\ELVEFLOW\ESI
SOFTWARE_&_SDK\ESI_V3_02_05\SDK_V3_02_05\SDK_V3_02_05\Python_32'.encode('ascii'))#add the path of the LoadElveflow.py
import time, csv
import numpy as np
from ctypes import *
from array import array
from Elveflow32 import *

log_file_path = <Path to log file>
destroyed = False
exit_flag = False
get_pressure = c_double()
pressure_log = []
flowRate_log = []
set_channel = c_int32(int(1))

print("Adding OB1..")
# see User guide to determine regulator type NI MAX to determine the instrument name
Instr_ID = c_int32()
error = OB1_Initialization('01DF9B9B'.encode('ascii'), 5, 0, 0, 0, byref(Instr_ID))
# all functions will return error code to help you to debug your code, for further information see user guide
# print('error:%d' % error)
# print("OB1 ID: %d" % Instr_ID.value)

if error == 0 and Instr_ID.value == 0:
    print('OB1 added successfully \n')
print('Adding flow sensor..')
# add one analog flow sensor
error = OB1_Add_Sens(Instr_ID, 1, 4, 0, 0, 7) # 4 means 80ul/min
if error == 0:
    print('Flow sensor added successfully \n')

# Calibration
print('Calibrating..')
Calib = (c_double*1000)() # always define array that way, calibration should have 1000 elements
Calib_path='C:\Users\Arun\Desktop\Calibration\Calibration.txt'
error = Elveflow_Calibration_Load(Calib_path.encode('ascii'), byref(Calib), 1000)
if error == 0:
    print('Calibration loaded \n')
else:
    error = OB1_Destructor(Instr_ID.value)
    destroyed = True

set_pressure = c_double(float(0))
error = OB1_Set_Press(Instr_ID.value, set_channel, set_pressure, byref(Calib),1000)

# exit_flag = True

with open(log_file_path, 'wb') as f:
    writer = csv.writer(f)
    writer.writerow(['Voltage', 'Flow-rate'])
f.close()

try:
    while not exit_flag:
        set_pressure = float(input('Set pressure (mbar): '))
        print('Pressure set to: %d' % set_pressure)
        if set_pressure > 1000:
            print('Pressure too high, breaking out')
            break
        set_pressure = c_double(set_pressure)

        error = OB1_Set_Press(Instr_ID.value, set_channel, set_pressure, byref(Calib),1000)

        while not exit_flag:
            voltage = input('Input current voltage (n to break): ')
            time.sleep(1)
            if voltage == 'n':
                break
            else:
                voltage = int(voltage)
            flowRate_log = []
            # Acquiring flow rate
            for i in range(0, 500):
                data_sens = c_double()
```

```python
                error=OB1_Get_Sens_Data(Instr_ID.value,set_channel, 1,byref(data_sens)) # Acquire_data =1 -> Read all the
analog value
                flowRate_log.append(data_sens.value)
            flowRate = np.mean(flowRate_log)
            print('Recording voltage: %d, flow-rate: %f' % (voltage, flowRate))
            with open(log_file_path, 'ab') as f:
                writer = csv.writer(f)
                writer.writerow([voltage, flowRate])
            f.close()
except KeyboardInterrupt:
    print('Force interrupt encountered, setting pressure to zero and shutting down OB1 connection')
    set_pressure = c_double(float(0))
    error = OB1_Set_Press(Instr_ID.value, set_channel, set_pressure, byref(Calib),1000)

    error = OB1_Destructor(Instr_ID.value)
    if error == 0:
        print('OB1 connection stopped')
    destroyed = True
except:
    set_pressure = c_double(float(0))
    error = OB1_Set_Press(Instr_ID.value, set_channel, set_pressure, byref(Calib),1000)
    error = OB1_Destructor(Instr_ID.value)
    if error == 0:
        print('Error encountered, OB1 connection stopped')
    destroyed = True
if not destroyed:
    set_pressure = c_double(float(0))
    error = OB1_Set_Press(Instr_ID.value, set_channel, set_pressure, byref(Calib),1000)
    print('End of program, pressure set to zero, OB1 connection stopped')
    error=OB1_Destructor(Instr_ID.value)
```

Appendix B – Si-MEMS Microvalves

This appendix contains the following sections:
1. Else Kooi Lab
2. MESA+ Lab

The initial approach to fabricate a microvalve was using Silicon microfabrication. This had to be changed to a hybrid-integration approach due to delays in the Si-fabrication. Significant work has been done in the design and development of these microvalves.

Two types of microvalves were initially designed. One type is a membrane microvalve and the other is a valve-plate microvalve. Schematics are shown in the following figure.
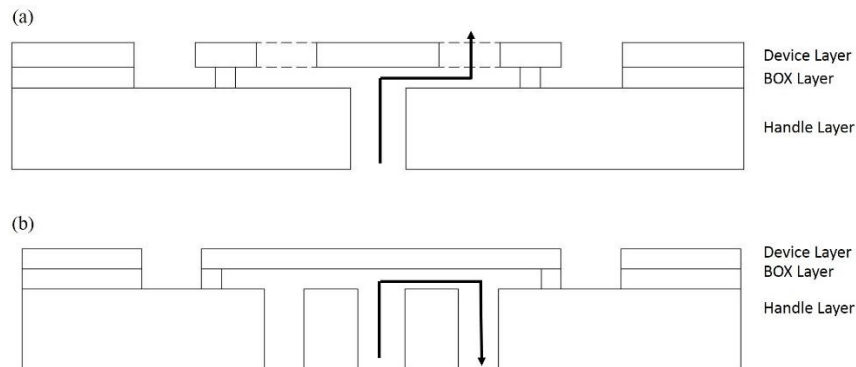
**Figure 17: Schematic of Membrane and valve-plate microvalves**

Both of these types were fabricated in two labs. Due to fabrication limitations in each, the design had to be modified. The fabrication process and the designs at each lab are shown below. Results are shown where applicable.

B.1 Microvalves from Else Kooi Lab

The following sections detail the work that has been done to fabricate the microvalves at the Else Kooi Lab (EKL).

B.1.1 Fabrication Process

The EKL MUMPS (Multi User MEMS Process Sequence) was used to fabricate these microvalves. Figure 18 shows the fabrication process sequence. A final long vapor HF step might be required to release the membrane in the membrane microvalve (> 2 hours), but this has not been tested yet.
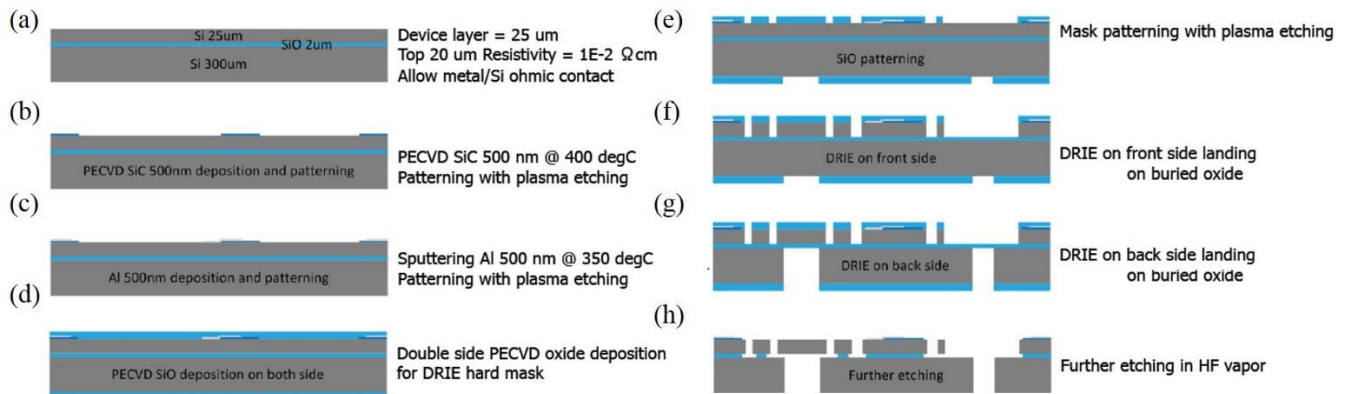
Figure 18: EKL MUMPS Process

B.1.2 Microvalve Designs

Four devices have been fabricated: a microactuator, a membrane microvalve, a valve-plate microvalve, and test-structures to test the etch-rate of vapor HF on SiO_2. The mask designs were made in L-Edit and are shown in Figure 19.
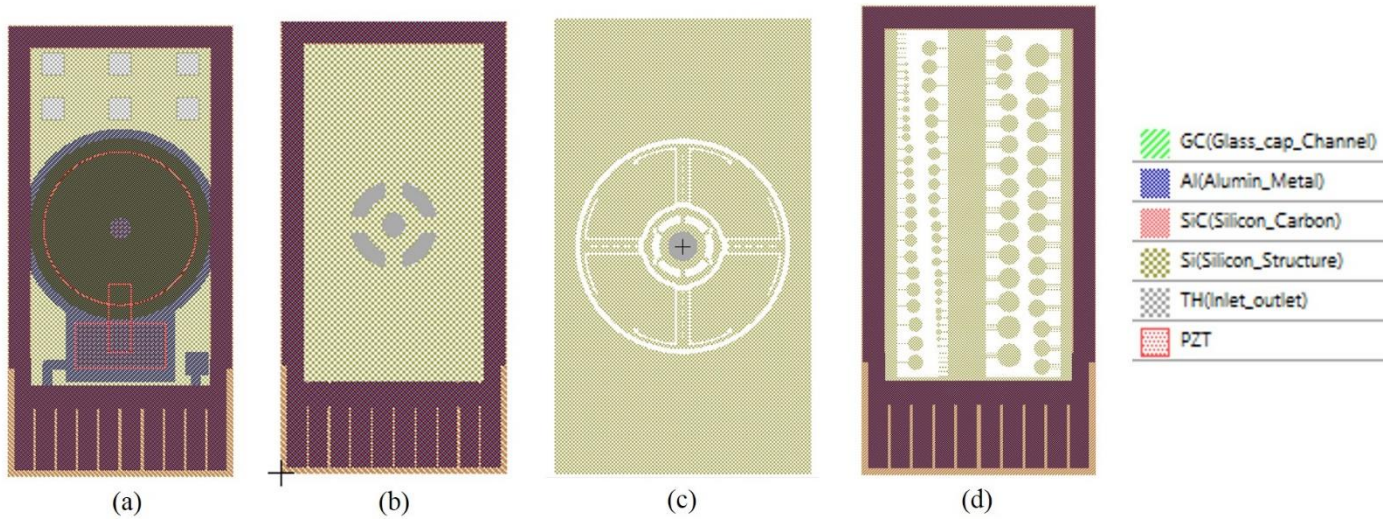
Figure 19: (a) Microactuator chip (b) Membrane microvalve (c) Valve-plate Microvalve (d) Test-structures

B.2   Microvalves from MESA+ Lab

A batch of the membrane and valve-plate microvalves were fabricated at the MESA+ Lab in the University of Twente. Due to a low under-etch distance (of the BOX layer) in their process, the microvalve designs had to contain many perforations so that the device layer could be released. This means that these devices are not suitable as microvalves but can be used to conduct basic mechanical analyses. The mask designs were made in CleWin.

B.2.1 Fabrication Process

(a)
- Substrate selection
- SOI 25-2-400
- Orientation: h100i
- Device layer: 25 um, P++
- Handle layer: 400 um, P+

(b)
- Wafer cleaning
- Wet Thermal Oxidation, 2 um
- Temperature, 1150 ∘ C
- Time: 12:00 h
- Measurement of oxide layer thickness

(c)
- Coating handle layer with photoresist, Olin 907-17
- Exposure, mask: HANDLE

(d)
- Etching of silicon dioxide in Adixen DE
- depth: 2µm
- time: ≈ 5 min

(e)
- Stripping resist, cleaning wafer

(f)
- Coating device layer with photoresist, Olin 907-17
- Exposure, mask: DEVICE

(g)
- Etching of silicon dioxide in Adixen DE
- depth: 2µm
- time: ≈ 5 min

(h)
- DRIE Etching of silicon in
- Adixen SE, top side
- Recipe: RB.HARS.
- depth: 25 µm
- time: ≈ 9 min.

(i)
- DRIE Etching of silicon in Adixen SE, bottom side
- Recipe: see section 6.2
- depth: 400µm
- time: ≈ 36 min.

(j)
- Stripping resist, cleaning wafer
- Fluor carbon removal
- O2 plasma cleaning, 800 Watt, 1 hour
- Piranha cleaning, 30 min

(k)
- Etching of oxide in 50% HF
- Time: ca. 2 min. until oxide at top and bottom side is removed

(l)
- Vapor-HF to release structures and devices
- Time: 45 min

(m)
- Release samples by removing surrounding frame
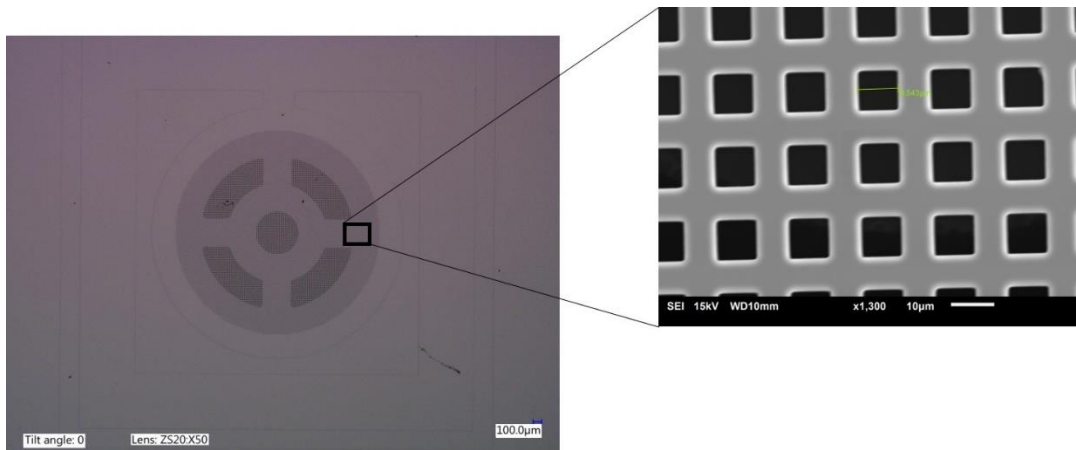- Measurement/Inspection of samples

Figure 20: Fabrication Process Sequence at MESA+ Lab
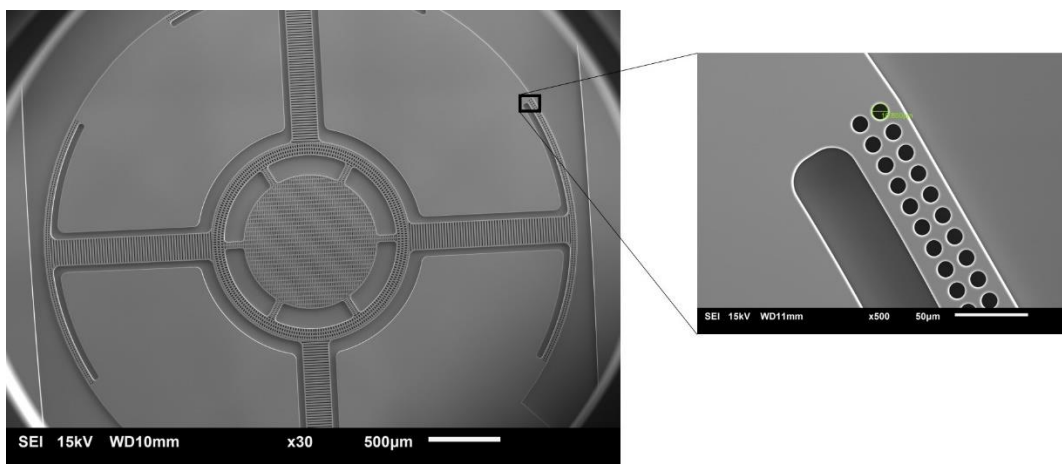
B.2.2 Microvalve Designs
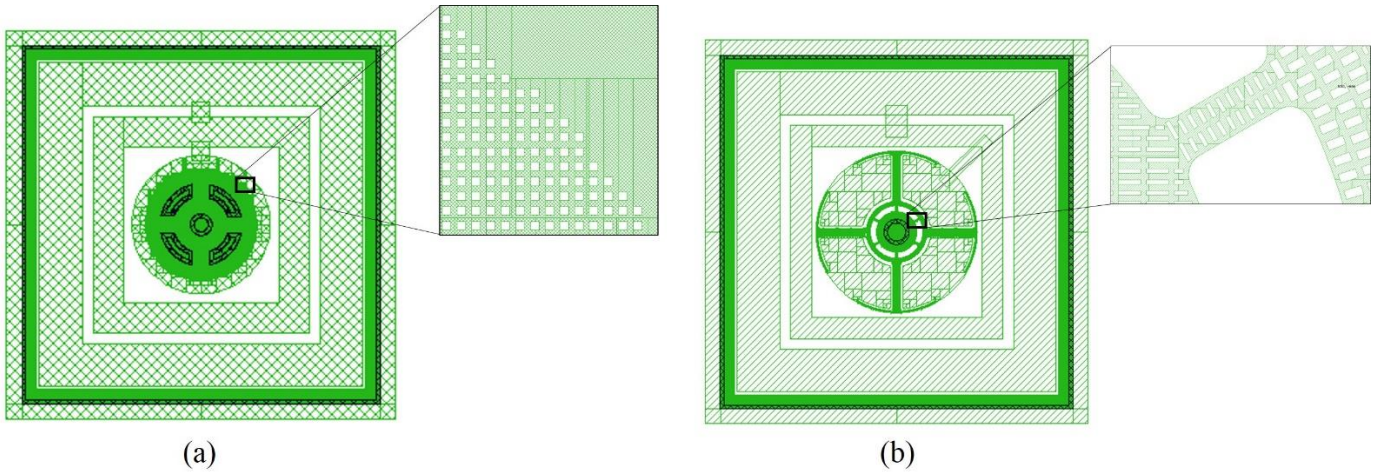
Figure 21: (a) Membrane microvalve with inset showing perforations (b) Valve-plate microvalve with inset showing perforations

B.2.3 Fabrication Results

Figure 22: Fabricated membrane microvalve with zoomed inset showing perforations

Figure 23: Fabricated valve-plate microvalve with zoomed inset showing perforations